Iowa Research Online
The University of Iowa's Institutional Repository

University of Iowa
Iowa Research Online

Theses and Dissertations

Fall 2012

Detection of erosion/deposition depth using a low frequency passive radio frequency identification (rfid) technology

Iordanis Vlasios Moustakidis
University of Iowa

Copyright 2012 Iordanis Vlasios Moustakidis

This thesis is available at Iowa Research Online: https://ir.uiowa.edu/etd/1490

Recommended Citation
Moustakidis, Iordanis Vlasios. "Detection of erosion/deposition depth using a low frequency passive radio frequency identification (rfid) technology." MS (Master of Science) thesis, University of Iowa, 2012.
https://doi.org/10.17077/etd.lcwy2kd4.

Follow this and additional works at: https://ir.uiowa.edu/etd

Part of the Civil and Environmental Engineering Commons

DETECTION OF EROSION/DEPOSITION DEPTH USING A LOW FREQUENCY PASSIVE RADIO FREQUENCY IDENTIFICATION (RFID) TECHNOLOGY

by

Iordanis Vlasios Moustakidis

A thesis submitted in partial fulfillment
of the requirements for the Master of
Science degree in Civil and Environmental Engineering
in the Graduate College of
The University of Iowa

December 2012

Thesis Supervisor: Professor Athanasios (Thanos) N. Papanicolaou

Copyright by

IORDANIS VLASIOS MOUSTAKIDIS

2012

All Rights Reserved

Graduate College
The University of Iowa
Iowa City, Iowa

CERTIFICATE OF APPROVAL

_____

MASTER'S THESIS

_____

This is to certify that the Master's thesis of

Iordanis Vlasios Moustakidis

has been approved by the Examining Committee
for the thesis requirement for the Master of Science
degree in Civil and Environmental Engineering at
the December 2012 graduation.

Thesis Committee: _____
Athanasios (Thanos) Papanicolaou, Thesis Supervisor

_____
Salam Rahmatalla

_____
Christopher Wilson

To my parents Vlasis and Vasso and my brothers Thodoris and Nikos

You could not step twice into the same river; for other waters are ever flowing on to you.
Heraclitus (535 - 475 BCE)

ACKNOWLEDGMENTS

First and foremost I offer my sincerest gratitude to my supervisor, Professor Athanasios (Thanos) Papanicolaou, who has supported me throughout my thesis with his advice, guidance and patience. I attribute the level of my Master's degree to his encouragement and effort and without him this thesis would not have been completed or written. I also would like to express my appreciation to Dr. Salam Rahmatalla and Dr. Chris Wilson for serving on my thesis defense committee.

I also thank my team mates Achilleas Tsakiris, Will Ettema, Ben Abban, Dr. Filippo Bressan, Dimitrios Dermisis, Ken Wacha, and Tommy Surtato, as well as the TI engineers, Hebert Meier and Klemens Sattlegger, for their help and support during my research. Here, I feel the need to extent my grateful thanks to my "second" family back in Fort Collins, CO, Prof. Evan Vlachos, Panagiotis Oikonomou, Dr. Galatios Moschonas, the Brown family (Brian, Maro, Sierra and Teagan) and all my friends there for their truly support and friendship. I would also wish to thank the IIHR people; professors, graduate students, technical and administrative staff for warmly welcoming me to this great scientific institution and making my transition as smooth as possible.

Lastly, and more importantly, I would like to thank my family members, my father Vlasios, my mother Vasiliki and my brothers Theodoros and Nikolaos for their unconditional love and support. Without their encouragement, I would not have finished the degree.

ABSTRACT

This thesis presents an experimental study both in the laboratory and field to develop and test a method for continuously measuring and monitoring scour using an automated identification technology known as Radio Frequency Identification (RFID). RFID systems consist of three main components, namely (a) the reader which controls the system, (b) the transponder (derived from transmitter/responder) that transmits data to the reader and (c) the excitation antenna that allows the communication between the reader and the transponder.

The study provides an insight into the RFID technology and develops the framework for using this technology to eventually address two central themes in river mechanics and sediment transport; (a) the determination of the active layer thickness and (b) the scour/deposition depth around a hydraulic structure. In particular, this study develops the methodology for relating the signal strength of a radio frequency (RF) device with the distance between an excitation antenna and the RF device.

The experiments presented herein are classified into two main groups, (1) the laboratory and (2) the RF signal vs. the detection distance experiments (field experiments). The laboratory experiments were designed to understand the effect of key RFID parameters (e.g., transponder orientation with respect to the excitation antenna plane, maximum antenna-transponder detection distance), measured in terms of the transponder return RF signal strength for various antenna-transponder distances, transponder orientations with respect to the excitation antenna plane and different mediums in between the excitation antenna and the transponder, on the overall performance of the RFID system. On the other hand, the RF signal vs. the detection

distance experiments were based on the results obtained during the laboratory experiments and focused on developing calibration curves by relating the transponder return RF signal strength with the distance between the excitation antenna and a transponder.

The laboratory results show that the dominant RFID parameters affecting the system performance are (a) the transponder orientation towards the excitation antenna plane and (b) the medium type in between the excitation antenna and the transponder. The differences in reading distances were attributed to the transponder inner antenna type, while the effect of the medium was related with the void ratio, where higher porosity materials have, less RF signal strength decay. The parameter that governs the RF signal strength decay was found to be the distance between the excitation antenna and the transponder (erosion process experiments). The RF signal strength decays almost linearly with distance, while the rate of the RF signal strength decay is controlled by the material type in between the excitation antenna and the transponder (deposition process experiments).

The RF signal vs. the detection distance experiments demonstrate that the reading distance of the RFID system can be significantly increased by using a custom made excitation antenna. The custom made excitation antenna not only increases the reading distance between the antenna and the transponder to nearly 20 ft., but also allows the user to manipulate the excitation antenna's shape and size to meet the specific landscape requirements at the monitoring site.

TABLE OF CONTENTS

LIST OF TABLES ix

LIST OF FIGURES x

CHAPTER

1. INTRODUCTION 1

1.1 Problem statement 1

2. BACKGROUND AND LITERATURE REVIEW 6

2.1 Introduction 6
2.2 Types of bridge scour 6
2.3 Existing bridge scour inspection and monitoring methods 11
2.3.1 Physical probes local scour inspection devices 12
2.3.1.1 Sounding poles 12
2.3.1.2 Sounding weights 13
2.3.2 Sonar sound local scour inspection systems 13
2.3.3 Ground Penetrating Radar (GPR) 15
2.3.4 Time-Domain Reflectometer (TDR) 16
2.3.5 Fiber Bragg Grating (FBG) 17
2.4 Use of the Radio Frequency Identification (RFID) Technology 22
2.4.1 RFID particle tracers 23
2.5 Limitations related to the low frequency passive RFID technology reported in literature 26
2.5.1 RFID system operational limitations 27
2.5.2 Limitations of the RFID technology related to RF signal properties 28

3. HYPOTHESIS AND OBJECTIVES 31

3.1 Hypothesis 31
3.2 Scope and objectives 32

4. INSTRUMENTATION AND EXPERIMENTAL SETUP 35

4.1 Instrumentation and experimental setup 35
4.1.1 RFID system by TI 36
4.1.2 RFID system by HiTAG 39

5. METHODOLOGY 43

5.1 Parametric experiments 43
5.1.1 Transponder orientation (ORIENT) effects on the transponder return RF signal 45
5.1.2 Transponder housing (HOUS) effects on the transponder return RF signal 47
5.1.3 Coupling effects on the transponder return RF signal 48

5.1.4 Medium (MEDM) effects on the RF signal strength decay 50
5.1.5 Effects of sand and gravel porosity on the RF signal propagation and decay 51
5.2 Replication of real case scenarios in the laboratory: evaluating the performance of the RFID system during the erosion and deposition processes 53
5.2.1 RF signal strength decay during the erosion (EROS) process 54
5.2.2 RF signal strength decay during the deposition (DEP) process 57
5.2.3 Quantify scour (SCR) using the Leopold chain method around a bridge pier model 59
5.3 The RF signal strength vs. detection distance experiments 61
5.3.1 Development of a custom made excitation antenna for achieving the maximum antenna-transponder detection distance 62
5.3.2 Development of the transponder return RF signal strength decay calibration curve in air using the custom made excitation antenna 67
5.4 Radio Frequency Signal 67
5.4.1 Analysis of the obtained RF signal 68
5.4.2 Different methods of analyzing the RF signal 69

6. RADIO FREQUENCY (RF) SIGNAL STRENGTH DECAY EXPERIMENTAL RESULTS 74

6.1 Introduction 74
6.2 Parametric experiments 74
6.2.1 Transponder orientation (ORIENT) effects on the transponder return RF signal 75
6.2.2 Transponder housing (HOUS) effects on the transponder return RF signal 78
6.2.3 Coupling effects on the transponder return RF signal 80
6.2.4 Medium (MEDM) effects on the RF signal strength decay 82
6.2.5 Effects of sand and gravel porosity on the RF signal propagation and decay 85
6.3 Sensitivity analysis 85
6.4 Quantify transponder return RF signal strength decay during the erosion and deposition processes 89
6.4.1 RF signal strength decay during the erosion (EROS) process 89
6.4.2 RF signal strength decay during the deposition (DEP) process 90
6.4.3 Quantify scour (SCR) using the Leopold chain method around a bridge pier model 92
6.5 The RF signal strength vs. detection distance experiments 94
6.5.1 Development of a custom made RFID antenna for achieving the maximum antenna- transponder detection distance 94
6.5.2 Development of the transponder return RF signal strength decay calibration curve in air using the custom made RFID antenna 96
6.6 Uncertainty analysis 98

7. CONCLUSIONS, CONTRIBUTIONS AND RECOMMENDATIONS 104

REFERENCES 107

LIST OF TABLES

Table

1-1 Total highway damage repair costs for selected floods 3

2-1 Different methods to measure clear-water and live-bed scour around structures and their limitations 9

2-2 Particle tracers employed in live-bed scour studies. 20

5-1 Summary of the experiments performed 44

5-2 Summary of the RF signal strength vs. detection distance experiments performed 61

5-3 Custom made, closed rectangular loop shape excitation antenna summary attempts 65

6-1 Average detection distances for the different encasings under different orientations 79

6-2 Factors considered for the sensitivity analysis 87

LIST OF FIGURES

Figure

1-1 The Willow Creek bridge failure, where the bed elevation was lowered due to erosion. Extensive erosion can expose the subsoil leading to the formation of an abrupt step in the channel bed, varying from few centimeters to many meters in depth. This abrupt step is known as a head-cut and progresses upstream putting at greater risk the structural integrity of the bridge. 4

1-2 A sketch of a typical bridge waterway, where flow that passes through a bridge constriction is directed towards the bridge embankments. The different media based on which the bridge foundations are established are also presented.....4

1-3 A bridge failure in Wild River, Minnesota case caused by the interrelated action of scour and debris accumulation against the structure. This is common for small bridges, where bridge openings narrow the natural channel and form an obstacle to the flow.....5

1-4 Schematic representation of a low frequency, passive Radio Frequency IDentification (RFID) system developed by Texas Instruments (TI).....5

2-1 Scour types at a bridge site. 8

2-2 Operational frequencies of the most common used scour monitoring systems.....11

2-3 Sounding pole device.....14

2-4 Sounding weight device.....14

2-5 Fixed fathometer sonar system. 18

2-6 Ground Penetrating Radar (GPR) system.....18

2-7 Time Domain Reflectometer (TDR) system's main parts.....19

2-8 Fiber Bragg Grating system.....19

2-9 Painted particle tracers employed in a gravel bed river study. 24

2-10 Magnetic particle tracers.....25

2-11 The components of an Active RFID system (Reader, active transponders and antennas) 25

2-12 The components of a passive RFID system (Reader, passive transponders and antennas). 26

3-1 Schematic representation of the implementation of the Leopold chain method for continuously monitoring scour around bridge piers.....34

4-1 RFID systems used in this study; (A) A low frequency (134 kHz), passive Radio Frequency Identification (RFID) system from TI (excitation antennas specifications: (1) large rectangular loop shape antenna RI-ANT-G01E – 0.70x0.27 m and (2) small square loop shape antenna RI-ANT-G02E – 0.20x0.20 m) and (B) a low frequency (125 kHz), passive Radio Frequency Identification (RFID) system from HiTAG (antenna specifications: a six-edged polygon loop shape antenna (0.86x0.52) 36

4-2 Transponder detection software for the TI RFID system, developed in IIHR. 41

4-3 Communication between the excitation antenna and multiple transponders; (A) without the anti-collision feature and (B) with the anti-collision feature 42

5-1 Transponder orientations with respect to the excitation antenna plane; (a) perpendicular and (b) parallel 46

5-2 Size comparisons for the transponder and particles used. From left to right: (a) "naked" transponder, (b) glass particle and (c) concrete-tungsten particle. 48

5-3 Transponder located inside the excitation antenna's frame. 49

5-4 Experimental setup for testing the medium effects on the transponder return RF signal; D is the maximum detection distance achieved between the excitation antenna and the transponder. 51

5-5 Log-normal sand particle size distribution. 52

5-6 Log-normal gravel particle size distribution. 53

5-7 Erosion process experimental setup. 55

5-8 Erosion process experimental phases - schematic representation. 56

5-9 Deposition process experimental setup. 57

5-10 Deposition process experimental phases - schematic representation. 58

5-11 Leopold chain method experimental setup to quantify scour around a model bridge pier. 60

5-12 Field experimental setup: a view of the developed custom made excitation antenna (10x6 ft.) employed for the field experiments. 66

5-13 RF signal time series; (A) Example of the RF signal time series (as they were obtained via a digital oscilloscope), using the TI system and (B) a sketch showing the points at which the RF signal was recorded. 71

5-14 RF signal main parts. 72

5-15 One RF signal cycle (~ 0.1 seconds) - time length of each RF signal part: (A) the whole RF signal, (B) the "step" and the "oscillating" RF signal parts and (C) the "step" part of the RF signal 72

5-16 Different methods for computing the RF signal strength decay 73

5-17 Development of the RF signal strength decay curves by using the drop in voltage of transponder return RF signal with respect to the "charging" part of the RF signal 73

6-1 Transponder detection success percentage rate as a function of the antenna - transponder distance, for each transponder used in this experimental series. 77

6-2 Transponder's return RF signal strength decay in air when the transponder is located at close proximity or within the excitation antenna frame. 81

6-3 RF signal strength decay curves developed in various mediums (i.e., air, water, dry sand and dry gravel). 84

6-4 RF signal decay curves for (a) sand and (b) gravel material types. 84

6-5 Sensitivity analysis curves for (a) water, (b) dry sand and (c) dry gravel mediums, for the favorable transponder orientation. 88

6-6 Sensitivity analysis curves for (a) water, (b) dry sand and (c) dry gravel mediums, for the unfavorable transponder orientation. 88

6-7 The RF signal strength decay curve for the erosion process experiments. 90

6-8 The RF signal strength decay curve for the deposition process experiments. 91

6-9 Transponder return RF signal strength decay calibration curve in air, using the custom made RFID antenna. 97

6-10 Uncertainty analysis plot for the transponder return RF signal strength decay using the ISO/BIMP (1993) protocol for the TI LF passive RFID system with the 120 mm transponders, along with the custom made RFID antenna, when AIR was in between the antenna and the transponder. 103

CHAPTER 1

INTRODUCTION

1.1. Problem Statement

The term scour is used to define the removal of channel bed sediments under the erosive action of the flow. Excessive scour can dramatically affect channel stability by exposing the subsoil and laterally eroding the riverbanks (Ettema et al. 2006) (Figure 1-1). This channel instability greatly increases the potential for failure of the hydraulic structures located in the channel. During 2008, the state of Iowa alone has spent $403 million on restoration and replacement projects for its more than 5,000 bridges. Table 1-1 presents the total highway damage repair costs for selected floods, as they were reported by Mueller (2000).

The design of stable bridge foundations remains challenging, since bridges cannot conform to a dynamically changing riverine environment. Rivers continuously adjust their banks and beds to efficiently accommodate flow and sediment discharges. Moreover, at bridge crossings, the main channel constricts causing increased stream flow velocities and turbulence beneath the bridge opening resulting in excessive bridge scour (Figure 1-2). Subsequently, the bed sediments around bridge piers and abutments are washed away, compromising the bridge foundations.

Scour around bridge foundations (e.g., piers and abutments) can lead to their failure during high floods (Figure 1-3). Bridge scour has been identified as a problem at a national scale, being both an economic burden and a threat to public safety. In recent

history, more bridge failures have been attributed to scour than all other causes combined (Murillo 1987; Shirhole and Holt 1991; Kattell and Eriksson 1998).

It is obvious that with nearly 500,000 bridges in the U.S., annual inspection of all these bridges for scour is a nearly impossible task. In fact, most bridges are only inspected every 3 to 4 years. Additionally, the methods employed to inspect scour around bridge piers and abutments cannot be used during high floods, when the maximum scour occurs. Thus, there is an imperative need for an automated bridge scour monitoring system that can continuously monitor the scour depth around a bridge pier, especially under high flood conditions, and provide to the bridge maintenance personnel an early warning system when scour reaches a critical depth.

To address the critical need for a continuously monitoring bridge scour system, we intend to use Radio Frequency Identification (RFID) technology, which utilizes radio frequency (RF) waves to transfer information between a reader and a transponder (short for transmitter/responder) via an excitation antenna (Nichols 2004; Dziadak et al. 2009). The reader consists of a set of circuit boards that transmits an RF signal through an excitation antenna to a transponder. The excitation antenna ensures the two way communication between the reader and the transponder through the electronic circuits (e.g., antenna tuning board). The excitation antenna is connected to a tuning board, which keeps that the excitation antenna is at the same frequency with the reader allowing for proper communication with the transponder. The transponders consist of circuits that send out a coded ID once they have received a wake up signal from the reader (Nichols 2004). The excitation antenna relays this coded ID to the reader, which passes it to a host device, or computer (Figure 1-4).

In this study we will employ a low frequency (LF) (134.2 kHz), passive RFID technology to develop a robust system for continuously monitoring bridge scour. In order to achieve this goal, the key RFID parameters will be identified and subsequently analyzed to obtain a better understanding of this relatively new technology and then laboratory and field experiments will be designed to test the performance and efficiency of this technology in continuously monitoring scour.

Table 1-1 Total highway damage repair costs for selected floods.

Flood Location and Year	Repair Costs
Midwest - 1993	$178,000,000
Georgia - 1994	$130,000,000
Virginia - 1995	$ 40,000,000

Figure 1-1 The Willow Creek bridge failure, where the bed elevation was lowered due to erosion. Extensive erosion can expose the subsoil leading to the formation of an abrupt step in the channel bed, varying from few centimeters to many meters in depth. This abrupt step is known as a head-cut and progresses upstream putting at greater risk the structural integrity of the bridge (after Ettema et al., 2006).

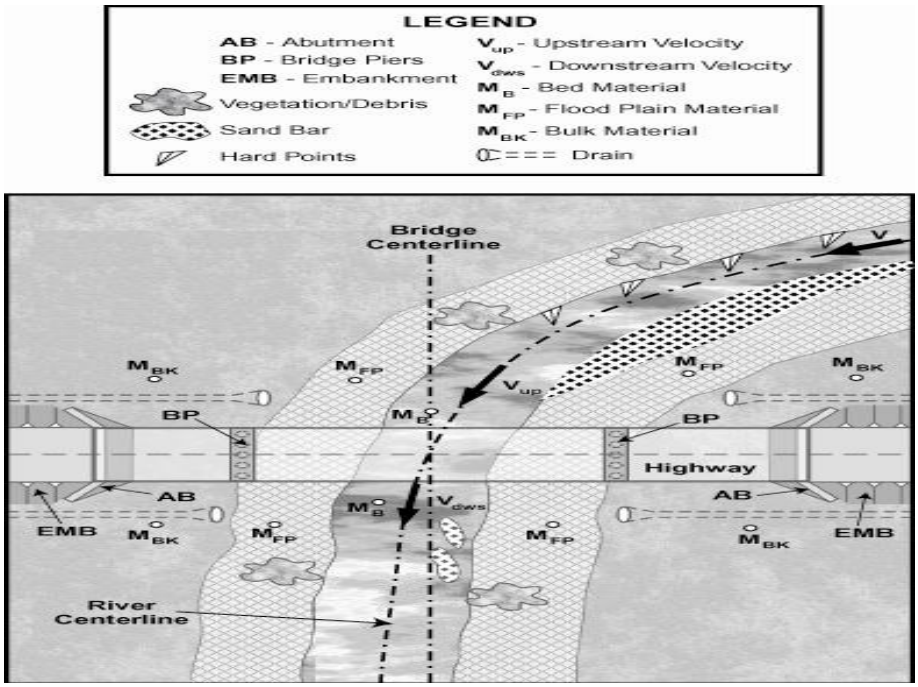

Figure 1-2 A sketch of a typical bridge waterway, where flow that passes through a bridge constriction is directed towards the bridge embankments. The different media based on which the bridge foundations are established are also presented (after Ettema et al., 2006).

Figure 1-3 A bridge failure in Wild River, Minnesota case caused by the interrelated action of scour and debris accumulation against the structure. This is common for small bridges, where bridge openings narrow the natural channel and form an obstacle to the flow (after Ettema et al., 2006).

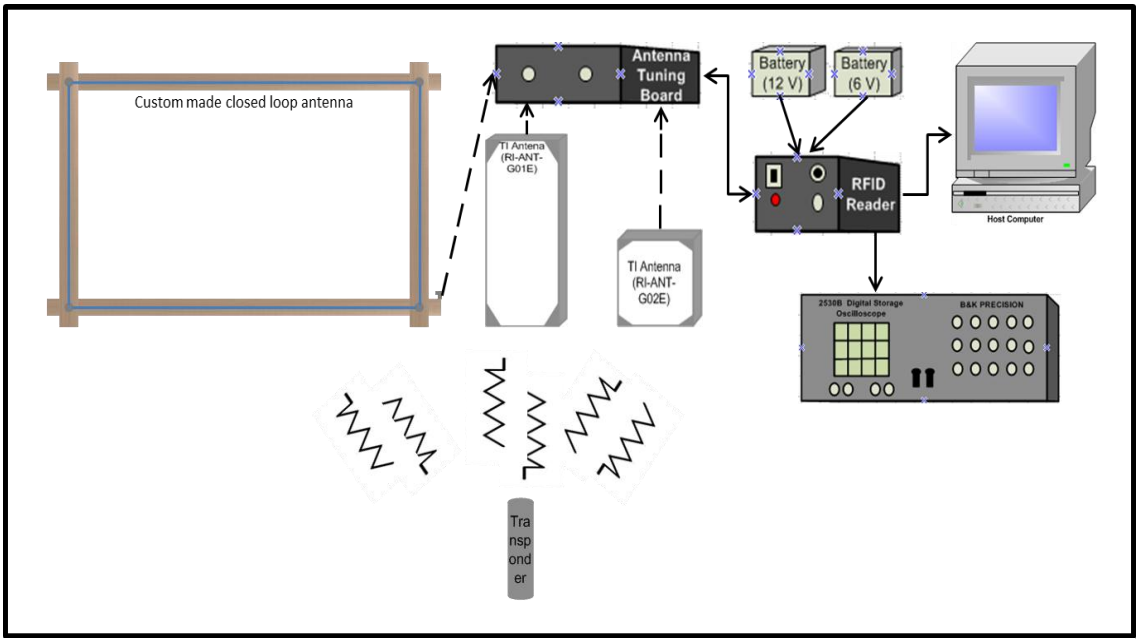

Figure 1-4 Schematic representation of a low frequency, passive Radio Frequency IDentification (RFID) system developed by Texas Instruments (TI).

CHAPTER 2

BACKGROUND AND LITERATURE REVIEW

2.1. Introduction

This chapter focuses on a critical literature review of scour considering that the application of the RFID technology will be used for a scour analysis. The literature review will discuss the most prominent scour processes around bridge piers. The presence of bridge structures in a river creates unsteady, non-uniform flow conditions and introduces complex flow-sediment interactions which are outlined in literature by Gill (1972), Melville (1975), Davoren (1985), Kwan (1988) and Koken and Constantinescu (2008) for abutments/dikes and Kirkil (2008), Melville (1975), Ettema (1980), Dongol (1994), Melville and Chiew (1999) for cylindrical piers.

2.2. Types of bridge scour

There are two types of scour that can occur at a bridge site (Figure 2-1) and are commonly known as

- General scour
- Local scour

General scour is independent of the existence of a hydraulic structure. It occurs when certain criteria are met, such as an increase in the flow discharge due to floods or water releases from a dam upstream, gravel and sand mining in river bed or flood plains and discontinuity in sediment transport due to a dam or changes in the watershed land use. In other words, general scour occurs when the availability of sediment is below the

channel sediment transport capacity. In literature, two types of general scour have been reported, (1) long-term scour and (2) short-term scour. The differentiation between those two types of general scour is based on the time scale of the evolution of the scour hole. The long-term general scour occurs at a considerably longer time scale (several years or longer), and includes progressive degradation and lateral bank erosion. The short-term general scour occurs by a single or several closely-spaced flood events.

Local scour is solely caused due to the presence of hydraulic structures and is generated by the interactions between the flow and the obstacle (e.g., bridge piers and abutments, spur dikes). As flow approaches the structure, it decelerates and flows downward due to pressure gradient at the upstream face of the structure. This downflow generates horseshoe vortices, which are responsible for scouring sediment near the structure (Kwan 1984 and 1988; Melville and Coleman 2000).

The local scour depth is affected by the width, length, and projected length of the obstacle into the flow. Shen et al. (1966), Lemos (1975), Kwan (1984) and Melville and Coleman (2000) found that the local scour depth is proportionally dependent on the structure diameter. In addition, Kirkil (2004) found that the strength of the vorticity field behind the structure and the frequency of the vortex shedding equally affect the evolution of the scour hole and its depth. All these complex flow-obstacle-sediment interactions increase the level of uncertainty in predicting scour depth. In fact, most scour formulae provide information only once the scour depth reaches equilibrium (Breusers et al. 1997; Melville and Sutherland 1988; Richardson et al. 1993 and Kuhnle et al. 2002). Therefore, prediction of the transient local scour depth remains challenging.

Local scour can occur either as clear-water or live-bed scour (Melville and Coleman, 2000; Ettema et al., 2006; Brunner, 2010). Clear-water scour occurs under transport limited conditions. In other words, the shear stress exerted by the flow on the channel bed is below the critical shear stress threshold required to entrain the sediment particles. Whereas, live-bed scour is defined as the process at which erosion is not spatially limited around a hydraulic structure. In this case, the shear stress exerted by the flow on the bed is higher than the critical shear stress and thus the particles are entrained into motion.

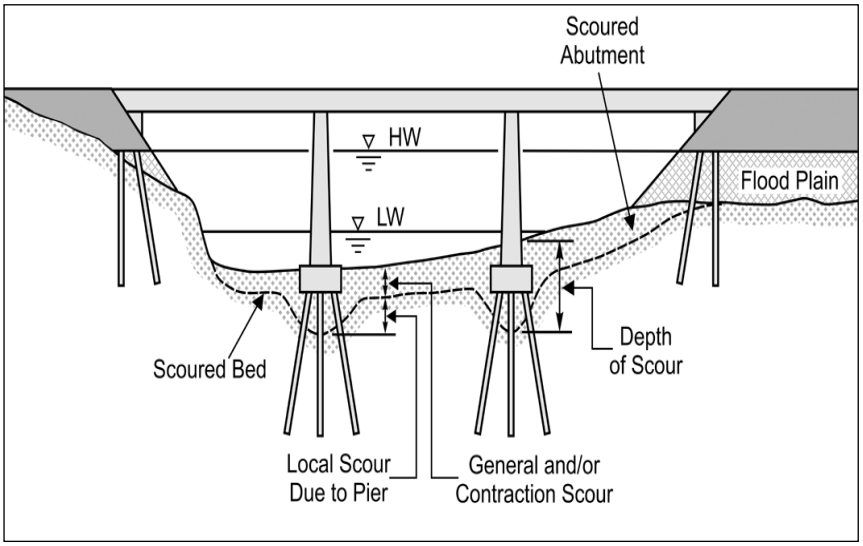

Figure 2-1 Scour types at a bridge site (after Ettema et al. 2006).

Table 2-1 Different methods to measure clear-water and live-bed scour around structures and their limitations.

Methods	Authors	Limitations
Sounding Pole	Lefter (1993); Lagasse (1998); and Fukui and Otuka (2002)	a) Cannot operate under debris and/or ice accumulation b) Difficulty to implement during high velocities c) Susceptible to bed surface penetrating d) Manual operation e) Limited length
Sounding Weights	Van Wilson (1994); Haeni et al. (2000); and Van Wilson (2001)	a) Cannot operate under debris and/or ice accumulation b) Time consuming measurements c) Susceptible to bed surface penetrating d) Manual operation e) Limited length
Sonar Sound Reflectometer	Gorin and Haeni (1989); Mason and Sheppard (1994); Hayes and Drummond (1995); De Falco and Mele (2002); Nassif et al. (2002); and Hunt (2005)	a) Air and/or sediment entrainment can affect measurement quality b) Not very accurate under large flow depths (>2 m) and high velocities (>3 m/s) c) Sensitive to noise caused from turbidity d) No real time scour measurements

Table 2-1 Continued.

Methods	Authors	Limitations
Ground Penetrating Radar	Horne (1993); Forde et al. (1999); Webb et al. (2000); Park et al. (2004); and Anderson et al. (2007)	a) Very expensive b) Labor intensive c) Professional data interpretations required d) Sensitive to noise from turbidity e) No real time scour measurements f) Not operational in saline waters
Time-Domain Reflectometer (TDR)	Yankienlun and Zabilansky (1999); Yu and Zabilansky (2006); and O'Connor and Dowding (2006)	a) Easily dispersed signal b) Functionality limited by dust and muddy water c) Susceptible to corrosion d) Sensitive to electromagnetic noise
Fiber Bragg Grating (FBG)	Schulz et al. (1998); Lin et al. (2004); Lin et al. (2006); and Deng and Cai (2010)	a) Further field testing is required to assess the robustness of the method b) Very expensive c) Noise due to vibrations caused by debris, air bubbles and fluid turbulence d) Special care required to protect the optical fiber sensors

2.3. Existing bridge scour inspection and monitoring methods

Table 2-1 presents the various bridge scour inspection methods, which have been employed by the Department of Transportation (DOT) bridge-inspection personnel in order to measure clear-water scour around bridge piers and abutments and live-bed scour, along with their limitations. Figure 2-2 present the operational frequencies of the most common used scour monitoring systems.

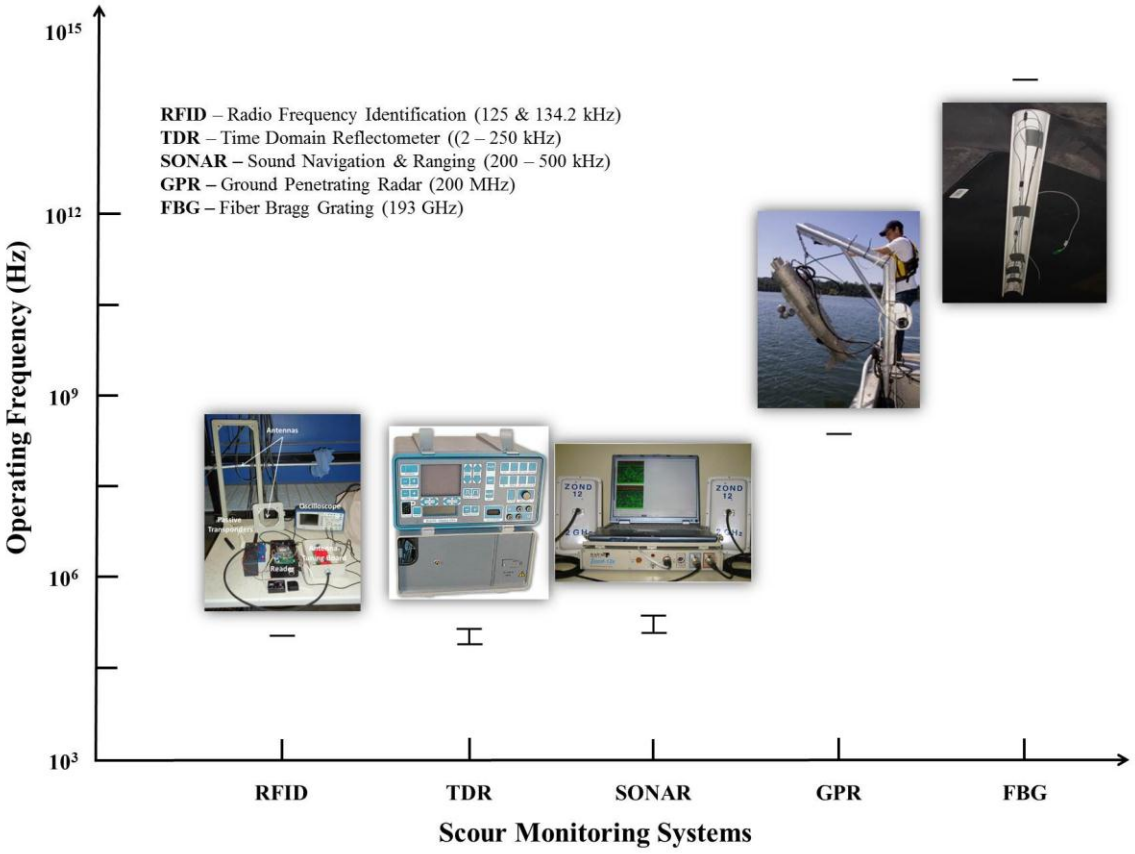

Figure 2-2 Operational frequencies of the most common used scour monitoring systems.

2.3.1. Physical probes local scour inspection devices

2.3.1.1. Sounding poles

Sounding poles (Figure 2-3) are long rods that are typically 12 to 18 ft. (3.66 to 5.5 m) and are used to examine the channel bed around bridge piers and abutments, as well as in shallow water channels to measure the flow depth. The poles are divided into 1-ft. intervals that are marked with different colors in order to enable a better indication of the depth. This is a simple technique with limited applicability that provides poor results. Sounding poles can penetrate in bed surface (Lagasse et al. 1998; Ettema et al. 2006), especially in sand-bed rivers, affecting the accuracy of the scour measurements. In addition, the implementation of this technique during floods is almost impossible during high flows (Ettema et al. 2006) and can put at risk the life of the bridge inspection crew (Fukui and Otuka 2002). Using sounding poles is further limited by the presence of debris and ice accumulation at the bridge site, since the scour hole cannot be reached (Ettema et al. 2006).

2.3.1.2. Sounding weights

Sounding weights (Figure 2-4) are torpedo-shaped objects attached to the bottom end of a measuring rod. Typically, sounding weights are made of lead with aluminum tail fins, to stabilize the pole against the flowing water. Sounding weights can also be used as bedload sediment samplers (e.g., Helly-Smith bedload sampler). Sounding weights are another version of the sounding poles to measure local scour, and therefore the same limitations apply (e.g., susceptibility to bed surface penetration, difficulties in

implementing during floods, and inoperable under debris and ice accumulation at the bridge site).

2.3.2. Sonar sound local scour inspection systems

Sonar, including fathometers and acoustic depth sounders, (Figure 2-5) has been used extensively in measuring bridge scour (Strom and Papanicolaou 2005). Sonar stands for Sound Navigation and Ranging and was initially developed during World War II. The principle behind sonar involves measuring the travel time of an acoustic wave pulse (sound) emitted from a transducer and its reflected echo due to the channel bed. Sonar devices typically operate at a frequency range of 200 to 500 kHz (Lagasse et al. 2001; DeFalco and Mele 2002; Strom and Papanicolaou 2005) and are either mounted to a pier, connected to a data logger (i.e. fathometer), or are portable (i.e. acoustic depth sonar).

Even though sonar has been used extensively, there are limitations that reduce its efficiency and applicability. The quality of the measurements is affected by the presence of air bubbles and fluidized/suspended sediment between the transducer and the river bed since part of the acoustic wave is reflected back to the transducer by the suspended particles increasing the signal to noise ratio. (Nassif et al. 2002; Ettema et al. 2006). Moreover, the accuracy of the data obtained, especially when portable sonar devices are used, during high floods, where the flow depth is more than 2 m and flow velocities higher than 3 m/s, is quite poor (Schall and Price 2004; Ettema et al. 2006). The relatively high cost of the equipment comparatively to physical probes, along with the

need for specially trained personnel to interpret the data, make the sonar solution less attractive.

Figure 2-3 Sounding pole device (after Lagasse et al. 2001).

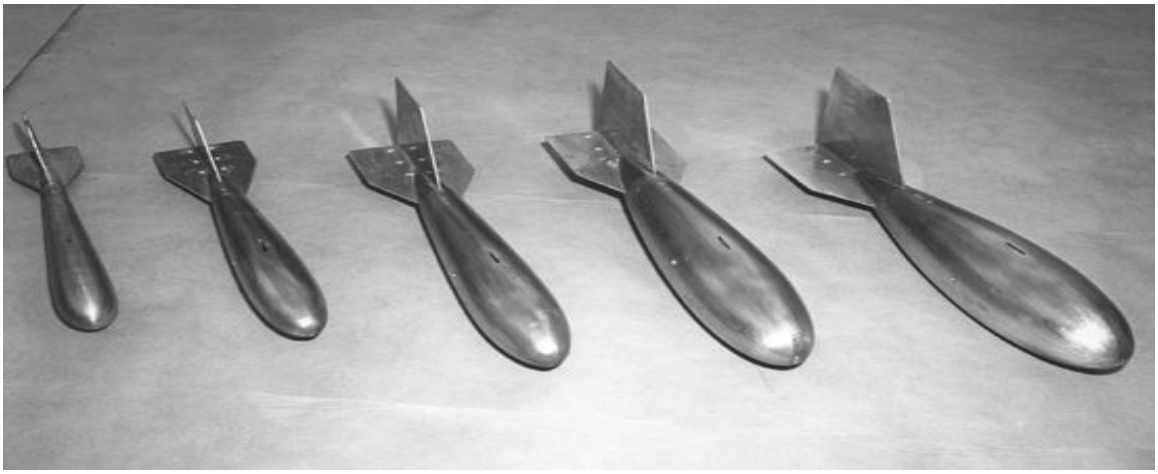

Figure 2-4 Sounding weight device (after Ettema et al. 2006).

2.3.3. Ground Penetrating Radar (GPR)

GPR (Figure 2-6) is a nondestructive surveying device that emits a short RF pulse and receives the reflected echo of that transmitted signal. The transmitted RF signal propagates until a discontinuity in the electromagnetic properties of the soil is encountered. At the boundary of the discontinuity, only a portion of the emitted pulse is reflected back to the receiving antenna with the remainder continuing to propagate into the boundary surface until another discontinuity is reached. The electromagnetic properties of the soil (i.e., permittivity and conductivity) and the magnitude of the discontinuity are the two major factors that affect the strength and intensity of the reflected signal.

GPR system consists of two coupled antennas, namely the transmitting and the receiving antennas, which are housed together. GPR systems emit frequencies from those antennas in the range of MHz, typically 200 MHz (Webb et al. 2000). The choice of the GPR system operational frequency is of great importance for the success of the study/project and extra consideration is required, since the level of detail of the information obtained and the RF signal penetration depth depend on the type of the RF signal (low vs. high RF signal). More specifically, high RF (HRF) signals can detect even slight changes in the soil body continuity and thus more detailed information can be extracted, but they present a poor signal penetration depth, which is further deteriorated by the existence of soil moisture. On the other hand, low RF (LRF) signals can penetrate deeper into the sediment column, without being severely affected by the presence of soil moisture, but the level of detail obtained is considered moderate.

GPR systems have not been extensively used in measuring clear-water local scour, since the equipment is very expensive compared to other methods (Horne 1993; Forde et al. 1999). Moreover, this method requires intensive labor for performing scour measurements and the results need to be interpreted by specially trained personnel (Horne 1993; Forde et al. 1999). The GPR scour inspection method cannot be used for real time scour measurements, since it is a portable device (Horne 1993; Forde et al. 1999; Webb et al. 2000). According to Webb et al. (2000), GPR is very sensitive to noise caused by turbidity increasing the noise to signal ratio and are not suited to saline waters due to the electrical conductivity of the salt waters that reduces the penetration depth (Van Overmeeren et al. 1997).

2.3.4. Time-Domain Reflectometer (TDR)

TDR (Figure 2-7) generates and emits pulses of electromagnetic waves through a transmission line at a constant velocity. The propagation velocity is a function of the speed of light, the electrical and physical characteristics of the transmission line and the surrounding media (Yankielun and Zabilansky 1999). When the propagating electromagnetic wave reaches a discontinuity in the dielectric properties at the interface of two materials (e.g., water and sediment), a portion of the electromagnetic wave is reflected back to the source, while another portion of the initial electromagnetic wave continues to propagate into the encountered material.

According to Yankienlun and Zabilansky (1999) and Lin et al. (2004), a major drawback of this system is the easily dispersed signal, which can severely affect the accuracy of the measurements. Lin et al. (2004) and (2005) reported TDR is susceptible

to electromagnetic noise from the surrounding environment, which also affects the accuracy of the measurements. Since a metallic coaxial cable is used (Yankienlun and Zabilansky 1999; O'Connor and Dowding 2006) the TDR system is also susceptible to corrosion and mud.

2.3.5. Fiber Bragg Grating (FBG)

The FBG system was developed based on the distributed Bragg reflector and consists of sensors placed into a fiber optic cable. For scour monitoring, the system is buried into the river bed at the upstream face of a bridge pier. As scour progresses, the FBG sensors are exposed to higher levels of natural light radiation. This radiation is characterized by a specific wavelength which coincides with the wavelength period of the FBG sensors and ranges from 1500 to 1600 nm, with typical values around 1550 nm. Thus, when the two wavelengths are the same, there is a change in the status of the sensors being exposed to this radiation, which is an indication that the bridge scour reaches a known depth, at which the sensor was initially buried. The resolution of the FBG system can be modified by increasing the number of the sensors in use. In literature has been reported that this method is susceptible to noise due to suspended sediment, air bubbles and fluid turbulent (Lin et al. 2004 and 2005). Further field testing is required to evaluate the performance and the reliability of this system in continuously monitoring local scour around bridge piers, since the optical fiber sensors used are sensitive to collisions with debris and high velocity fluids. Figure 2-8 A, B and C show the sensors and the fiber core, the experimental setup and the flume application of the FBG system, respectively.

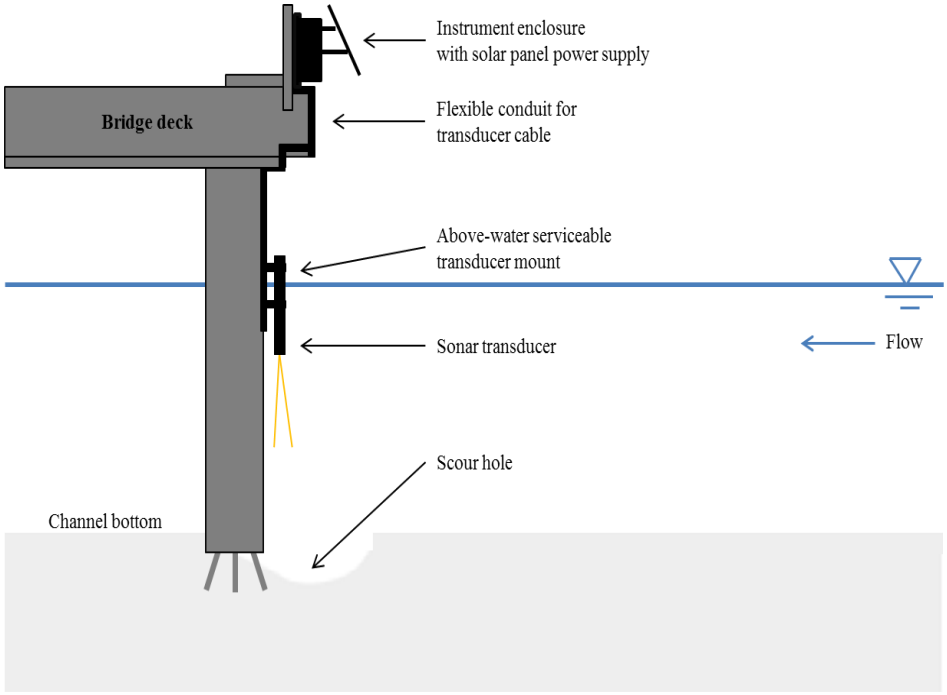

Figure 2-5 Fixed fathometer sonar system (after Ettema et al. 2006).

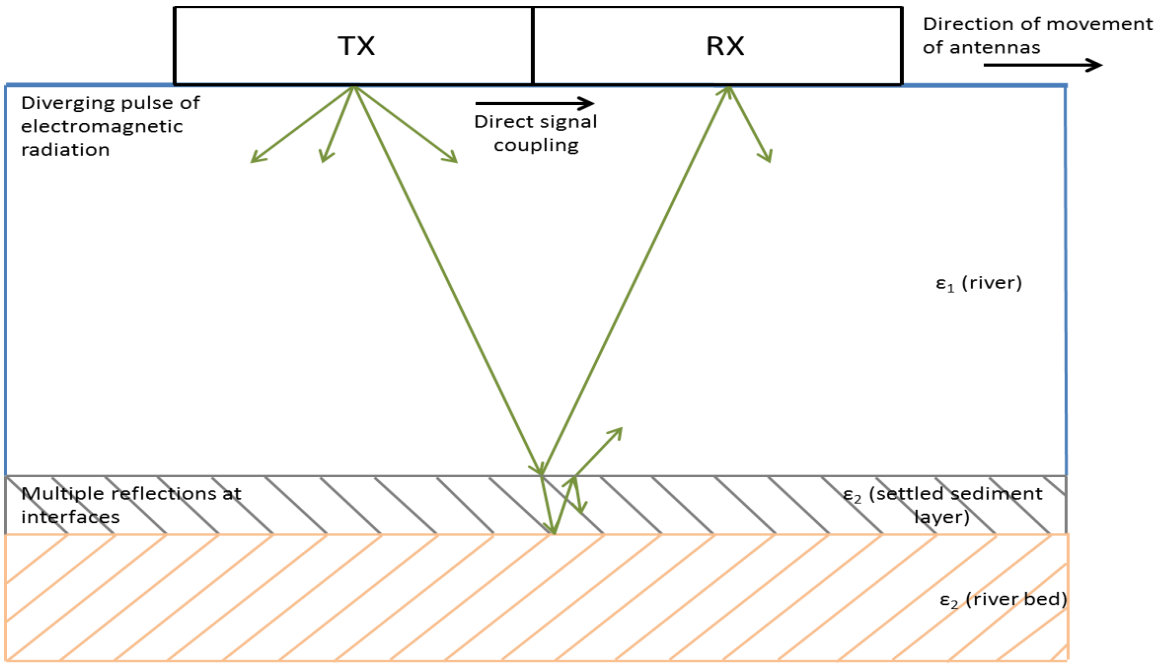

Figure 2-6 Ground Penetrating Radar (GPR) system (after Millard et al. 1998).

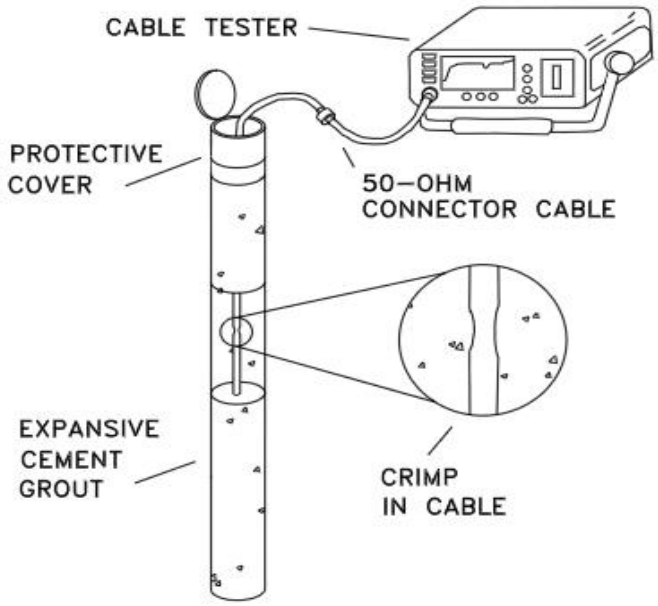

Figure 2-7 Time Domain Reflectometer (TDR) system's main parts (after O'Connor and Dowding 2006).

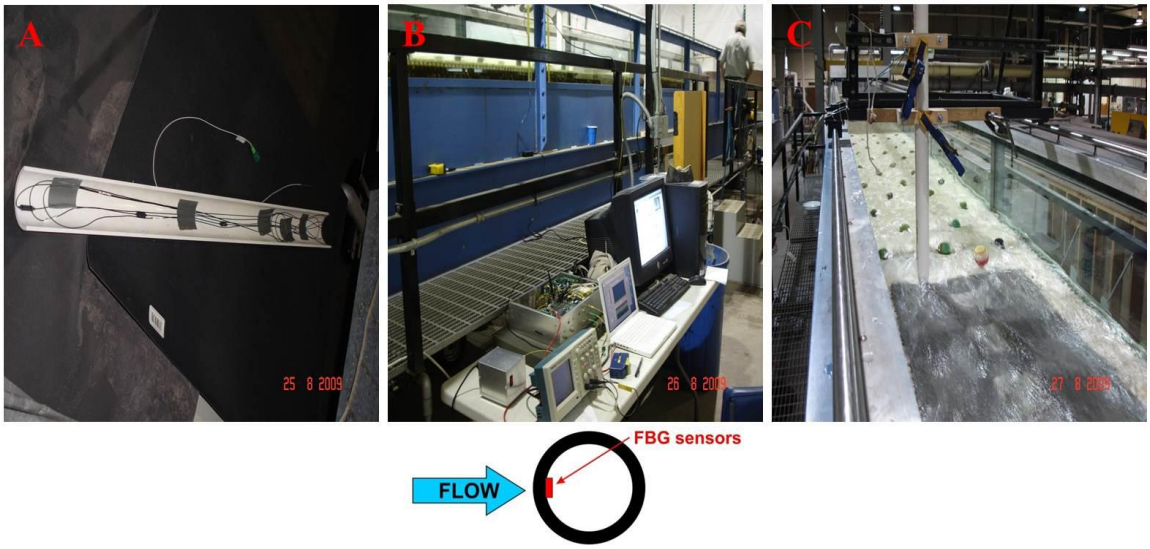

Figure 2-8 Fiber Bragg Grating system.

Table 2-2 Particle tracers employed in live-bed scour studies.

Methods	Authors	Limitations
Painted Tracers	Leopold et al. (1966); Emmett et al. (1990); Hassan et al. (1992); Church and Hassan (1992); Schmidt and Ergenzinger (1992); Haschenburger (1996); and Wilcock (1997)	a) Very low recovery rates (10 - 15%) b) Short lifetime (reliable until the paint fades) c) Difficulty in identifying the particles and measuring the distance traveled d) Time consuming to track down the particles.
Magnetic Tracers	Arkell et al. (1982); Hassan et al. (1984); Custer et al. (1987); Ergenzinger et al. (1989); Ashworth and Fergunson (1989); Laronne and Duncan (1992); Haschenburger and Church (1998); Sear et al. (2000); and Church and Hassan (2002)	a) Moderate recovery rates (40 - 50%) b) Difficulty in identifying the tags and measuring the distance traveled c) Difficulty in measuring the depth of the buried tags d) Interference between naturally magnetic material and the magnetic tags.

Table 2-2 Continued.

Methods		Authors	Limitations
Radio Frequency Identification (RFID) Systems	Active RFIDs	Habersack (2001); Merced Irrigation District (DIC) and Natural Resource Scientists Inc. (2003); Keskilammi et al. (2003) and McNamara and Borden (2004)	a) High cost transponders b) Large size transponders – the battery is embodied into the transponder c) Limited lifespan of the transponders d) Battery failure e) The signal cannot penetrate through saturated sediment f) Only commercially available antennas can be used – the maximum detection distance cannot be manipulated. g) The temperature can affect the lifetime of the battery.
	Passive RFIDs	Nichols (2004); Lamarre et al. (2005); Allan et al. (2005); Lauth and Papanicolaou (2008); Lauth and Papanicolaou (2009); Curtiss et al. (2009); Camenen et al. (2010); Papanicolaou et al. (2010) and MacVicar and Roy (2011)	a) Currently, short reading distances (the maximum distance between the excitation antenna and the transponder varies from few centimeters to less than a meter) b) Vulnerable to electrical noise c) Presence of metal structures can detune the system's magnetic field d) A higher powered reader is required (since the transponder needs to be charged by the reader)

2.4. Use of the Radio Frequency Identification (RFID) Technology

In 1980s and 1990s the development of the Radio Frequency Identification (RFID) technology and especially the low frequency (134.2 kHz) passive RFID technology allowed for the study of sediment transport from the Lagrangian perspective (Nichols 2004; Lamarre et al. 2005; MacVicar and Roy 2011; Liebault et al. 2012; Bradley and Tucker 2012). RFID is a wireless automated identification technology that utilizes/transmits RF waves to transfer information between the receiver and a transponder via an excitation antenna. An RFID system consists of three main parts, namely (a) the reader, (b) the excitation antenna and (c) the transponders. This pioneering technology, due to its high recovery rates of around 90% (Lamarre et al. 2005), gives researchers the opportunity to investigate the motion of individual particles, by knowing their exact position at any time, including the time lag between two successive particle movements and the distance traveled in each movement. Thus, the virtual velocity concept, as it was introduced by Einstein (1937), can be determined. For comparison, the painted particle tracing technique, although it is a simple and low cost method, suffers from very low recovery rates (~10 – 15%) (Figure 2-9). The magnetic particle tracing technique (Figure 2-10) on the other hand, although it is characterized by higher recovery rates (~ 40 – 50%) compared to the painted particles, still suffers from difficulties in spotting and identifying the particles and thus estimating the distance traveled. See Table 2-2 for other tracers and their recovery rates.

Another advantage of the RFID technology is that the RFID transponders can be successfully detected by the system, even though they are buried, allowing for the study of the active layer thickness, (D_{AL}), which is of primary importance for numerical studies

to quantify the amount of sediment eroded/deposited within a channel reach. In literature there have been reported various values for the thickness of the active layer, introducing important error and uncertainty on the bedload formulas. For gravel bed streams, the thickness of the active layer is assumed to be equal to D_{94} (Papanicolaou et al. 2004), while for sand bed rivers, the active layer thickness is assumed to be 2 times the D_{50} (Einstein and Chien 1953). For the case of cohesive bed rivers the active layer thickness has a vertical variability of seven layers (Ziegler et al. 2000). These assumptions are not always valid, since there are cases where the thickness of the active layer in sand bed rivers can be more than three gain diameters (Sumer et al. 1996). In Table 2-2 the most commonly used types of particle tracers are presented along with their limitations.

2.4.1. RFID particle tracers

In the case of active RFID transponders (Figure 2-11), the power source (i.e., battery) is embodied into the transponder, affecting their size. For this reason, researchers are to use active transponders mainly for coarse gravel or cobbles-bed rivers studies, where the median particle distribution ranges from 16 to 256 mm (e.g. Habersack 2001; Merced Irrigation District and Natural Resources Scientists Inc. 2003; McNamara and Borden 2004). Due to the large transponder size and limited battery lifespan, as well as the high transponder's cost (~ $300/transponder), potential battery failure, and limited penetration depth into saturated sediments (Personal communication with Telonics and personal experience), active RFIDs are not really suited for scour measurements. Instead, the passive RFID particle tracing technique (Figure 2-12) has been recently used in scour studies since it incorporates important technical features such as low transponder cost,

ability to penetrate into saturated sediment, and low susceptibility to metal surfaces that increase the effectiveness of the RFID technology in riverine environments. The particle recovery rates reported in literature using passive RFID vary from 87% to 96% (Lamarre et al. 2005), yet another important parameter making the passive RFID technology suitable for sediment transport studies. The development of this technology, allowed researchers to monitor single particle's displacement movements, enabling the transition from the Eulerian to Lagrangian particle description feasible.

Figure 2-9 Painted particle tracers employed in a gravel bed river study (after Hendrick et al. 2010).

Figure 2-10 Magnetic particle tracers (after Sear 2003).

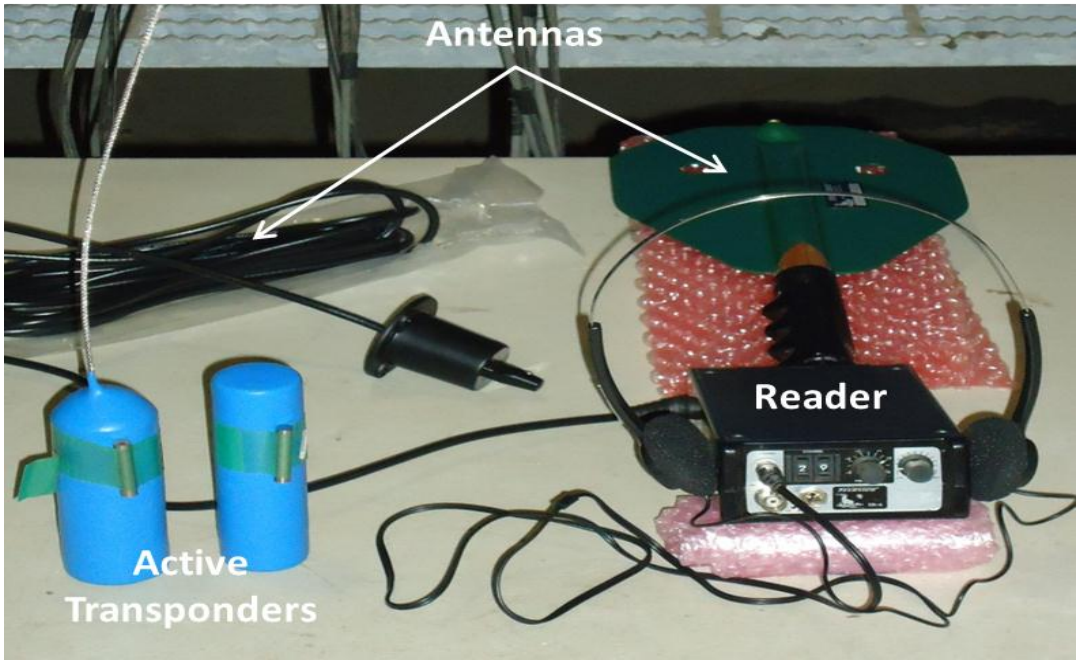

Figure 2-11 The components of an Active RFID system (Reader, active transponders and antennas).

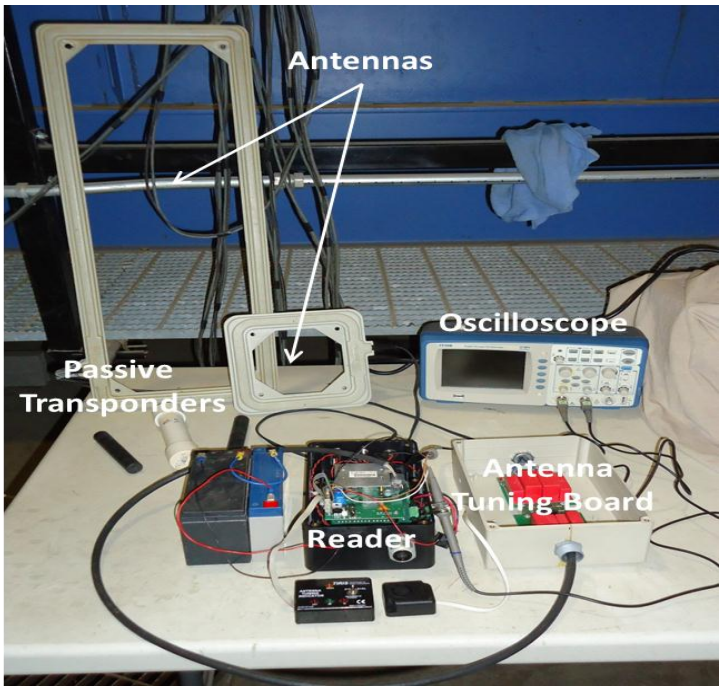

Figure 2-12 The components of a passive RFID system (Reader, passive transponders and antennas).

2.5. Limitations related to the low frequency passive RFID technology reported in literature

The limitations presented for the passive RFID systems herein are categorized into two groups, namely (a) RFID system operational limitations and (b) limitations of the RFID technology related to RF signal properties.

2.5.1. RFID system operational limitations

Several studies have reported the short detection distance between the excitation antenna and a transponder, which varies from few centimeters to less than a meter as a major deficit of the passive RFID system (Nichols 2004; Hassan and Chatterjee 2006; Lauth and Papanicolaou 2008; Papanicolaou et al. 2010). Since this is a passive system, the transponder is activated by the energy transferred from the reader through the excitation antenna's electromagnetic field. The RF signal strength from the excitation antenna decays with the square of the distance traveled (Equation 2-1) and limiting the distance that the system can successfully activate the transponder.

$$P_1 = P_o\left(1/d^2\right) \qquad \text{Equation 2-1}$$

where P_1 is the power density at a distance d from the source; and

P_o is the power density of the source;

d is the distance between the source and the measurement point.

Another limitation of most commercially available systems is the absence of an anti-collision feature (Papanicolaou et al. 2010), which would allow the system to read multiple transponders simultaneously. Most RFID systems do not support multiple readings, if the transponders are found at a close proximity to one another. In this case, the signals coming from the multiple transponders "collide", thus impairing the communication between the excitation antenna and all the transponders. An anti-collision feature enables the system to prioritize the communication between the

excitation antenna and a transponder when multiple transponders are detected simultaneously.

Finally, it has been recently reported in literature that the transponder's orientation with respect to the excitation antenna plane can significantly affect the maximum antenna-transponder detection distance and thus the overall performance of the RFID system (Nichols 2004; Allan et al. 2006; Lauth and Papanicolaou 2008; Dziadak et al. 2009; Papanicolaou et al. 2010).

2.5.2. Limitations of the RFID technology related to RF signal properties

In this subsection the emphasis is on limitations of the passive RFID system due to the RF signal strength attenuation and propagation through different mediums. Reportedly, one factor that can affect the performance of the RFID technology is the presence of nearby metal structures (Curtin et al. 2007; Cormos et al. 2007; Huang and Chang 2007; Papanicolaou et al. 2010). Metal structures interfere with the RF signal by absorbing part of the radiated energy causing decay in the RF signal strength, thereby limiting antenna-transponder detection distances.

Furthermore, experiments performed by Saarenketo (1998), Metje et al. (2007) and Dziadak et al. (2009) highlighted the effect of soil water content (or soil moisture) on RF signal strength attenuation. It was found that the presence of water in the soil column increased decay rate of the RF signal strength limiting the RF signal propagation through the medium.

In Dziadak et al. (2009), the same soil was tested under three different water contents (i.e., degrees of saturation). Their results showed that higher water contents in a

soil produced faster RF signal strength decay, matching the Saarenketo et al. (1998) findings, due to its efficiency to absorb and reflect the electromagnetic waves.

Metje et al. (2007) also showed that the variability in soil water content and temperature significantly affected the propagation of the RF signal. Water absorbs part of the RF signal and, as a permanent dipole, uses this energy to polarize its molecules and reach a more stable energy level.

This behavior of water is closely related with the value of its dielectric constant, which is a quantity that measures the ability of a substance to store electrical energy in an electric field. The dielectric constant of a substance is a function of its temperature. Weast (1986) and Hasted (1993) found that as the temperature of a substance increased, the value of its dielectric constant decreased, causing the rate of the RF signal strength attenuation to increase. Wraith and Or (1999) showed that there are interactions between the soil surface area and water content, where finer soils and/or low water content favor an increase in the dielectric constant with increasing temperature, while coarse soils and/or high water content favor a decrease in the dielectric constant, under the same temperature conditions. These results were attributed to competing effects of temperature on the dielectric constant of bulk and hindered soil water. Ulaby et al. (1986) developed an expression for computing the bulk dielectric constant, ε_b, of saturated soils, based on the dielectric constants of the dry sediment and water and their corresponding volume fractions.

$$\varepsilon_\varepsilon = \varepsilon_s v_s + \varepsilon_w v_w \qquad \text{Equation 2-2}$$

where ε_s is the dielectric constant of dry sediment;

ε_w is the dielectric constant of water;

ν_s is the volume fraction of sediment; and

ν_w is the volume fraction of water.

Finally, Al-Shamma'a et al. (2004) and Shaw et al. (2006) studied the effects of water salinity on the RF signal strength attenuation. These experiments revealed that as water salinity increased, the rate at which the RF signal attenuates increased. The following pattern developed where the RF signal strength attenuated faster at low distances, while at longer distances the rate of decay became more gradual.

CHAPTER 3

HYPOTHESIS AND OBJECTIVES

3.1. Hypothesis

Despite the detailed and laborious experiments that studied scour around structures, there are still several factors and influential processes that are not fully understood. This is due to the lack of field measurements during the scour critical events. Moreover, most scour predicting formulae provide information once the scour depth reaches equilibrium, meaning that the dynamic nature of the scour process is not captured, introducing important error and uncertainty. Thus, there is high uncertainty in the prediction of the maximum scour depth. This problem is further magnified by the fact that these formulae were developed based on data obtained via laboratory experiments and not from real field data, introducing additional error on the prediction of the maximum scour depth. So despite the recognized need for a continuously, or at least a more frequent, scour monitoring system at a bridge site, the existing scour monitoring methods cannot provide continuous data regarding the evolution of a scour hole. The hypothesis considered herein is that an automated system, based on the low frequency passive RFID technology, could provide unique continuous measurements, even during high flow events that are critical to scour development, which could enhance the predictive ability of scour evolution. To our knowledge, few studies have considered passive RFID systems for such a type of application.

3.2. Scope and objectives

The main question to be addressed in this thesis is: "Can an advanced automated technique, such as RFID, be used to continuously quantify scour, with or without the presence of hydraulic structures?". In order to answer this question, the overarching objective of this study is to develop a framework for a robust and autonomous system that continuously monitors scour at a bridge site, by relating a transponder's return RF signal strength with the distance between the excitation antenna and the transponder through calibration curves for various mediums. The secondary objectives of this study are (a) to cast more light on the principles of the low frequency passive RFID technology by performing specially designed experiments and (b) to address the RFID technology limitations by properly modifying the RFID system components.

In order for these objectives to be achieved, low frequency passive RFID transponders were utilized under two different experimental series. In the first experimental series (laboratory experiments), the behavior and effects of key RFID parameters on the overall system performance were investigated, as well as the strength of the transponder's return RF signal. This experimental setup included the use of single RFID transponders, which were buried into different types of media (e.g., air, water, dry sand, dry gravel and 100% saturated sand) at various depths and orientations with respect to the excitation antenna plane (perpendicular vs. parallel), as well as with different encasing materials ("naked", glass, concrete-tungsten and PVC). The results of this experimental series were designed to provide a better understanding of this relatively new technology for developing benchmark conditions for different media, transponders orientations and housing materials, as well as revealing the limitations of the system. In

addition, these results were considered to design an appropriate method to continuously monitoring scour at a bridge site.

The second experimental series (the RF signal vs. the detection distance experiments) was designed to relate the transponder's return RF signal strength with the distance between the excitation antenna and the transponders, which is key information for the development of a continuous monitoring clear-water local scour system. Herein, the Leopold chain method was considered (Leopold et al. 1966). This method relies on the principle that the exposed portion of the chain lays atop of the bed and is nearly parallel. We attached transponders at predetermined locations (depths) along a plastic chain with known length. The chain was subsequently driven into the bed substrate at locations where the maximum scour was expected. The chain retained the transponders perpendicular to the excitation antenna plane, so that they were continuously detected by the RFID system. Once scour occurs, the transponders no longer remained perpendicular to the bed, but instead were oriented parallel to the excitation antenna plane and thus did not provide the same RF signal strength, an indication that scour has reached a known depth, at which the transponder was initially buried (Figure 3-1).

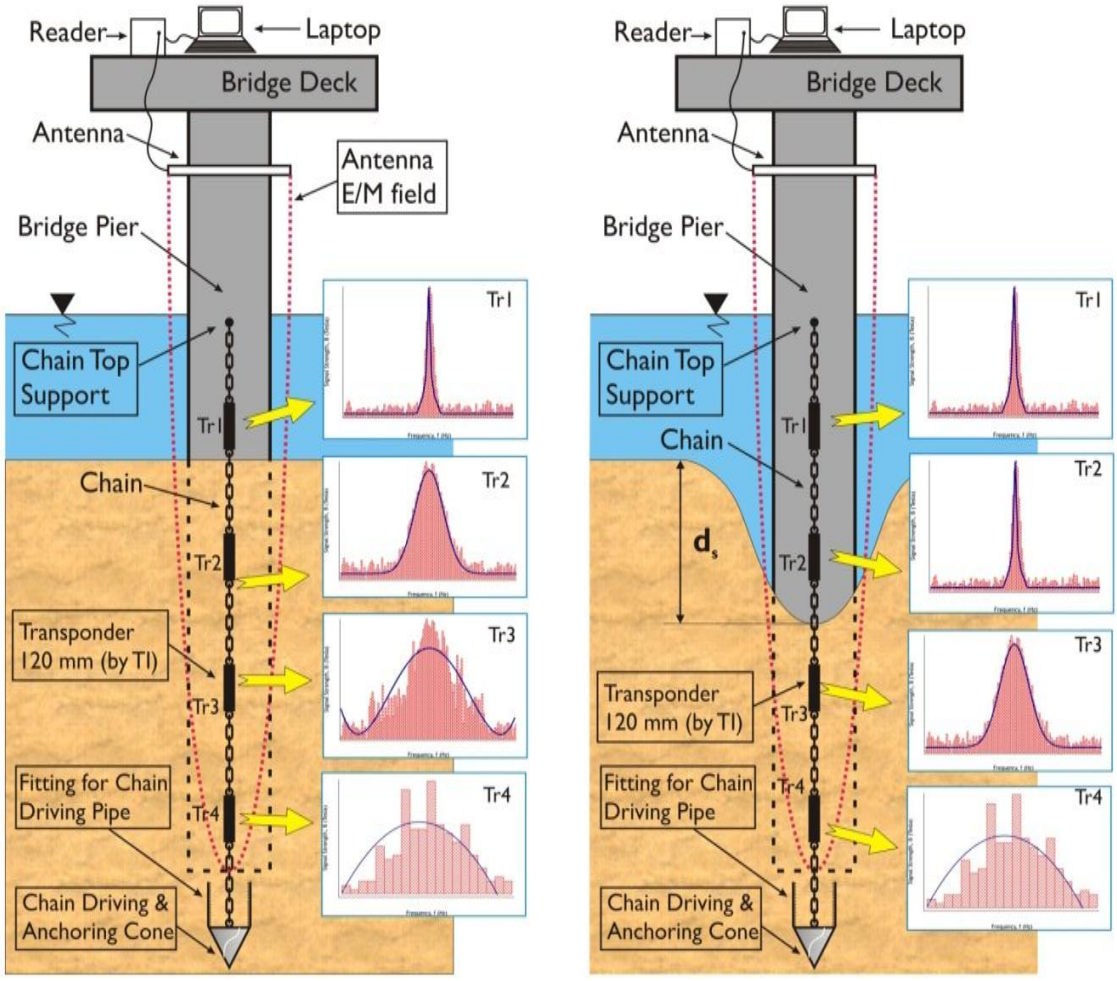

Figure 3-1 Schematic representation of the implementation of the Leopold chain method for continuously monitoring scour around bridge piers (courtesy of Papanicolaou et al. 2010).

CHAPTER 4

INSTRUMENTATION AND EXPERIMENTAL SETUP

In chapter 4 a detailed description of the instrumentation and the experimental setup are presented. This chapter is organized according to the follow structure. First, the RFID technology is presented and the basic features are discussed. Then, the instrumentation employed in this study along with its capabilities and limitations are described in great detail in order for the reader to obtain a better insight into the RFID equipment.

4.1. Instrumentation and experimental setup

For the purposes of this study, two RFID systems, namely (a) Texas Instruments (TI) and (b) HiTAG were used (Figure 4-1). Both RFID systems operate in a low frequency band (134.2 kHz and 125 kHz, respectively). The reasons for selecting low frequency RFID systems were that low RF waves (LF) can penetrate deeper into saturated sediment and are less affected by surrounding metal surfaces than high RF (HF) waves. These properties of the LF waves were extremely important to achieve the goals of this study, namely that the RFID technology will be used for continuously measuring scour around a bridge pier. In addition, the TI and HiTAG RFID systems are passive, which again means that the transponders use the electromagnetic field created by the excitation antenna to charge. Additionally, passive RFID transponders are less expensive (~$20 / transponder) and have a relatively unlimited lifespan, unlike the active transponders, which are more expensive (~$300 / transponder), battery-dependent, and

have approximately 2 years lifespan, as well as are much heavier, since the battery is embodied into them.

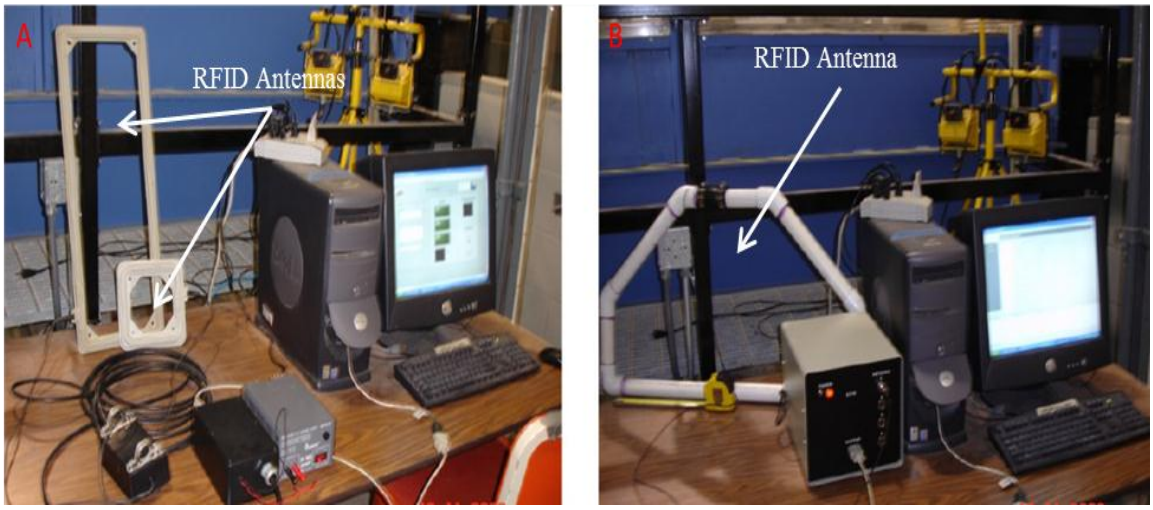

Figure 4-1 RFID systems used in this study; (A) A low frequency (134 kHz), passive Radio Frequency Identification (RFID) system from TI (excitation antennas specifications: (1) large rectangular loop shape antenna RI-ANT-G01E – 0.70x0.27 m and (2) small square loop shape antenna RI-ANT-G02E – 0.20x0.20 m) and (B) a low frequency (125 kHz), passive Radio Frequency Identification (RFID) system from HiTAG (antenna specifications: a six-edged polygon loop shape antenna (0.86x0.52) (courtesy of Papanicolaou et al. 2010).

4.1.1. RFID system by TI

The TI low frequency (134.2 kHz), passive RFID system is similar to the RFID system used by Nichols (2004) and consists of three main parts. The first part is the

reader, which is a set of two boards/circuitry, namely the control (RI-CTL-MB2A-03) and the radio frequency (RI-RFM-008B-00) modules. The frequency module converts the RF waves transmitted by the transponder into electrical signals that can be then processed by the control module and sent to the host computer. The control module is the interface between the frequency module and the PC, which is used to control the system (Papanicolaou et al 2010). Essentially, the control module converts the RF signals received from the transponder into the serial number (ID) of the transponder and transmits this information over a serial line to the host PC. The type of reader used in this study is considered as the most powerful and durable offered by TI. Thus, the RF signal emitted by the reader is very strong, which considerably increases the maximum detection distance between the excitation antenna and the transponder (personal communication with TI engineers).

The excitation antenna is the second component and also consists of circuits (e.g., antenna tuning module) that ensure the two-way communication between the reader and the transponder. Two excitation antennas were used in this study, (1) a large rectangular loop shape antenna (RI-ANT-G01E) with dimensions of 0.70x0.70 m and (2) a small square loop shape antenna (RI-ANT-G02E) with dimensions of 0.20x0.20 m. The two excitation antennas can be interchangeably connected to the reader by switching two pin type connectors.

Another advantage that the TI RFID system offers is that a custom made excitation antenna can be connected to the reader. This option allows the user to build an optimal antenna by manipulating the size, material and shape of the antenna to increase the maximum detection distance. A 10 m long waterproof twinax cable was used to

connect the selected excitation antenna with the reader. The length of the twinax cable can be up to 120 m. For lengths more than 120 m, the resistance will increase resulting in reduced antenna voltage, directly affecting the maximum antenna-transponder detection distance (Oregon RFID 2012). The antenna tuning module (Large Tuner Board) tunes the excitation antenna with the reader to ensure that the outgoing RF signal emitted by the frequency module is at the correct frequency for proper communication between the reader and the transponder.

The passive transponders are the third component and embody circuits that allow the information sent by the reader to be stored and sent back as a response RF signal to the reader; a miniature antenna that supports the two-way communication between the reader and the transponder and capacitors to store the charge up energy transferred through the excitation antenna's electromagnetic field (Nichols 2004).

Two transponder types were selected for this study. The 23 mm long, cylindrical, low frequency, passive transponders (RI-TRP-WEHP-30) and the 120 mm long, cylindrical, low frequency, passive transponders (RI-TRP-W9TD) were used. The low acquisition cost of each transponder permitted the purchase of a large number of transponders of the two types. Each transponder came with 80 bit Read/Write memory, which enabled the assignment of a unique identification number (transponder ID) on each transponder. The ability to assign each transponder with a unique serial number was the basis for developing, in IIHR - Hydroscience & Engineering laboratory, a code in C++ language, which records the number and the detection time of each transponder and exports the output in a text file format (Figure 4-2). The entire TI RFID system is powered by two batteries of 12 and 6 Volt connected in series and resulting in 18 Volt

power supply. The maximum RFID system allowed voltage is 20 Volts (TI Series 2000 Reader System Reference Guide, 2008).

The TI RFID system operates as half-duplex. In other words, one read cycle (lasts approximately 0.1 seconds) has two phases:

- Phase 1 (or "emitting" phase) where for the first 0.05 seconds the reader sends RF waves at the frequency of 134.2 kHz, to charge the transponder's circuitry (transponder's internal capacitors) and
- Phase 2 (or "listening" phase) where for the last 0.05 seconds the reader is receiving the RF signal from the transponder. Therefore, the half-duplex system ensures the regular and undisturbed communication between the reader and the transponder, since when the one is in the "emitting" mode, the other is in the "listening" mode.

Finally, a 25 MHz digital storage oscilloscope by B&K PRECISION (2530B) was connected to the RFID reader radio frequency board, to the J1 connector's pins #1, 2, 6 and 10, which corresponded to logic ground, transmitter control input for activation of the transmitter (active low, internal pull-up resistor), logic level compatible receiver clock output and analog receiver signal strength test pin functions, respectively. The digital oscilloscope was used to record and export the shape and form of the RF signal.

4.1.2. RFID system by HiTAG

The HiTAG low frequency (125 kHz), passive RFID system also consists of three main parts. The reader, which is developed by Phillips (HTRM-01 Long Range Reader), that converts the RF waves transmitted by the transponder into the serial number of the transponder and processes this information at a terminal device (e.g., host computer).

The HiTAG reader incorporates the anti-collision feature, which enables the reader to communicate with a transponder when multiple transponders are located within the electromagnetic field of the excitation antenna. The anti-collision feature is based on the RTF ("Reader Talks First") protocol, which ensures that the reader can prioritize the communication between the excitation antenna and one transponder at the time, when multiple transponders are detected (Figure 4-3). Once the first transponder is interrogated, the anti-collision function sets the already detected transponder in mute status and proceeds with the interrogation of the transponder detected next. The process is repeated until all the transponders within the excitation antenna electromagnetic field are interrogated. The antenna tuning module is incorporated to the reader to tune the excitation antenna with the reader in order to ensure that the outgoing RF signal is at the correct frequency for proper communication between the reader and the transponder. The excitation antenna is the second component. This system came with four identical, six-edged, polygon loop shape antennas (HTLRX) with dimensions of 0.86x0.52 m. The excitation antennas were encased in PVC pipes to ensure waterproof conditions in order to successfully operate under water. This RFID system can simultaneously support up to four antennas connected to the same reader via the multiplexer (HTM4-I) feature. A custom code was developed in C++ language to allow the fully automated use of the anti-collision feature and the ability to switch between the excitation antennas, when more than one excitation antenna is connected to the reader. The custom C++ code records the serial number (ID) and the detection time of each transponder along with the excitation antenna number used for detection, and exports the output in a text file format; and (c) the passive transponders. The 22 mm long, cylindrical transponders (HTS2048) used in

this study, support the Read/Write function and come with 2048 bits of memory and the anti-collision feature. A unique identification number is assigned to each transponder.

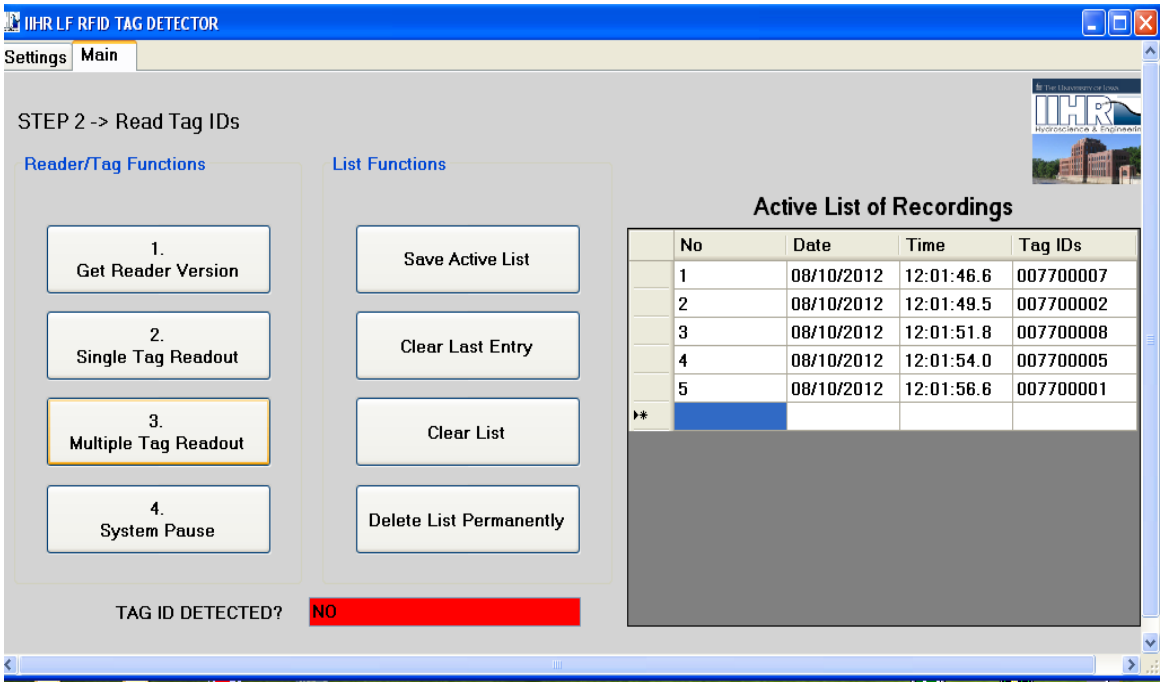

Figure 4-2 Transponder detection software for the TI RFID system, developed in IIHR.

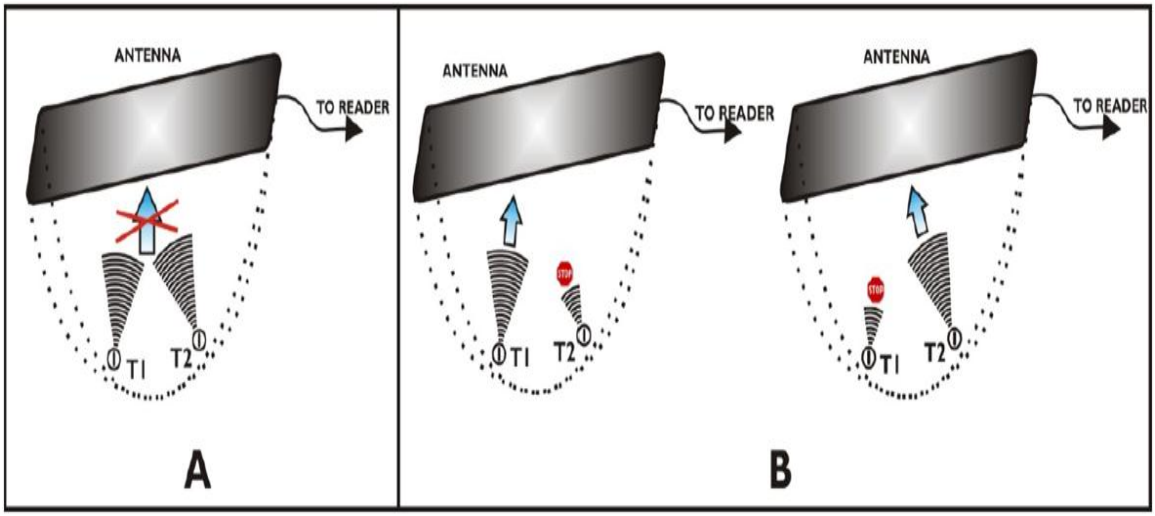

Figure 4-3 Communication between the excitation antenna and multiple transponders; (A) without the anti-collision feature and (B) with the anti-collision feature (courtesy of Papanicolaou et al. 2010).

CHAPTER 5

METHODOLOGY

In this chapter, the experimental conditions and setups are discussed and analyzed along with the RF signal, sensitivity and error analyses. Two experimental series were considered that address the objectives of this study (i.e., the parametric experiments and the RF signal strength vs. detection distance experiments), which were designed based on the outcomes of the parametric experiments. The nature of the experiments performed herein was to gain a deeper insight into the behavior of the RFID system under different controlled conditions. The parametric experiments were conducted at IIHR - Hydroscience & Engineering of the University of Iowa, while the RF signal strength vs. detection distance experiments were conducted in a quarry located at Coralville, IA.

5.1. Parametric experiments

A total of 8 experiments were conducted in the laboratory to study the key RFID parameters and the overall performance of the TI RFID system. Table 5-1 presents a summary of the experiments performed herein. All experimental runs were repeated at least 5 times for repeatability.

For each experiment, the baseline condition of the maximum antenna-transponder detection distance is presented in terms of D_{max_air}. More specifically, the maximum antenna-transponder detection distance that was used as a baseline condition to carry out the comparisons for each experiment were based on the experimental setup. In other

words, $D_{max_air_23}$ and $D_{max_air_120}$ are the maximum antenna-transponder detection distances, 0.6 and 2 m respectively, reported by the manufacturer for the TI 23 and 120

Table 5-1 Summary of the experiments performed.

Experimental series #	Experimental description	Number of runs
P1	Transponder orientation (ORIENT) effects on the transponder return RF signal	15
P2	Transponder housing (HOUS) effects on the transponder return RF signal	15
P3	Coupling effects on the transponder return RF signal	3
P4	Medium (MEDM) effects on the RF signal strength decay	4
P5	Effects of sand and gravel porosity on the RF signal propagation and decay	10
P6	RF signal strength decay during the erosion (EROS) process	2
P7	RF signal strength decay during the deposition (DEP) process	2
P8	Quantify scour (SCR) using the Leopold chain method around a bridge pier model	2

mm transponders. The $D_{max_air_120_barrel}$ is the reduced maximum antenna-transponder detection distance due to the limited barrel height (~0.55 m). During the scour experiments, where the Leopold chain method was employed, the maximum antenna-transponder detection distances for the favorable and unfavorable transponder orientations, $D_{max_Leo_sc_22}$ = 0.43 m and $D_{max_Leo_sc_unfav_22}$ = 0.101 m respectively, were choosen based on the maximum detection distances occurred for the specific experimental setup and the two transponder orientations (favorable vs. unfavorable).

5.1.1. Transponder orientation (ORIENT) effects on the transponder return RF signal

A total of 15 experimental runs were conducted to isolate the effects of the transponder's inner antenna and long axis orientation towards the excitation antenna plane. In all runs the transponder was considered "naked", meaning that it was encased in only the factory packaging, a reinforced poly-ether-imide encasing. This was considered as the baseline condition. For the baseline condition, the maximum antenna-transponder detection distance was considered to be 0.6 m ($D_{max_air_23}$), as it was reported by the manufacturer (TI Low Frequency 23mm Glass Transponder Manual 2001). The following equipment was used during these experiments: the TI low frequency, passive RFID system, the rectangular loop shape antenna, a TI 23 mm long, cylindrical transponder and a 25 MHz digital storage oscilloscope.

During these experiments 4 different transponders were used, while the transponders' long axis was placed at different orientations with respect to the excitation antenna plane and the largest detection distance was recorded (Figure 5-1). The antenna–

transponder distance was increased until the transponder was no longer detected by the excitation antenna. For each tested detection distance, the excitation antenna was swept over the transponder 16 times providing a total number of 64 chances to detect the transponder. The next step was to identify the effects of the transponder inner antenna on the maximum detection distance, along with the transponder's long axis orientation with respect to the excitation antenna plane.

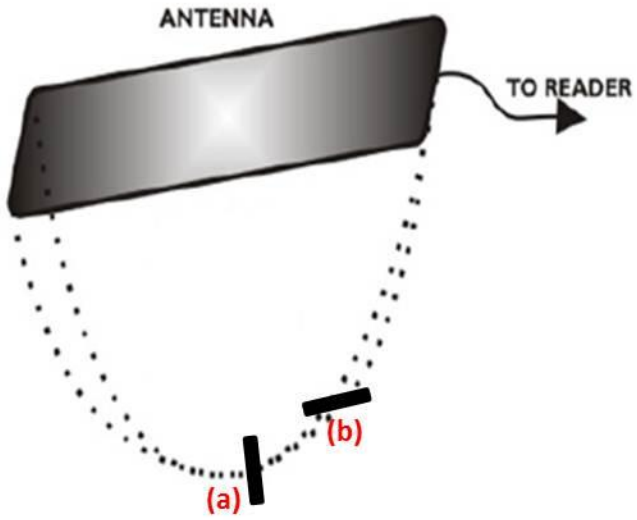

Figure 5-1 Transponder orientations with respect to the excitation antenna plane; (a) perpendicular and (b) parallel.

5.1.2. Transponder housing (HOUS) effects on the transponder return RF signal

Three different transponder housing materials (i.e., glass, concrete-tungsten and PVC) were tested and compared against a "naked" transponder in order to investigate the effects, if any, of the encasing on the strength of the transponder's return RF signal (Figure 5-2). A total number of 120 experimental runs were performed. The TI low frequency, passive RFID system was used along with the square loop shape antenna and the TI 23 mm long, cylindrical transponders. Again, the "naked" transponder and the maximum antenna-transponder detection distance reported by the manufacturer ($D_{max_air_23}$) formed the baseline condition.

Each transponder was assigned with a unique identification number. The main criterion for selecting the 23 mm transponder type was the transponder small size, which made them feasible to be installed into a 0.0254 m diameter spherical particle. Two types of spherical particles were used to house the transponders, namely a glass particle and a particle made of concrete coated with tungsten. The density of the encased particles matched the density of quartz (measured here equal to 2658 kg/m^3).

The glass particles were annealed in order to be drilled without cracking. During the annealing process, the glass particles were heated for 30 to 40 minutes at high temperatures (~ 600^{o}C), while the whole process lasted for approximately 12 hours. After being annealed, the glass particles were carefully drilled to house the transponder. When the transponder was placed inside the glass particle, it was sealed with silicon to keep the transponder in place.

The concrete-tungsten particles were made by first casting concrete particles and subsequently coating them with a thin film of tungsten, in order to match the sand density

for the known volume of the particle. For each type of material tested, the maximum detection distance was measured for two transponder orientations (a) when the transponder's long axis was oriented perpendicular to the excitation antenna plane and (b) when the transponder's long axis was oriented parallel to the excitation antenna plane. The obtained results were compared to the baseline condition.

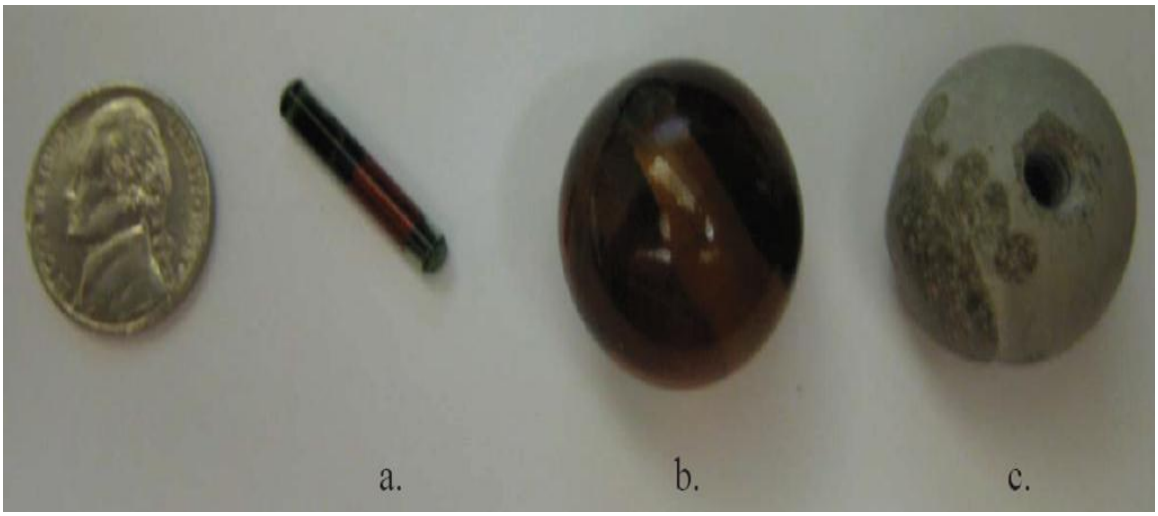

Figure 5-2 Size comparisons for the transponder and particles used. From left to right: (a) "naked" transponder, (b) glass particle and (c) concrete-tungsten particle (courtesy of Papanicolaou et al. 2010).

5.1.3. Coupling effects on the transponder return RF signal

Another very important parameter related to RF signal strength, that can affect the performance of the TI LF passive RFID system with the 120 mm long transponders, is

the minimum distance required between the excitation antenna and the transponder in order to ensure that the two electromagnetic fields created by the excitation antenna and the transponder's inner antenna do not interfere with each other in a way that further decay in the strength of the RF signal is caused (Personal communication with TI engineers). This effect has not been reported in the RFID literature. However, the interference of the two electromagnetic fields warranties further attention. Herein, 3 experimental runs were performed and each run was repeated 5 times. Initially, the transponder was placed inside the excitation antenna frame (0 cm distance between the excitation antenna and the transponder) (Figure 5-3) and the transponder return RF signal strength was recorded and exported via a digital storage oscilloscope. Then, the obtained RF signal time series were analyzed in MATLAB and the decay of the transponder's return RF signal strength was computed. The same procedure was also followed for the experimental runs for 2 and 4 cm distance between the excitation antenna and the transponder.

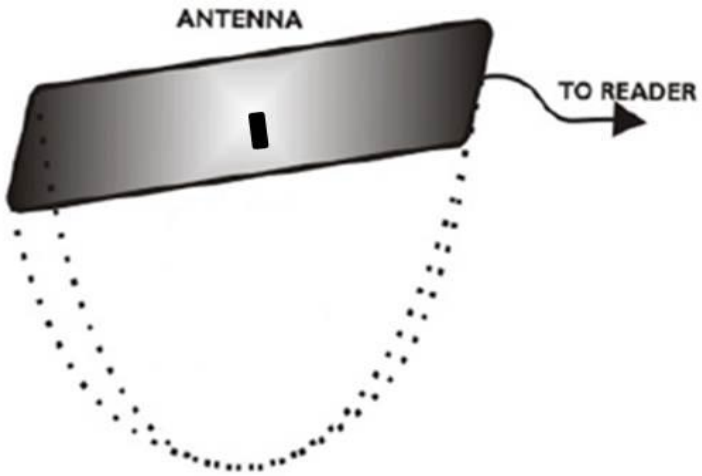

Figure 5-3 Transponder located inside the excitation antenna frame.

5.1.4. Medium (MEDM) effects on the RF signal strength decay

A number of 4 experimental runs were designed and performed to address the question of the effects of the medium type on the transponder return RF signal strength for the TI LF passive RFID system with the 120 mm transponders. Each experimental run was repeated 5 times. Four different types of material, namely air, water, dry sand and dry gravel were considered and tested, for two transponder's long axis orientations, perpendicular and parallel towards the excitation antenna plane, respectively.

A plastic barrel with diameter and depth of 0.55 and 0.71 m respectively, resulting in a total volume of 0.169 m^3 was employed to accommodate the experiments. The use of a plastic barrel to carry out the experiments was mainly sought because plastic does not affect the RF signal characteristics and the process of adding and removing material was simplified. The distance between the excitation antenna and the transponder for successfully detecting the latter was measured ($D_{max_air_120_barrel}$ = 0.55 m) and recorded and the shape and the form of the transponder's return RF signal was analyzed at four measuring points corresponding to $D_{max_air_120_barrel}$, $3D_{max_air_120_barrel}/2$, $D_{max_air_120_barrel}/2$ and $D_{max_air_120_barrel}/4$ of the detection distance, for each experimental case. The transponder return RF signal time series were recorded via a digital oscilloscope and then analyzed in MATLAB to estimate the RF signal decay for each medium used. Figure 5-4 shows the experimental setup followed herein.

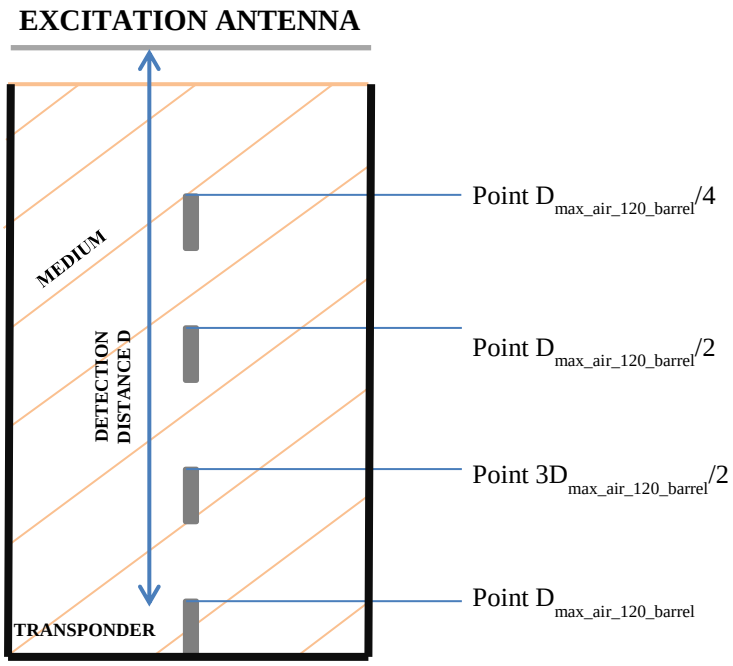

Figure 5-4 Experimental setup for testing the medium effects on the transponder return RF signal; D is the maximum detection distance achieved between the excitation antenna and the transponder.

5.1.5. Effects of sand and gravel porosity on the RF signal propagation and decay

In these experimental series, the sand and gravel medium types used in the previous experiments (section 5.1.4) were further analyzed herein to study the effects of the void ratio (e) on the transponder return RF signal strength decay. Ten sand and gravel samples were analyzed to estimate the average void ratio corresponded to each type of material. The average void ratio for sand and gravel was found to be equal to 32.4% and 40.1% respectively. The mean particle diameter (d_{50}) for the sand and gravel

material was found to be 0.0019 and 0.0132 m, respectively. Figures 5-5 and 5-6 show the sand- and gravel- size grain distribution as they occurred after the sieve analyses.

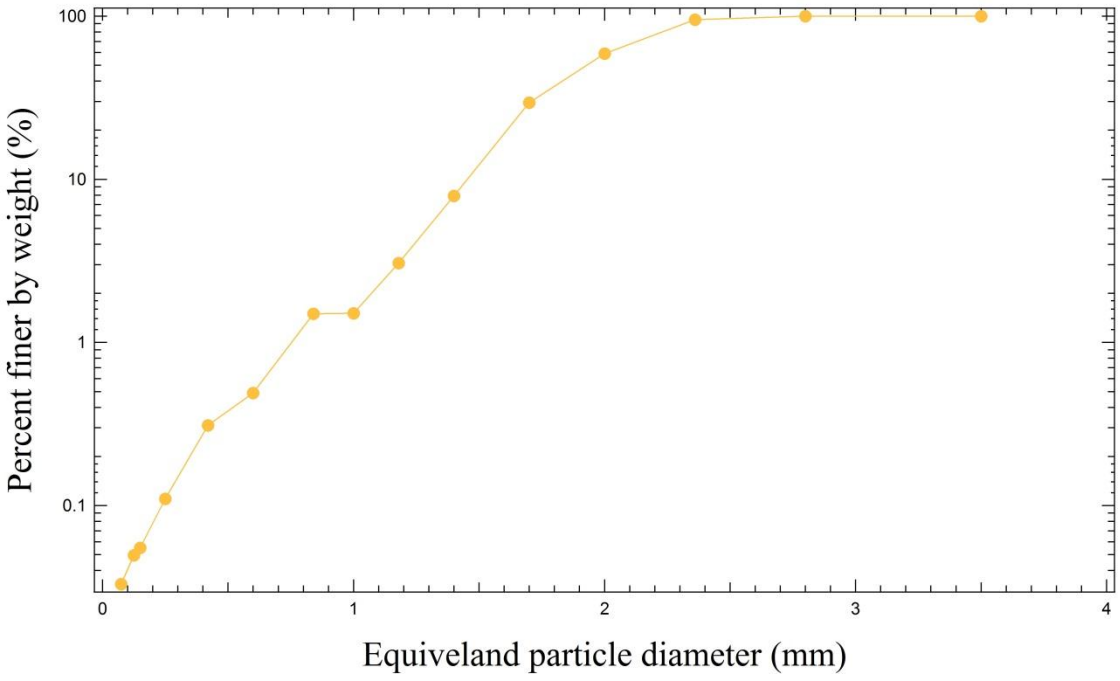

Figure 5-5 Log-normal sand particle size distribution.

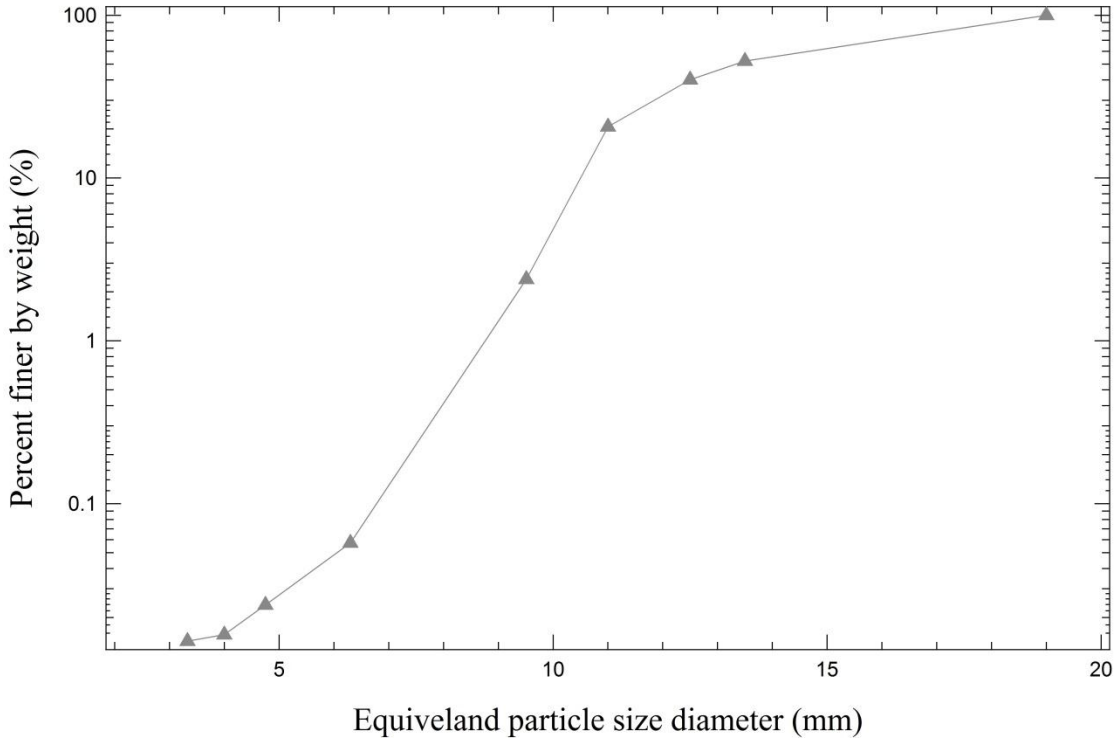

Figure 5-6 Log-normal gravel particle size distribution.

5.2. Replication of real case scenarios in the laboratory: evaluating the performance of the RFID system during the erosion and deposition processes

In these experimental series, the TI LF passive RFID system with the 120 mm long transponders was employed. A 0.95 m long, 0.31 m wide and 1 m deep trough located at the IIHR - Hydroscience & Engineering Model Annex facilities of the University of Iowa, was selected for conducting these series of experiments. The selection of a trough was made after considering its advantages, such that its dimensions were much greater compared to the plastic barrel ones, meaning that the distance between

the excitation antenna and the transponder was 0.33 m longer and thus, more accurate and detailed measurements could be performed regarding the maximum detection distance (Trough's Volume (V_{tr}) = 0.306 m^3, Plastic Barrel's Volume ($V_{p.b}$) = 0.169 m^3). For these experiments, the maximum antenna-transponder detection distance that was used as the baseline condition was $D_{max_air_120}$ = 2 m, according to the manufacturer (TI Low Frequency 120mm Cylindrical Transponder Manual 2001). Also, the front part of the trough was constructed of wooden beams placed on top of each other, therefore, it was easier to add and remove material during the experiments by increasing or decreasing the number of the wooden beams in the trough sidewall. An insulation sheet was placed inside the trough to prevent water leaking. Sand material (d_{50} = 0.0019 m) was added to cover most of the trough's volume (the sediment column height inside the trough was 0.78 m) and then the trough was filled with water until the sand was completely (100%) saturated and the water depth above the sand column reached the height of 0.15 m. The excitation antenna was placed 0.045 m above the water surface.

5.2.1. RF signal strength decay during the erosion (EROS) process

The scope of this experimental setup was to replicate, as much as possible, the real scour process. The maximum detection distance between the excitation antenna and the transponder was measured (37% of $D_{max_air_120}$) and recorded and the shape and the form of the transponder's return RF signal was taken at six measurement points corresponded to 5.5, 17, 22, 27, 32 and 37% of $D_{max_air_120}$. Figures 5-7 and 5-8 show the experimental conditions and setup followed in this experimental series. A plastic chain was attached to the transponder in order to make easier its upward movement to the

predetermined points of measurement. The transponder was first buried into the sediment column at the maximum depth for which the transponder was successfully detected (37% of $D_{max_air_120}$) by the RFID system and then through the attached chain the transponder was raised into different predetermined depths (antenna-transponder distances) and the transponder return RF signal strength was recorded each time.

Figure 5-7 Erosion process experimental setup.

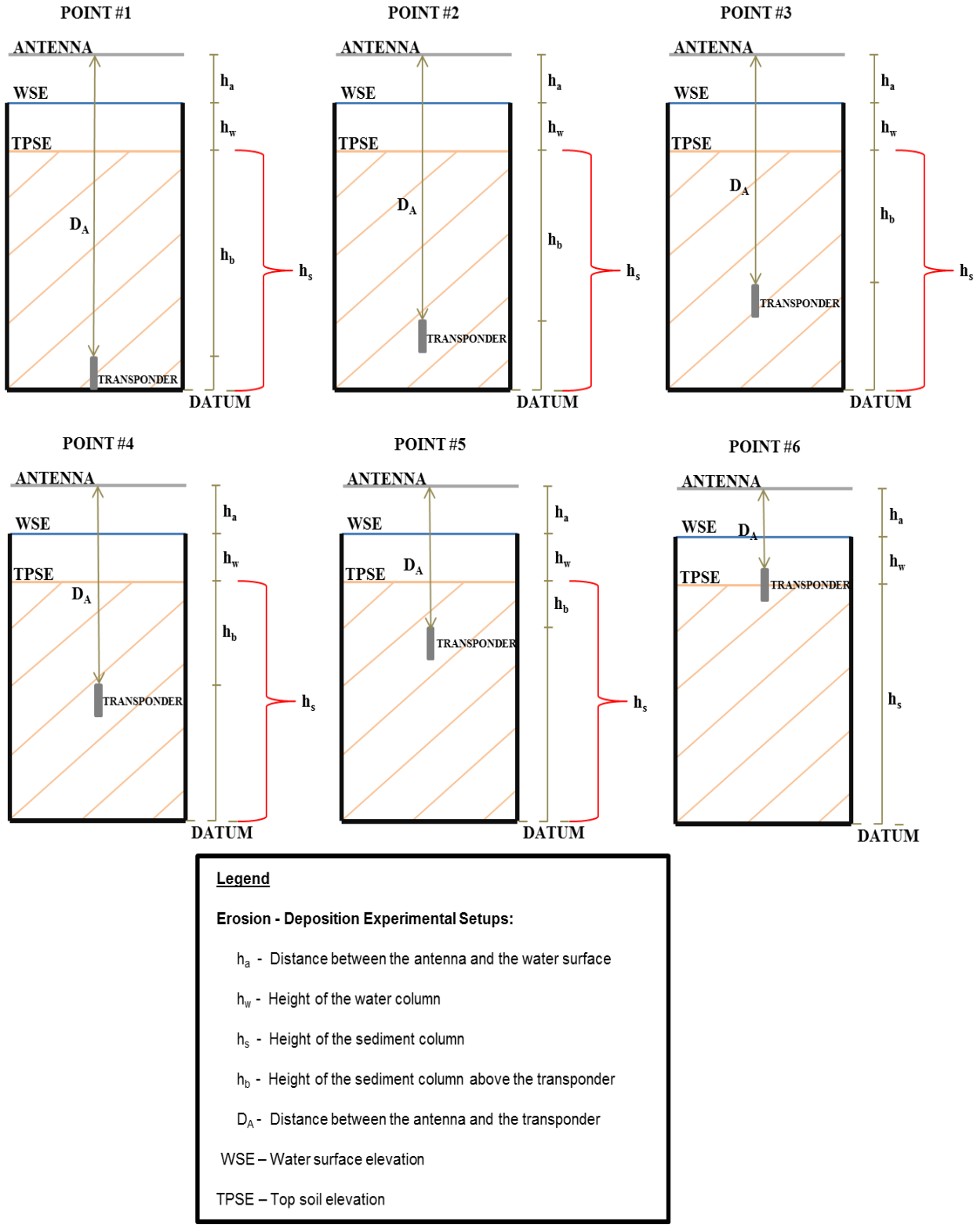

Figure 5-8 Erosion process experimental phases - schematic representation.

5.2.2. RF signal strength decay during the deposition (DEP) process

In this experimental series, the TI LF passive RFID equipment with the 120 mm long transponders was tested in quantifying the deposition height occurred above the transponder by relating the transponder return RF signal strength decay with the known deposition height. The transponder was placed at a fixed distance from the excitation antenna (37% of $D_{max_air_120}$), which also corresponded to the maximum antenna-transponder detection distance achieved for this experimental setup. For this experiment, the maximum detection distance between the excitation antenna and the transponder was equal to 0.745 m. Sand material (d_{50} = 0.0019 m) was gradually added above the transponder to replicate the deposition process. Six measurement points were also considered herein, where the height of the sediment column above the transponder, for each measurement taken, was 5.5, 17, 22, 27, 32 and 37% of $D_{max_air_120}$, in order all the experiments performed in this study to be consistent. The trough was filled with water until the sand was completely (100%) saturated and the water surface was kept constant at the same level with the erosion experiment. The excitation antenna was placed 0.045 m above the water surface. Figures 5-9 and 5-10 present the experimental conditions and setup followed in this experimental series.

Figure 5-9 Deposition process experimental setup.

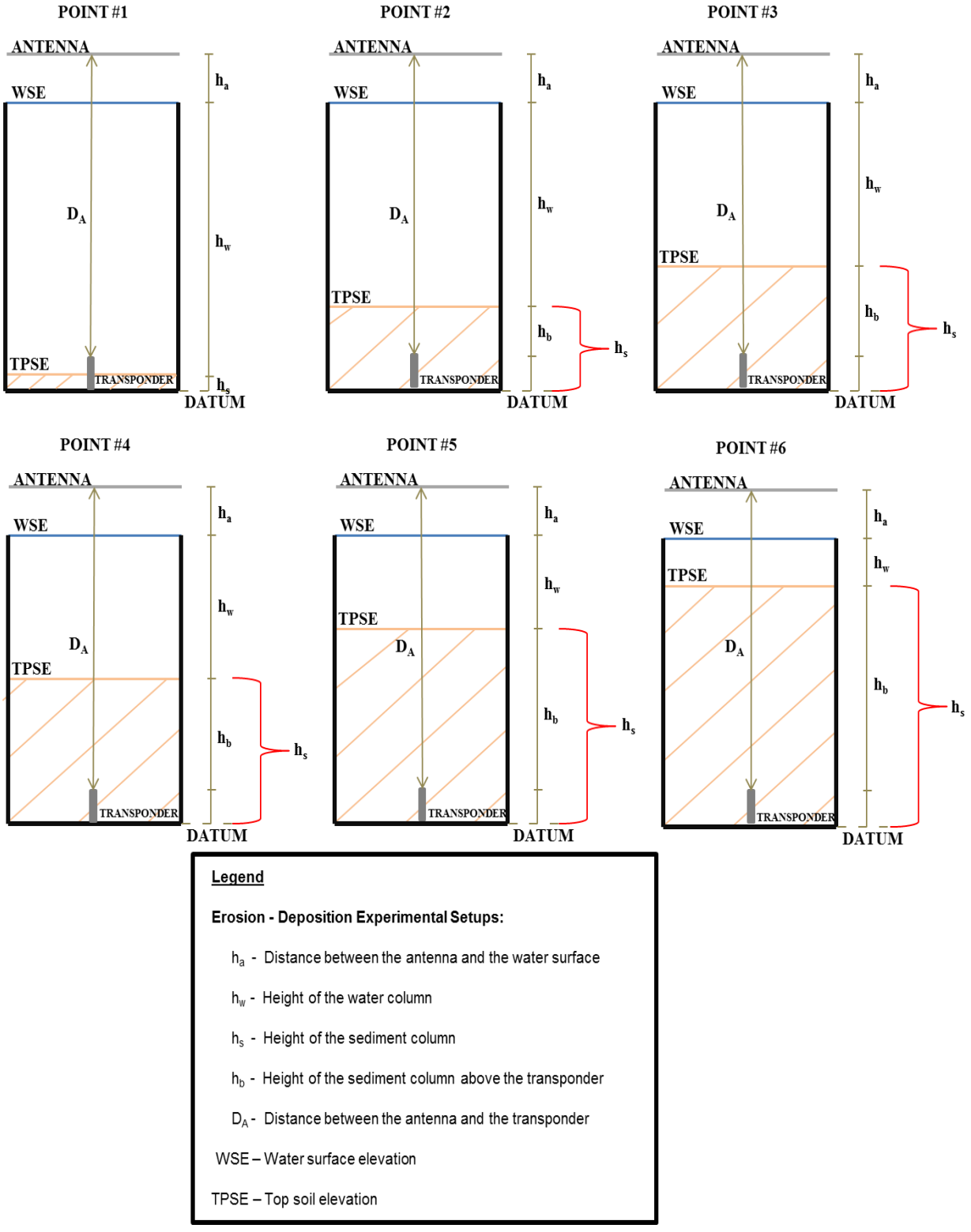

Figure 5-10 Deposition process experimental phases - schematic representation.

5.2.3. Quantify scour (SCR) using the Leopold chain method around a bridge pier model

This experimental series was designed to test the performance of the HiTAG low frequency (125 kHz), passive RFID system along with a HiTAG six-edged polygon shape antenna (HTLRX) and the 22 mm long, cylindrical, read/write (HTS2048) transponders on quantifying scour around a model bridge pier, following the Leopold chain method, as it was first introduced by Leopold et al. (1966). For this experiment, the HiTAG RFID system was preferred over the TI RFID system, since the HiTAG RFID system incorporates the anti-collision feature, which allows the detection and interrogation of multiple transponders located into the excitation antenna's electromagnetic field without the communication between the reader and the multiple transponders collapsed.

The experimental setup (Figure 5-11) included a 1 m long, 0.6 m wide and 0.8 m deep, acrylic tank to accommodate the Leopold chain method scour experiments. A 0.195 m long chain was built with 5 transponders attached to each other through 4 strings of 0.02 m long fishing line. The model bridge pier was replicated by a 0.8 m long, 0.127 m (5 inches) in diameter PVC pipe that was fixed into the bottom of the experimental tank and covered with sand (d_{50} = 0.0019 m) up to 0.53 m of its height. The chain was buried vertically into the sand column, in front of the upstream face of the model bridge pier, in the location where the maximum scour was expected to occur. The transponders were placed on the chain in such a way that their long axis orientation to be favorable (perpendicular) to the excitation antenna plane. Water was recirculated into the experimental tank at constant discharge of 0.00074 m^3/sec through a jet nozzle using a

1/3 HP pump, while the water depth was maintained at 0.04 m. The jet nozzle, 0.004 m in diameter, was pointed towards the bridge pier, where the buried chain located to create scour around the pier. Two acrylic plates of dimensions of 0.05x0.15 m were inserted vertically into the sand bed on each side of the pier, forming a funnel with an angle of 60^{o}, to prevent the surrounding sand material from infiltrating the developing scour hole. Once the scour occurred and the transponders were exposed, they would reorient parallel to the excitation antenna plane and thus, the transponder return RF signal strength would be reduced and the transponder would be no longer detected by the excitation antenna. This state would indicate that the bridge scour reached the known depth, at which the transponder was initially buried.

Figure 5-11 Leopold chain method experimental setup to quantify scour around a model bridge pier.

5.3. The RF signal strength vs. detection distance experiments

Once the key parameters affecting the RFID efficiency were identified under controlled conditions (parametric experiments), the TI RFID system was further tested in a field set-up. The goals of the RF signal strength vs. detection distance experiments were to (a) considerably increase the maximum antenna-transponder detection distance and (b) develop calibration curves for the transponder return RF signal strength in air and sediment (i.e., sand and gravel), so that the RFID method can be successfully employed in real-field applications. Table 5-2 presents the RF signal strength vs. detection distance experiments considered herein.

Table 5-2 Summary of the RF signal strength vs. detection distance experiments performed.

Experimental test #	Experimental description	Repeatability of the experiment
Q1	Development of a custom made excitation antenna for achieving the maximum antenna-transponder detection distance	2
Q2	Development of the transponder return RF signal strength decay calibration curve in air using the custom made excitation antenna	10

5.3.1. Development of a custom made excitation antenna for achieving the maximum antenna-transponder detection distance

The detection distance between the excitation antenna and the transponder is a function of more than one parameters, namely (a) the reader's transmitted power, (b) the size and shape of the RFID system's excitation antenna, (c) the size and shape of the transponder's inner antenna, (d) the presence of metal structures in close proximity to the RFID system, (e) the level of the electrical noise in the surrounding environment, (f) the transponder's long axis orientation with respect to the excitation antenna plane, (g) the material type in between the excitation antenna and the transponder and (h) the transponder's housing material. From the above listed parameters, the reader's transmitted power is limited by the legislation and the transponder's inner antenna dimensions are fixed based on the TI products specifications and characteristics. The consideration of an environment with low levels of electrical noise and absent of metal structures, e.g. parks, quarries, results in minimizing the effects of these factors. The transponder's long axis orientation towards the excitation antenna plane, the transponder's housing material and the type of material in between the excitation antenna and the transponder are determined by the nature of the application. Therefore, the only parameter that can be directly manipulated by the user is the size and shape of the RFID system's excitation antenna. A very important advantage of the TI RFID system, as it was discussed in section 4.1.1, is the compatibility of the reader with custom made excitation antennas. The construction of a custom made excitation antenna allows the user not only to considerably increase the maximum antenna-transponder detection distance, but also to manipulate the size and shape of the RFID system's excitation

antenna according to the specific requirements of each purpose and monitoring site (Hassan and Chatterjee 2006; Dziadak et al. 2009). However, there is an optimum in the increase of the excitation antenna's size after which the maximum antenna-transponder detection distance can dramatically deteriorate, since more ambient noise is picked up by the excitation antenna (TI Antenna Reference Guide 1996).

An excitation antenna has a certain inductance (L) value, which signifies its ability to store energy within the created electromagnetic field. The inductance is dependent on (a) the excitation antenna size and shape, (b) the wire type and size used for the loops, (c) the loops number, (d) the spacing between the loops and (e) the excitation antenna dimensions. For the case of the TI RFID system, the excitation antenna's inductance should not exceed 80 μH (TI Series 2000 Reader System Reference Guide 2002) otherwise; malfunctions can be caused to the transponder circuitries. The excitation antenna's inductance value can be directly measured using an inductance meter or computed using the formula:

$$L = \frac{1}{4\pi^2 f^2 C} \qquad \text{Equation 5-1}$$

where L is the excitation antenna's inductance (μH);

f is the RFID system's frequency (134.2 kHz); and

C is the capacitance (Farads).

These experiments were conducted at the Willow Creek Park, located at Iowa City, Iowa. The TI low frequency (134.2 kHz), passive RFID system and the TI 120 mm long, PVC encased, cylindrical transponders were employed for these experiments. A

piezoelectric buzzer device was connected to the RFID reader (connector J2 at Radio Frequency Module (RFM)), which allowed a sound indication that the transponder was detectable by the RFID custom made excitation antenna. Every time the transponder was detected by the reader, the piezoelectric buzzer made a very sharp sound; this sound was not made once the transponder was located outside the excitation antenna's electromagnetic field. It was through this process that the maximum antenna-transponder detection distance achieved for the different custom made excitation antennas. In Table 5-3 all the parameters taken into consideration for constructing the custom made excitation antenna are presented.

Another important antenna parameter that can affect its performance is the excitation antenna efficiency factor Q. The efficiency factor of an antenna quantifies the bandwidth of the RF signal and is defined as the ratio between the energy stored in a magnetic field and the radiated energy (Gustafsson and Nordebo, 2006). For the same voltage, high Q antennae are characterized by higher RF output signal than lower Q antennas, but they are more vulnerable to the presence of metal structures and miss-tuning. High Q antennae can also be used as filters that ignore signals that do not match with their bandwidth. The efficiency factor is dependent on antenna's resistance R, in the way that the lower antenna resistance results in a higher antenna efficiency factor. One direct way to manipulate the antenna's efficiency factor is through selecting the appropriate wire gage. In this study, three different copper wire gages were tested. The antenna's efficiency can be computed using the formula:

$$Q = \frac{2\pi f L}{R} \qquad \text{Equation 5-2}$$

Table 5-3 Custom made, closed rectangular loop shape excitation antenna summary attempts.

Attempt #	Antenna dimensions (ft^2)	Cable gage #	Number of loops	Loops spacing (inches)	Maximum detection distance achieved	Inductance (µH)
1	10x6	18	1	-	13.0	18
2	10x6	18	2	$\frac{5}{8}$	15.0	46
3	10x6	18	2	$1\frac{1}{4}$	14.5	48
4	10x6	18	3	1	16.5	87
5	10x6	18	3	$1\frac{3}{8}$	-	>80
6	10x6	14	2	1	15.5	45.5
7	10x6	14	2	$1\frac{1}{4}$	15.0	46
8	10x6	14	2	$1\frac{3}{8}$	17.0	45
9	10x6	14	2	$1\frac{1}{2}$	15.5	46
10	10x6	14	2	$1\frac{3}{4}$	14.0	45
11	10x6	14	3	$1\frac{3}{4}$	16.5	80
12	**10x6**	**12**	**2**	$\mathbf{1\frac{3}{8}}$	**17.5**	**45**
13	10x6	12	3	$1\frac{3}{4}$	15.0	82

where R is the antenna's resistance (Ohms).

In this experimental series, a number of 13 runs were performed to test the excitation antenna's performance for achieving the maximum antenna-transponder detection distance.

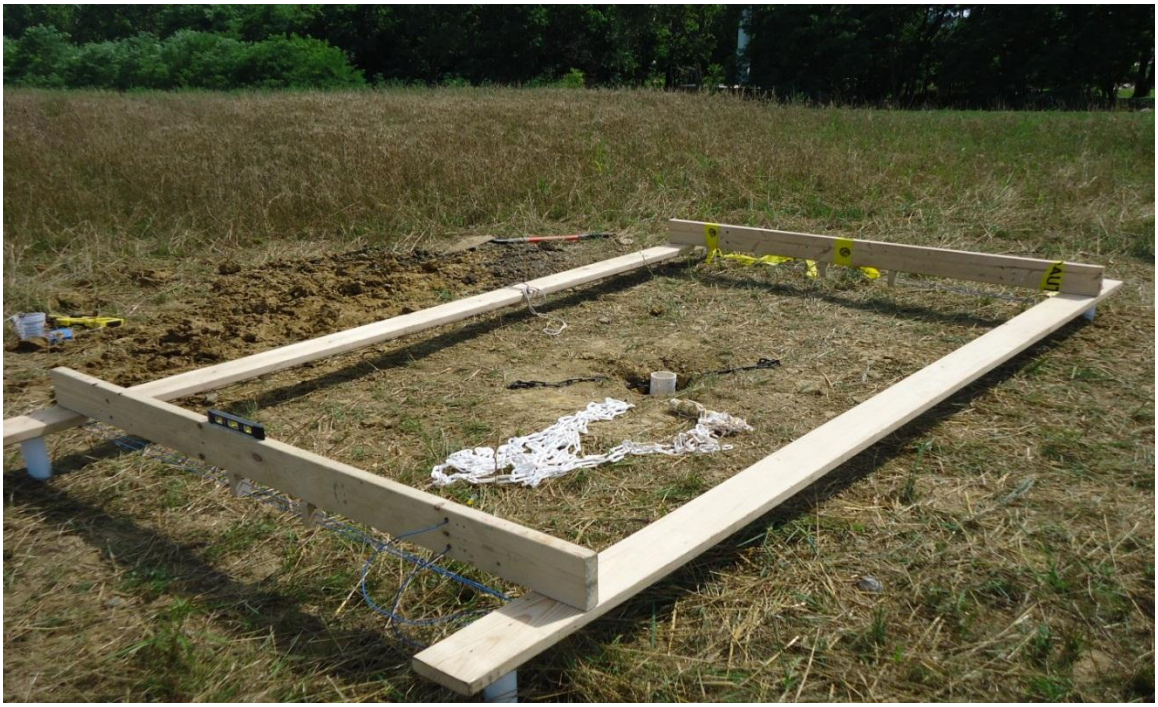

Figure 5-12 Field experimental setup: a view of the developed custom made excitation antenna (10x6 ft.) employed for the field experiments.

5.3.2. Development of the transponder return RF signal strength decay calibration curve in air using the custom made excitation antenna

The purpose of designing this experimental series was to develop calibration curves that related the transponder return RF signal strength with the distance in between the excitation antenna and the transponder in air. The decision of building the RF signal calibration curve in air was taken after considering the results occurred from the deposition experiments, which showed that the most important parameter for the RF signal decay was the distance between the excitation antenna and the transponder, whereas the height of the material above the transponder had little effect on the strength of the RF signal. For these experiments the TI low frequency (134.2 kHz), passive RFID system, along with the custom made excitation antenna (maximum detection distance achieved – 17.5 ft.) with dimensions of 10x6 ft. and the TI 120 mm long, PVC encased, cylindrical transponders were employed. A digital oscilloscope was used to record and export the shape of the RF signal at each measurement point considered. A total of 17 measurement points were considered corresponding to the maximum detection distance of 17 ft. achieved by using the custom made excitation antenna. Then, the obtained RF signal time series were analyzed in MATLAB and the corresponding calibration curve in air was built.

5.4. Radio Frequency Signal

In this section the RF signal, as it was recorded via a 25 MHz digital oscilloscope, is presented and analyzed. The RF signal is of great importance, since the whole analysis performed in this study is based on it. Figure 5-13 shows the shape and form of the RF

signal after plotting the raw RF signal time series in MATLAB. Each subplot in Figure 5-13A corresponds to a certain distance between the excitation antenna and the transponder, as it is shown in the descriptive experimental setup sketch below the time series subplots (Figure 5-13B).

5.4.1. Analysis of the obtained RF signal

The RF signal (in voltage) consists of three main parts. The first part or the big "plateau" (indicated with the green circle in Figure 5-14) corresponds to the transponder "charging" part and represents the energy required to activate the circuitry of the transponder. The energy is transferred from the reader to the transponder through the electromagnetic field of the excitation antenna and it is approximately 3 volts. This amount of energy is required to power up the inactive passive transponder in order the transponder to send back to the reader a response RF signal (TI Antenna Reference Guide 1996). This part of the RF signal lasts approximately 0.045 seconds (Figure 5-15A) and during this time length the reader is in the "sending" mode, while the transponder is in the "listening" mode. The second part of the RF signal is the transponder return RF signal or the "step" part of the RF signal (indicated with the green circle in Figure 5-14) which corresponds to the transponder response to the reader interrogation request RF signal. The transponder uses the energy stored in the excitation antenna's electromagnetic field to charge its circuitry and send back a replied RF signal to the reader. The voltage of the transponder return RF signal is reduced, since a part of the initially received energy was consumed to activate the transponder. The transponder return RF signal time duration is approximately 0.016 seconds (Figure 5-15B) and during

this time length the transponder is in the "sending" mode, while the reader is in the "listening" mode. Finally, the last part of the RF signal or the "oscillating" part (indicated with the red circle in Figure 5-14) represents the synchronization process between the reader and the interrogated transponder at which the reader is trying to establish the line of communication with the transponder. The time duration of this part is approximately 0.030 seconds (Figure 5-15C) and for this time length the reader is in the "sending" mode while the transponder is in the "standby" mode.

5.4.2. Different methods of analyzing the RF signal

Four methods of analyzing the RF signal were considered in this study, namely (a) analysis of the whole RF signal, (b) analysis of the transponder return RF signal combined with the RF signal oscillating part, (c) analysis of the transponder return RF signal and (d) analysis of the transponder return RF signal combined with the RF signal oscillating part based on the maximum peak histograms. For cases (a) and (b) the weighted average method was employed, based on the time duration of the contributing RF signal parts. For each measurement point, the RF signal strength decay was calculated by the formula:

RF signal strength decay (%) =

$$\left(1 - \frac{\text{mean voltage value of the RF signal parts considered}}{\text{mean voltage value of the transponder's charging part of the RF signal}}\right) \times 100$$

Equation 5-3

By examining the RF signal time series (Figure 5-13A) the transponder charging part of the RF signal is constant for all the measurement points considered herein and thus it was used as the base for estimating the RF signal strength decay. For cases (c) and (d), the average voltage values were calculated using the mean voltage value of each RF signal part and the mean voltage value of the bin corresponded to the maximum peak histogram, respectively.

Although all four methods tested herein could capture, at least at some degree, the general decay trend of the RF signal strength, only the analysis of the transponder return RF signal (case (c)) could depict the actual decay caused as the distance between the excitation antenna and the transponder changed. Specifically, in Figure 5-13A it is shown that the RF signal oscillating part has an almost constant average voltage value around to 1.8 volts, which is also lower than the average voltage value corresponds to the transponder return RF signal part. The third analysis method, named the transponder return RF signal and the RF signal oscillating part based on the mean voltage value corresponding to the maximum peak histogram, partially failed to capture the RF signal strength decay. This method cannot be considered as a trusted one, since the maximum peak histogram has the same probability to occur in the RF signal oscillating part, leading to extremely high decay values. This is due to the fact that the RF signal oscillating part mean voltage values are consistently lower than the ones corresponding to the transponder return RF signal. Therefore, this method can lead to biased results, where measurement points located closer to the excitation antenna showed to have greater signal decay than measurement points located further away from the excitation antenna. Figure

5-16 shows the RF signal strength decay curves for each method considered herein, while Figure 5-17 presents the way that these RF signal strength decay curves were developed.

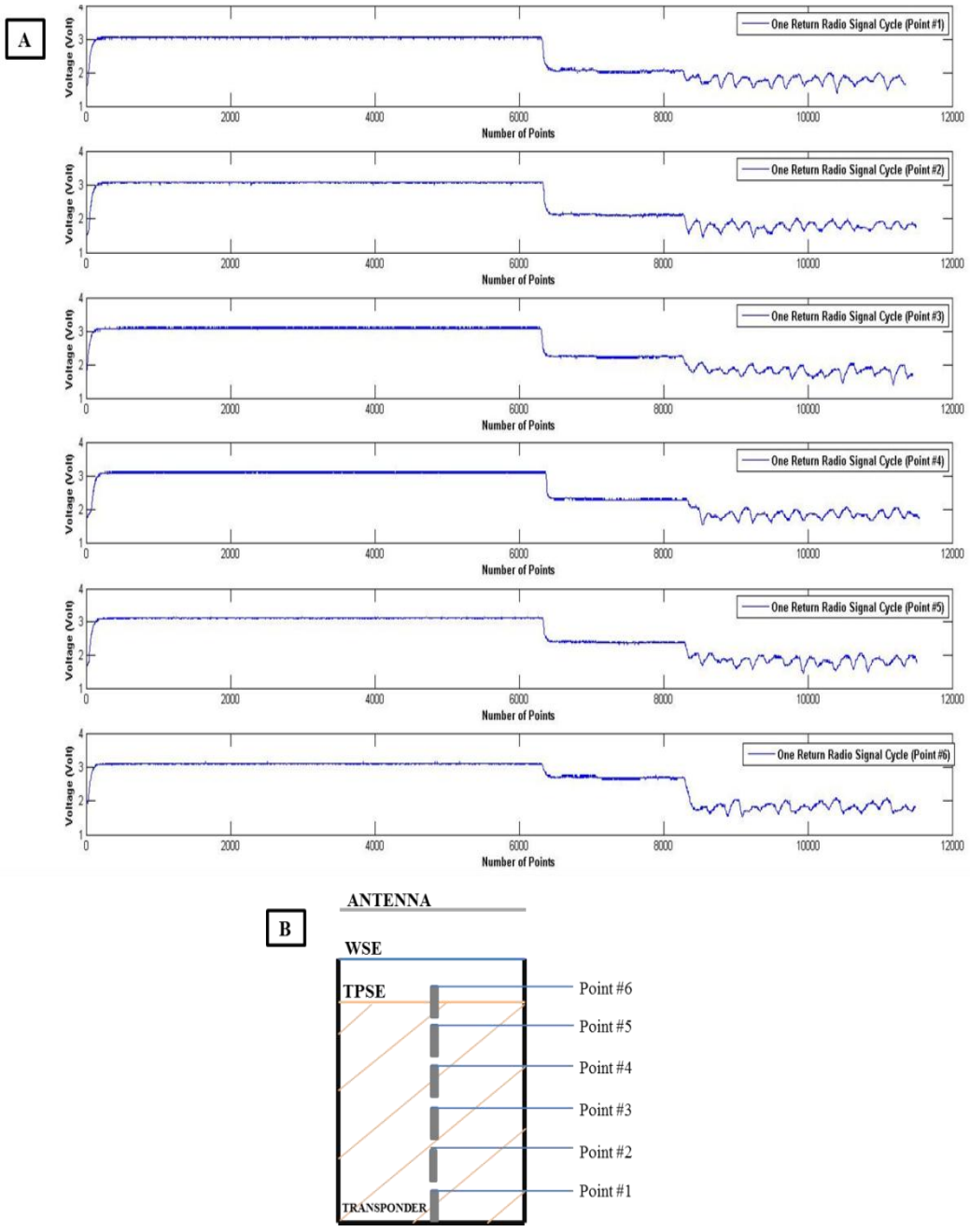

Figure 5-13 RF signal time series; (A) Example of the RF signal time series (as they were obtained via a digital oscilloscope), using the TI system and (B) a sketch showing the points at which the RF signal was recorded.

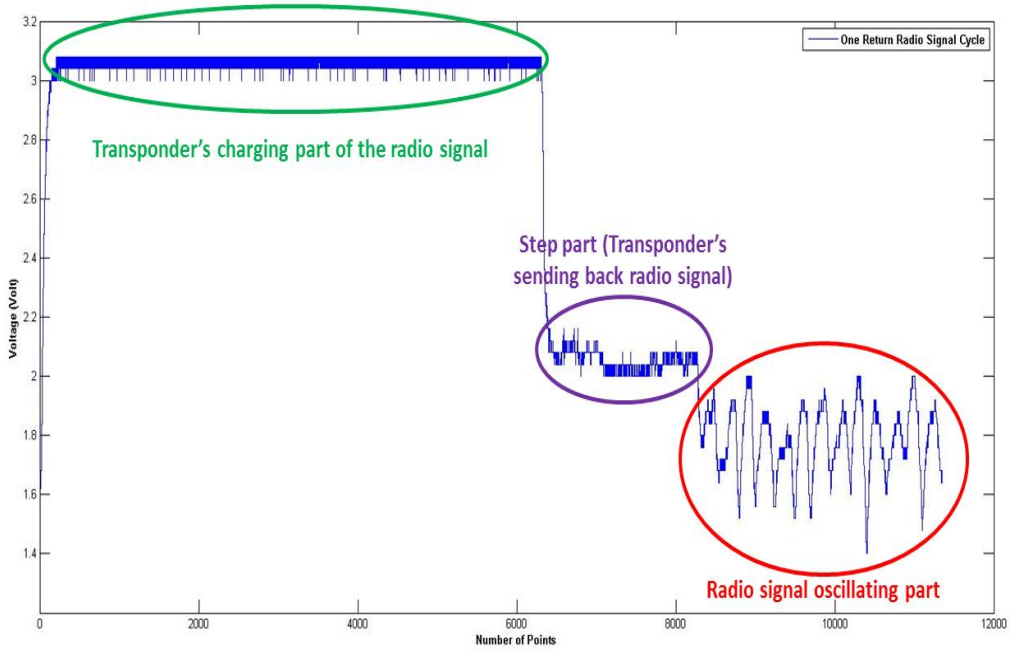

Figure 5-14 RF signal main parts.

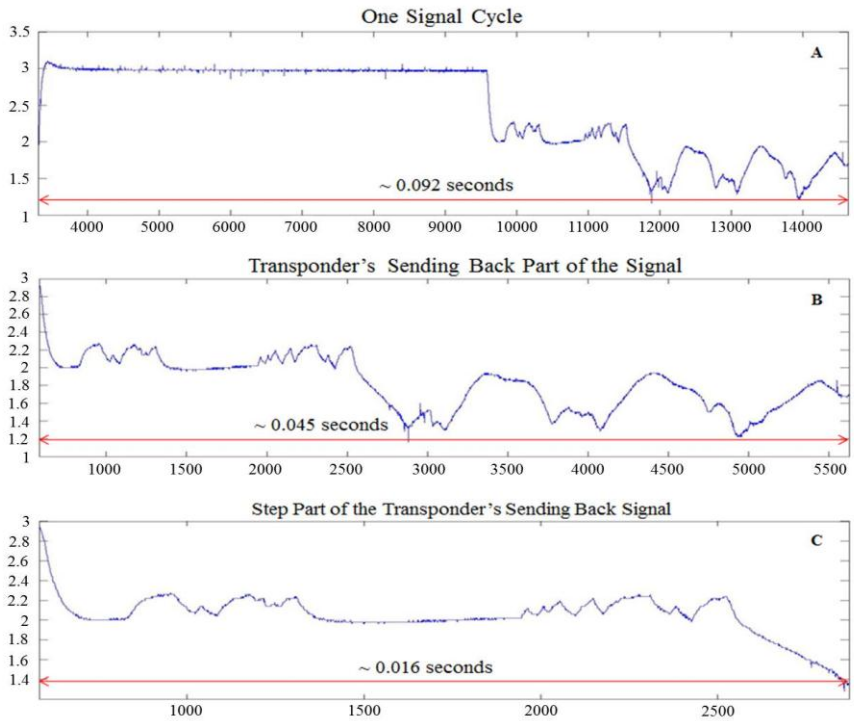

Figure 5-15 One RF signal cycle (~ 0.1 seconds) - time length of each RF signal part: (A) the whole RF signal, (B) the "step" and the "oscillating" RF signal parts and (C) the "step" part of the RF signal.

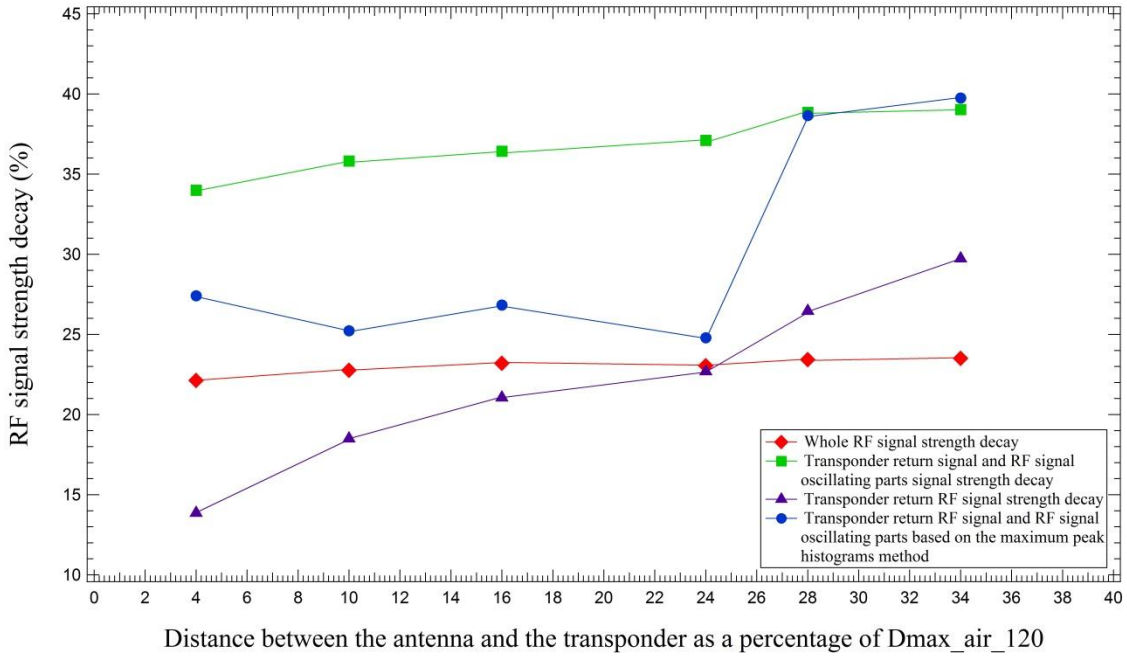

Figure 5-16 Different methods for computing the RF signal strength decay.

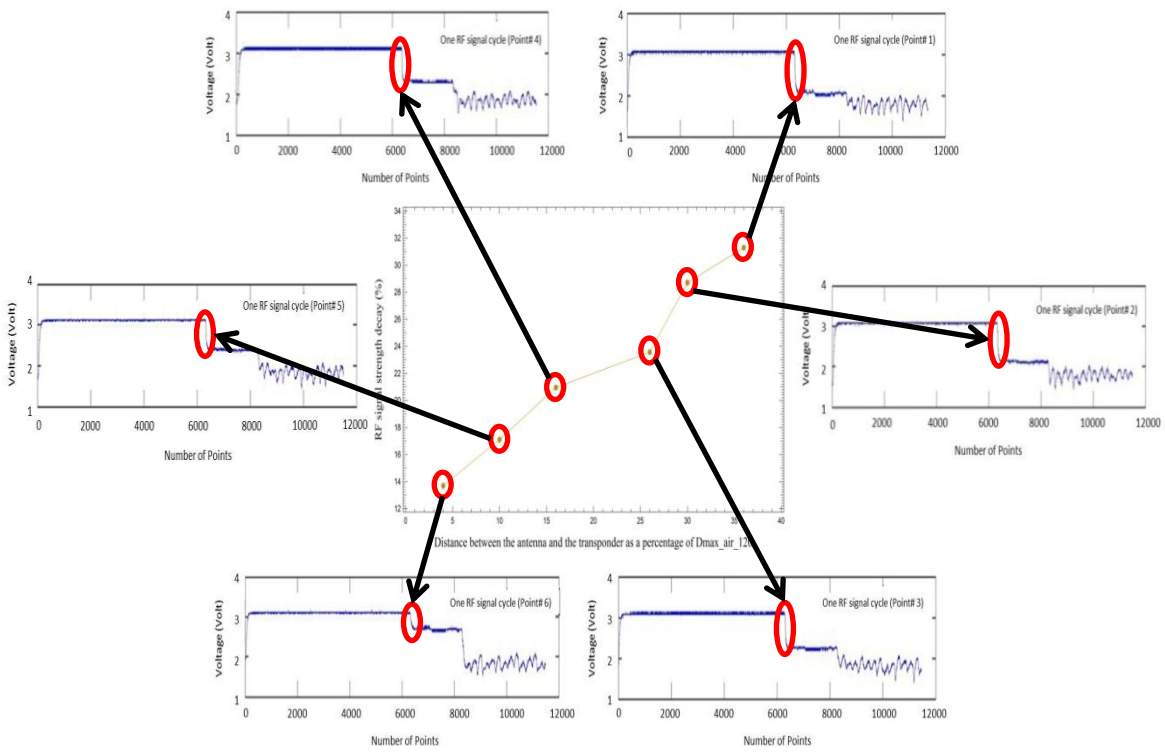

Figure 5-17 Development of the RF signal strength decay curves by using the drop in voltage of transponder return RF signal with respect to the "charging" part of the RF signal.

CHAPTER 6

RADIO FREQUENCY (RF) SIGNAL STRENGTH DECAY EXPERIMENTAL RESULTS

6.1. Introduction

This chapter presents the results of the following experiments:

(1) "Parametric" experiments, which were conducted to gain an insight of the effects that key RFID and environmental parameters have on the RF signal decay. These experiments were conducted at the IIHR – Hydroscience & Engineering Model Annex facilities.

(2) "RF signal strength vs. detection distance" experiments performed under various conditions representing real case scenarios, with the goal of evaluating the effectiveness of the RFID technology to detect erosion/deposition, in or without the presence of hydraulic structures. These experiments were conducted both in laboratory and field.

6.2. Parametric experiments

The parametric experiments were conducted under controlled conditions in the laboratory (see Chapter 5) and focused on the following aspects:

1. Testing the performance (i.e., in terms of transponder detection by the reader and transponder detection distance) of the RFID equipment in the context of transponder's return RF signal under various environmental conditions.

2. Analysis of the transponder's return RF signal.

The data for the parametric analysis are presented in terms of D_{max_air} (defined on page 1 in Chapter 5 for the different systems and set-ups considered here). Because the RFID technology was primarily developed to support applications in air, the RF signal strength decay curves for the different parametric conditions were in most cases compared with the baseline value of D_{max_air}. There were instances, however, that the value of D_{max_air} was compromised by the dimensions of the control volume (domain) used to run the experiments. For example, in some experiments the transponder distance from the RFID antenna was controlled by the maximum height of the barrel that was employed to simulate the river bed in the experiments.

6.2.1. Transponder orientation (ORIENT) effects on the transponder return RF signal

The medium considered for assessing the transponder orientation effects on its detectability was air. The system employed for these experimental series was the TI LF passive RFID with the 23 mm long transponders. The maximum detection distance ($D_{max_air_23}$) reported by the manufacturer is 0.6 m (TI Low Frequency 23mm Glass Transponder Manual 2001). Results from the 15 different orientation tests showed that the maximum detection distance occurred when the transponder's long axis was oriented perpendicular to the excitation antenna plane, which hereafter is referred to as the "favorable" transponder orientation. In this case, the intensity of the electromagnetic field created by the transponder obtained its highest value. On the contrary, when the transponder long axis was oriented parallel to the RFID antenna plane (defined here as the "unfavorable" transponder orientation), the minimum antenna-transponder detection

distance was recorded. In that latter case, the average detection distance between the antenna and the transponder decreased by 37%. As expected, different in-between transponder orientation positions provided intermediate detection distances, which were bounded between the minimum and maximum values of the antenna detection distance. A similar finding has been reported in the literature by Nichols (2004), Allan et al. (2006) and Papanicolaou et al. (2010).

As part of the ORIENT experiments we have further analyzed the transponder detectability performance by examining the success rate in detecting the transponder for the favorable orientation condition only. In other words, we have not only examined if the transponder was detectable but also how many times it became detectable. That is the success rate of detection which is evaluated here for different configurations.

We have recorded the detection success rate of four identical transponders. As a matter of fact, we have tested the detection limits and success rate of the RFID system for distances even greater than the one provided by the manufacturer ($D_{max_air_23}$ ~ 0.6 m). The four transponders were placed at identical distances each time from the antenna and numbered as transponders 1, 2, 3 and 4. They were spaced apart at all times by 0.38 m. The variability in the detection distance for each transponder was recorded by performing 16 sweeps per each chosen distance. The number of times the transponders were detected at different distances - averaged over the 16 sweeps – provides the success rate and is illustrated in Figure 6-1 in the form of % bars. The transponders can be successfully detected 100% of the time, when the antenna–transponder distance is $D_{max_air_23}$ ~ 0.6 m. The success rate of detection dropped, as expected, when the antenna–transponder distance became greater than 122% of $D_{max_air_23}$. Nonetheless and

to our surprise, the detection success rate remained relatively high in spite of the fact that the transponders distance surpassed the detection range reported by the manufacturer. Please note that for a distance greater than 122% of $D_{max_air_23}$, the RF signals between the antenna and transponders 1 and 3 were completely lost due to the interference of the electromagnetic fields created by the transponders internal antennas as they were found at a close proximity to each other (~0.38 m).

In a nutshell, the results of this section show that the transponder orientation does affect the antenna-transponder detection distance and for the favorable orientation position the maximum detection distance reported by the manufacturer can be exceeded by nearly 22%. In this case, the detection success rate dropped down to 63%. That implies that out of the 100 detection attempts, the transponder was detected 63 times. At $D_{max_air_23}$, the transponders can be successfully detected 100% of the time.

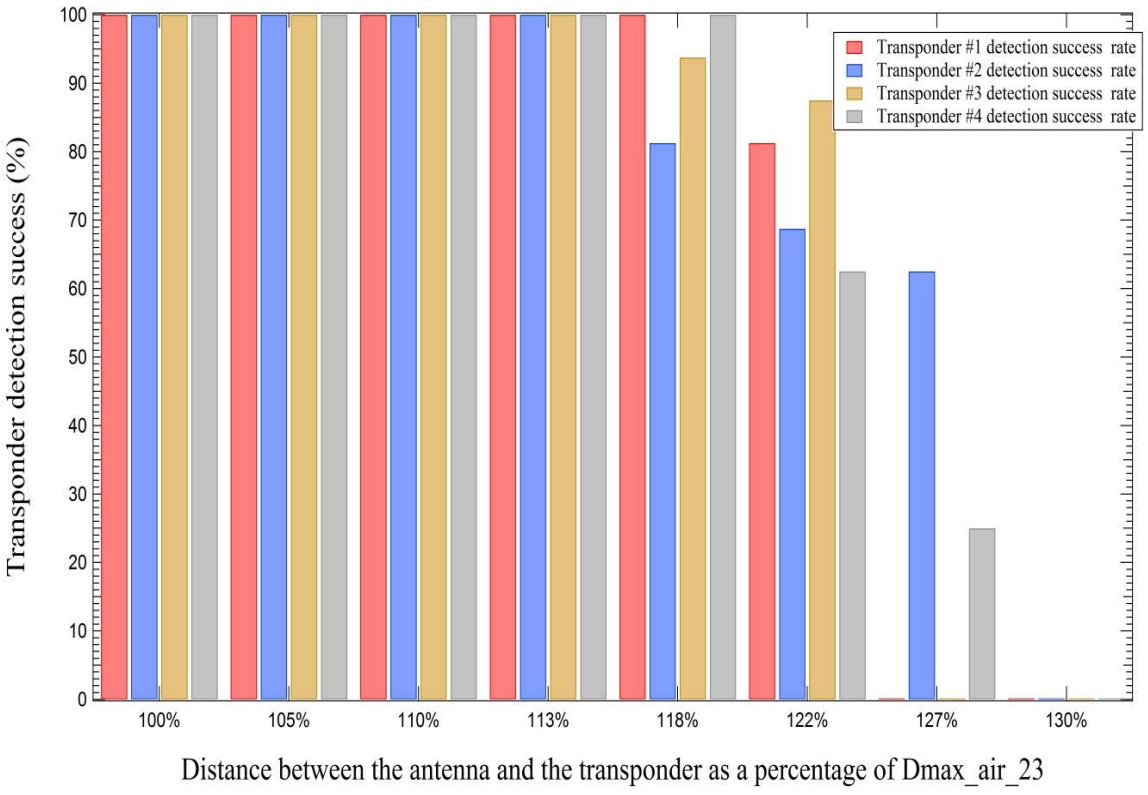

Figure 6-1 Transponder detection success percentage rate as a function of the antenna - transponder distance, for each transponder used in this experimental series.

6.2.2. Transponder housing (HOUS) effects on the transponder return RF signal

The medium considered in the HOUS experimental series was air as was the case with the ORIENT series. The system employed herein was the TI LF passive RFID with the 23 mm long transponders identical to the set-up used for the ORIENT series presented in section (6.2.1). The only difference with the ORIENT series experiments was that the transponders were encased or housed in different materials such as glass, concrete-tungsten, and PVC in order to examine the effect of housing material properties on the maximum antenna-transponder detection distance. Table 6-1 summarizes the results of the ORIENT and HOUS tests. The detection values given in Table 6-1 are the outcome of 15 runs per different housing and orientation combinations.

Results showed that the worst possible detection distance was encountered when the concrete-tungsten housing material was employed, for both transponder orientations, favorable and unfavorable. In this case, the detection distances dropped to 88% and 47% of $D_{max_air_23,}$ respectively. Out of the three encasing materials, the PVC material performed the best by providing the maximum antenna-transponder detection distance and the corresponding distance surpassed by 10% the reported $D_{max_air_23}$. Not lagging much behind, the glass housing gave an antenna-transponder detection distance 8% greater than the $D_{max_air_23}$ for the favorable transponder orientation and 1.5% reduction when it was compared to the PVC.

In conclusion, the results from this section revealed that the transponder encasing material affects the maximum antenna-transponder detection distance. Concrete-tungsten material had the poorest performance (88% of $D_{max_air_23}$) among the other materials considered herein. The PVC and glass encasing materials gave fairly similar maximum

antenna-transponder detection distances, with the PVC material performing the best. Nonetheless, the PVC encasing was preferable over the glass material due to its ease to use, rigidity to environmental stressors, availability and lower cost than glass. Based on these experimental findings, the transponders used for the remaining parametric and "RF signal strength vs. detection distance" experiments were PVC encased. Furthermore, in the remaining experiments we have used the favorable transponder orientation.

Table 6-1 Average detection distances for the different encasings under different orientations.

Housing material	*Naked		*Glass		*Concrete-Tungsten		*PVC	
Transponder orientation	**Perp.	***Par.	**Perp.	***Par.	**Perp.	***Par.	**Perp.	***Par.
Maximum detection distance obtained (m)	113% $D_{max_air_23}$	71% $D_{max_air_23}$	108% $D_{max_air_23}$	68% $D_{max_air_23}$	88% $D_{max_air_23}$	47% $D_{max_air_23}$	110% $D_{max_air_23}$	70% $D_{max_air_23}$

*Average of 15 iterations, the deviation was ± 2% in the reported values;

**Perp. = Perpendicular or favorable

***Par. = Parallel or unfavorable

6.2.3. Coupling effects on the transponder return RF signal

The medium considered in this experimental test was again air. However, the system employed herein was the TI LF passive RFID with the 120 mm long transponders. The maximum detection distance ($D_{max_air_120}$) reported by the manufacturer is 2 m (TI Low Frequency 120mm Cylindrical Transponder Manual 2001). It was deemed important that testing of the coupling effects or signal interference effects between the transponder internal antenna and the excitation antenna should be done for the 120 mm long transponders as the effect of coupling of the internal antennas of the 120 mm transponders should be more pronounced in this case than for the 23 mm transponders which have smaller internal antennas. Figure 6-2 presents the transponder's return RF signal strength decay curve with distance between the transponder and the excitation antenna. The overall trend of the decay curve is consistent with the reported trend in the literature that is, higher decay occurs as the distance between transponder and antenna increases. However, a paradoxical behavior has been observed when the transponder distance to the excitation antenna is less than 4% of $D_{max_air_120_barrel}$. Within that range, it was found that as the distance increases the RF signal strength dramatically decreases. When the transponder was placed at a distance of 1% of $D_{max_air_120_barrel}$, the decay observed in the RF signal strength was almost 30% and of the same order with the decay that corresponded to 20% of $D_{max_air_120_barrel}$. As the transponder was moved further away from the excitation antenna, the RF signal strength decay started to decrease until it dropped to the lower attenuation level, which corresponded to 4% of $D_{max_air_120_barrel}$. After that point, the RF signal strength started to increase and followed the expected semi-linear pattern. This phenomenon is called in the electromagnetic

theory as detuning of the transponder due to coupling effects and such an observation for this particular system and application has not been reported before in the literature. This paradoxical behavior is attributed to (a) the mutual signal coupling, which can cause the transponder to be detuned (personal communication with TI engineers) and (b) the fact that the transponder's return RF signal is electronically limited to protect the internal CMOS (Complementary Metal-Oxide-Semiconductor) circuitry for distances less than 4% of $D_{max_air_120_barrel}$ (personal communication with TI engineers). Based on the above, one could conclude that observations made for distances less than 4% of $D_{max_air_120_barrel}$ should not be considered in developing decay curves for the RF signal as it may lead to wrongful answers for scour detection as well as for other applications.

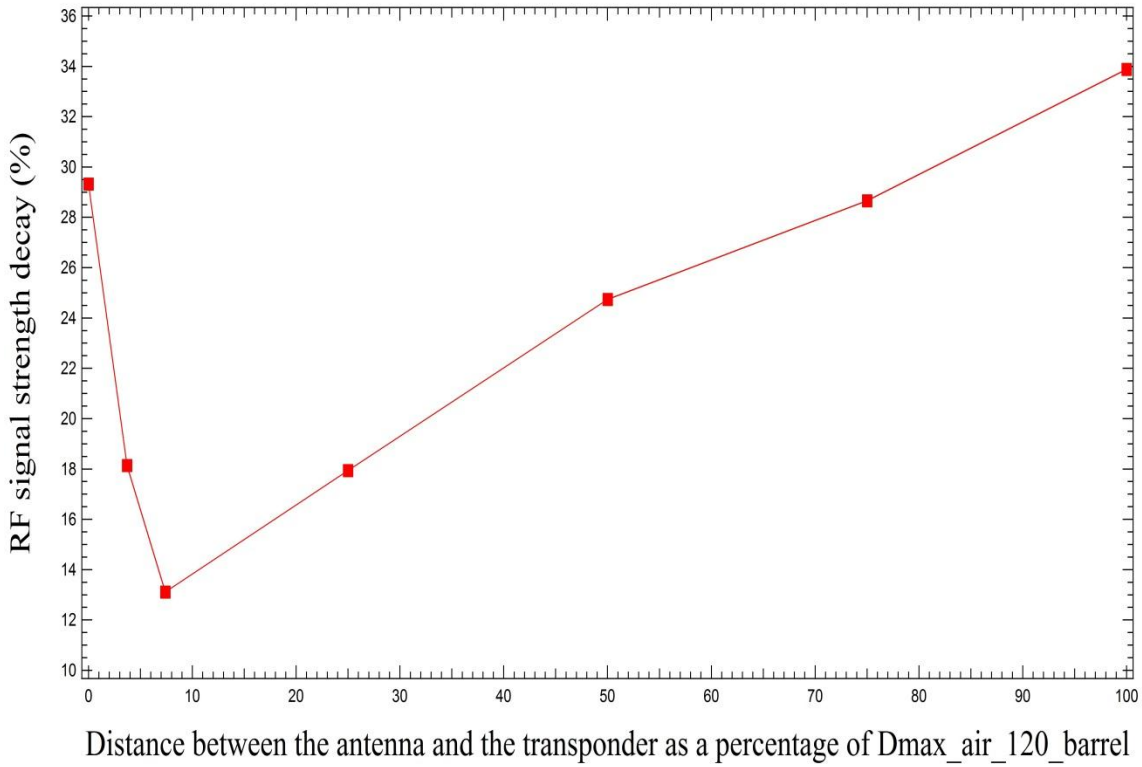

Figure 6-2 Transponder's return RF signal strength decay in air when the transponder is located at close proximity or within the excitation antenna frame.

6.2.4. Medium (MEDM) effects on the RF signal strength decay

The system considered in this section was the TI LF passive RFID with the 120 mm long transponders as this is the system to be ultimately considered for real world applications. In these experiments, the maximum antenna-transponder detection distance of 2 m achieved in air per the manufacturer, was compromised by the dimensions of the experimental setup (barrel) which were considered here as the maximum detection distance for an air medium defined as $D_{max_air_120_barrel} = 0.55$ m. Figure 6-3 demonstrates the transponder's return RF signal strength decay curves developed for each material type (i.e., air, water, dry sand and dry gravel) considered herein for the MEDM runs.

When air was the medium, the transponder's return RF signal strength suffered the minimum losses (Figure 6-3) compared to water, dry sand and dry gravel mediums. This behavior was expected, as there was no reflection of the RF signal in air.

In the case of water (Figure 6-3), the maximum antenna-transponder detection distance matched the $D_{max_air_120_barrel}$, although the decay rate of the transponder return RF signal strength in water was higher, but still comparable to the one for air. The transponder's return RF signal strength decay curve followed the same linear pattern of that for air.

In the case of dry gravel (Figures 6-3), the transponder's return RF signal strength decay curve also followed the linear decay pattern similar to the one for the air and water mediums. In this case, the maximum antenna-transponder detection distance matched the $D_{max_air_120_barrel}$ and the rate of decay of the transponder's return RF signal strength for dry gravel was similar to the one for water, except for the point that is located closer to

the RFID antenna (25% of $D_{max_air_120_barrel}$), where the RF signal strength decay was significantly higher.

Finally, in the case of dry sand (Figures 6-3) the maximum antenna-transponder detection distance dramatically decreased. In this case, the maximum antenna-transponder detection distance dropped to 64% of $D_{max_air_120_barrel}$ and the decay rate of the transponder's return RF signal strength was much higher than the ones corresponded to the other mediums considered herein (the slope of the decay curve for sand was much steeper than the ones for air, water and dry gravel).

These findings agree with the results presented by Dziadak et al. (2009), where the shortest antenna-transponder detection distance occurred when the transponder was buried into sand, while the detection distances corresponded to air and gravel were significantly longer. Therefore, the type of medium in between the antenna and the transponder affects the maximum antenna-transponder detection distance and can dramatically deteriorate the applicability and success of the RFID system. Dziadak et al. (2009) attributed this drop with the sand medium to its electromagnetic properties (i.e., magnetic permeability, permittivity, and conductivity) that affects the RF signal propagation into the sand medium.

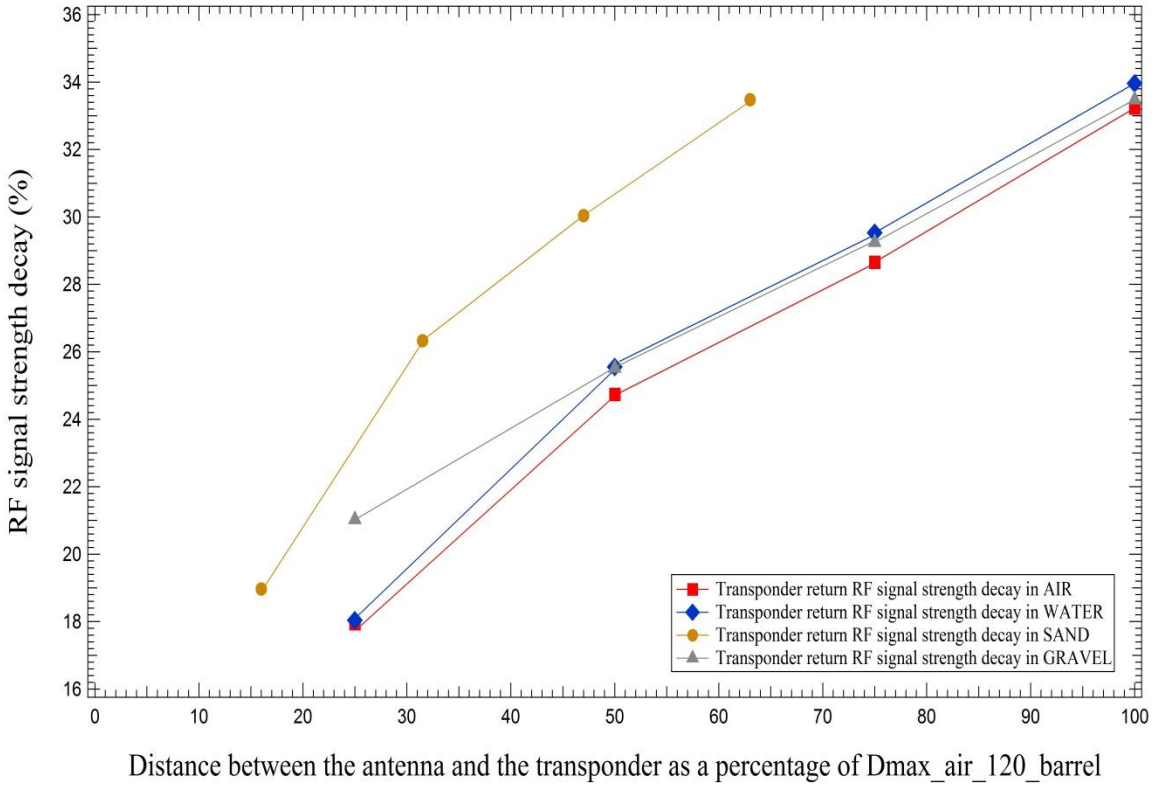

Figure 6-3 RF signal strength decay curves developed in various mediums (i.e., air, water, dry sand and dry gravel).

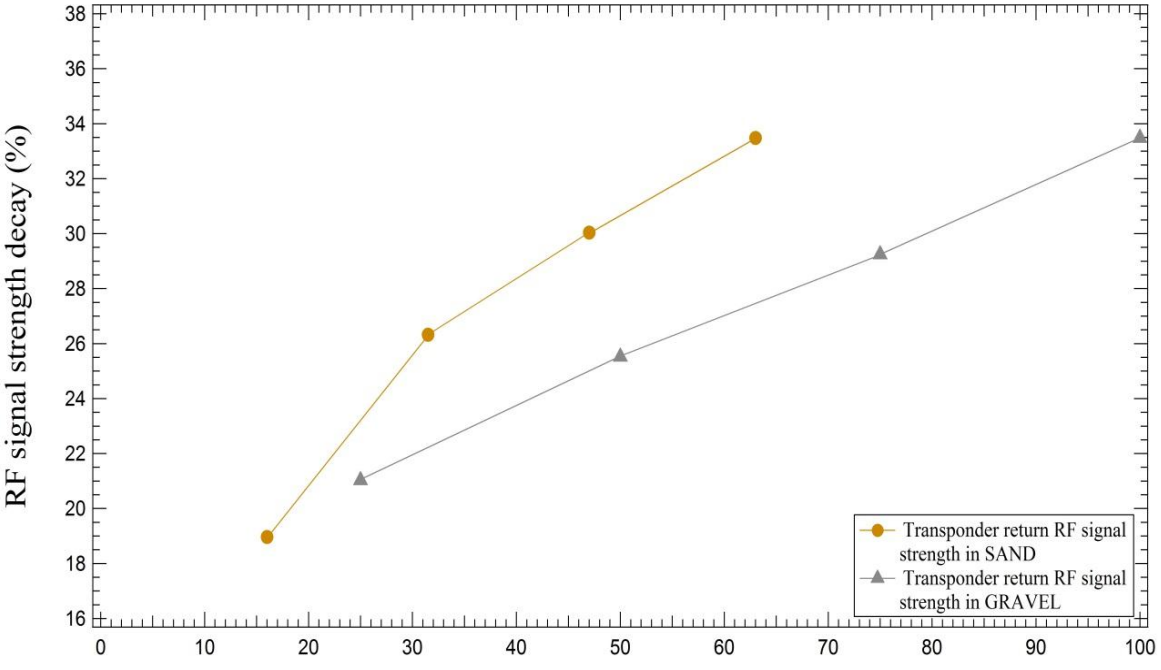

Figure 6-4 RF signal decay curves for (a) sand and (b) gravel material types.

6.2.5. Effects of sand and gravel porosity on the RF signal propagation and decay

The two material types considered herein were characterized by different void ratio values. The void ratio of sand and gravel were 32.4 and 40.1%, respectively. Figure 6-4 demonstrates the transponder's return RF signal strength decay curves for (a) sand and (b) gravel medium types. In case of sand, the maximum antenna-transponder detection distance (64% $D_{max_air_120_barrel}$) decreased by 37% compared to the one occurred for gravel ($D_{max_air_120_barrel}$). The slope of the transponder's return RF signal decay curve for sand was much steeper than the one corresponded to gravel, indicating that the RF signal propagates better through materials characterized by high void ratio values (i.e., gravel). These results also matched the ones reported by Dziadak et al. (2009), where the antenna-transponder detection distances in sand were constantly shorter from the ones in gravel.

6.3. Sensitivity analysis

The optimum RFID combination (air - perpendicular), which corresponded to the minimum rate of decay of the RF signal strength and the longest antenna-transponder detection distance ($D_{max_air_120_barrel}$), included (a) the favorable (perpendicular) transponder orientation and (b) air as a medium in between the antenna and the transponder. Table 6-2 shows the 6 key RFID parameters considered herein. The 6 combinations formed (i.e., water-perpendicular, dry sand-parallel) were compared with the optimum combination and the absolute error was computed based on the difference between the RF signal strength decay for each parameter combination and the optimum, for each measurement point. Figures 6-5 and 6-6 demonstrate the sensitivity curves, for

the 6 different RFID parameter combinations. More specifically, Figure 6-5 shows the sensitivity curves for various mediums (i.e., water, sand and gravel) when the transponder orientation was favorable. In case of water, the absolute error was less than 5% for all measurement points. For dry gravel, the absolute error obtained its maximum value at the first measurement point (the one closest to the RFID antenna), ~17%, while for the other three points the absolute error dropped below ~4%. On the contrary, in the case of dry sand, the absolute error was constantly higher compared to the ones for water and dry gravel, starting from ~12%, when the transponder was located closer to the RFID antenna, and raising above 30% for the rest measurement points. The sensitivity analysis for the favorable transponder orientation revealed that even though the transponder orientation is favorable, there are certain types of mediums (e.g., sand) that can lead to up to 30% error.

On the other hand, Figure 6-6 shows the sensitivity analysis curves for the unfavorable transponder orientation for the same types of mediums. The absolute error for all mediums was constantly higher, by an order of magnitude, compared to the one corresponding to the favorable transponder orientation. For the cases of water and dry gravel, their sensitivity curves followed a similar pattern with the corresponding absolute error values to be quite close to each other. However, the absolute error for these mediums, increased by almost 40% compared to the same mediums under the favorable orientation. For the case of dry sand, the maximum antenna-transponder detection distance was reduced by 80% of $D_{max_air_120_barrel}$, and the absolute error values were significantly higher, by an order of magnitude, than the ones corresponding to the other two mediums (water and dry gravel) for the same orientation. These results showed that

when the transponder was unfavorably orientated, the absolute error can be of at least one order of magnitude higher compared to the favorable one, while the combination of the unfavorable orientation with certain medium types (i.e., sand) can result in errors of up to two order of magnitude.

The above sensitivity analysis results indicated that the most sensitive RFID parameter is the transponder orientation, which can lead to significant error, while in combination with certain medium types (i.e., sand) the error can increase dramatically, with undesirable effects on the functionality and applicability of the RFID system.

Table 6-2 Factors considered for the sensitivity analysis

Transponder housing material	PVC		
Transponder orientation towards the antenna plane	Perpendicular	Parallel	
Medium in between the antenna and the transponder	Water	Dry Sand	Dry Gravel

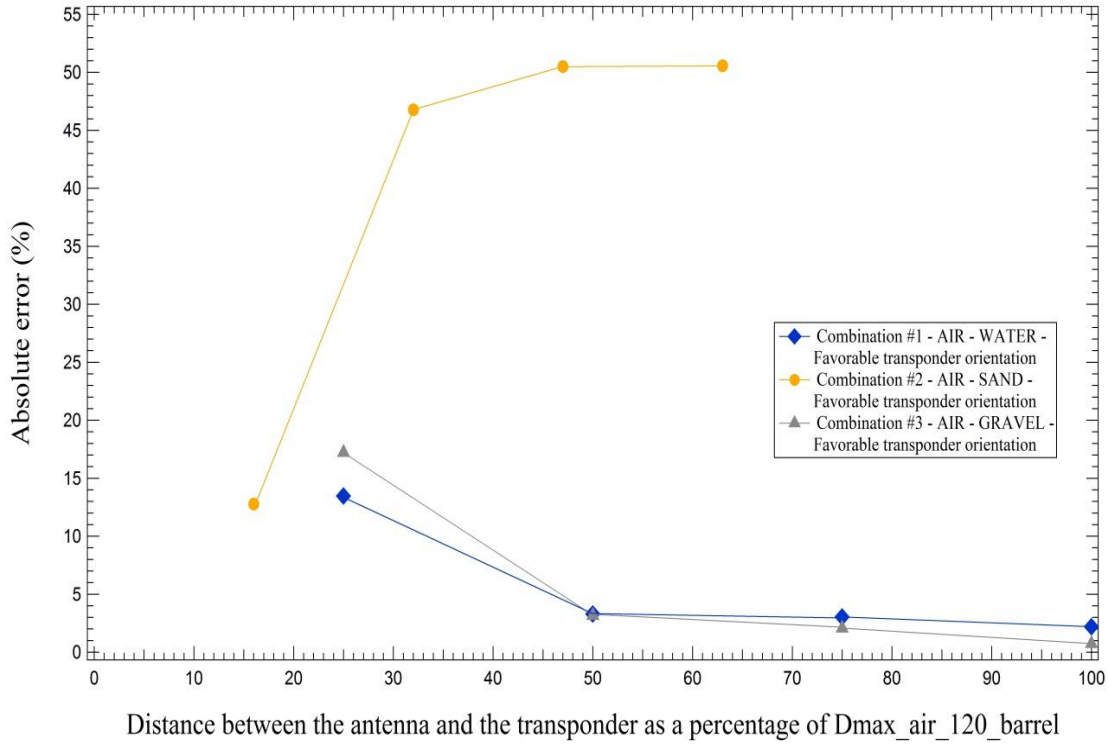

Figure 6-5 Sensitivity analysis curves for (a) water, (b) dry sand and (c) dry gravel mediums, for the favorable transponder orientation.

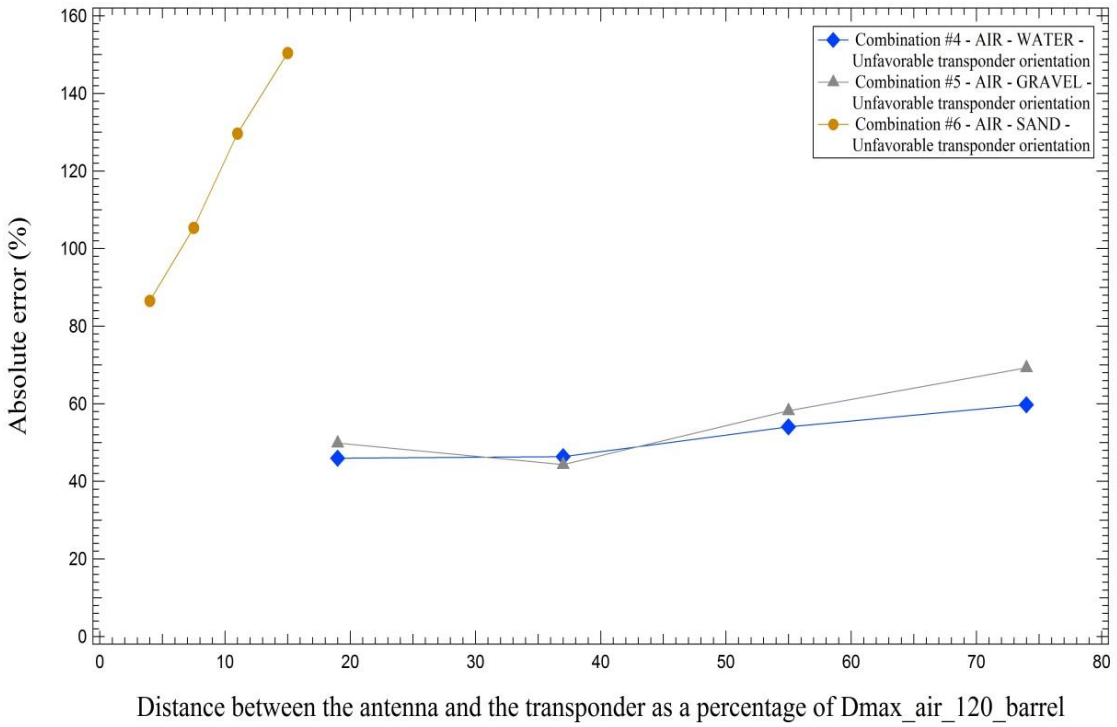

Figure 6-6 Sensitivity analysis curves for (a) water, (b) dry sand and (c) dry gravel mediums, for the unfavorable transponder orientation.

6.4. Quantify transponder return RF signal strength decay during the erosion and deposition processes

6.4.1. RF signal strength decay during the erosion (EROS) process

In these experimental series the TI LF passive RFID system with the 120 mm long transponders was used to quantify the scour depth evolution during the erosion process, by coupling the transponder's return RF signal strength with the distance between the antenna and the transponder. Initially the transponder was buried into sand material at the maximum antenna-transponder detection distance achieved for this experiment (37% of $D_{max_air_120}$). The RF signal strength was recorded at each of the six predetermined measurement points, which corresponded to 5.5, 17, 22, 27, 32 and 37% of $D_{max_air_120}$, reported by the manufacturer (see Figures 5-7 and 5-8 for details). Figure 6-7 presents the RF signal decay curve for the erosion process experiments.

The RF signal strength linearly decays as the distance between the antenna and the transponder increases. The correlation, r^2, of the RF signal strength decay curve is almost unity (0.99) indicating a strongly linear relationship between the RF signal strength decay and the distance between the antenna and the transponder. The decay pattern of the RF signal strength curve is in agreement with the wireless signal attenuation curve developed by Ko (2010), which shows the RF signal strength to decay with the distance between the antenna and the transponder.

The confirmation of the RF signal strength linear decay, as the antenna-transponder distance increased, reflects the RFID principle on which the RFID

technology was considered as the appropriate one for developing a real world continuously scour monitoring system.

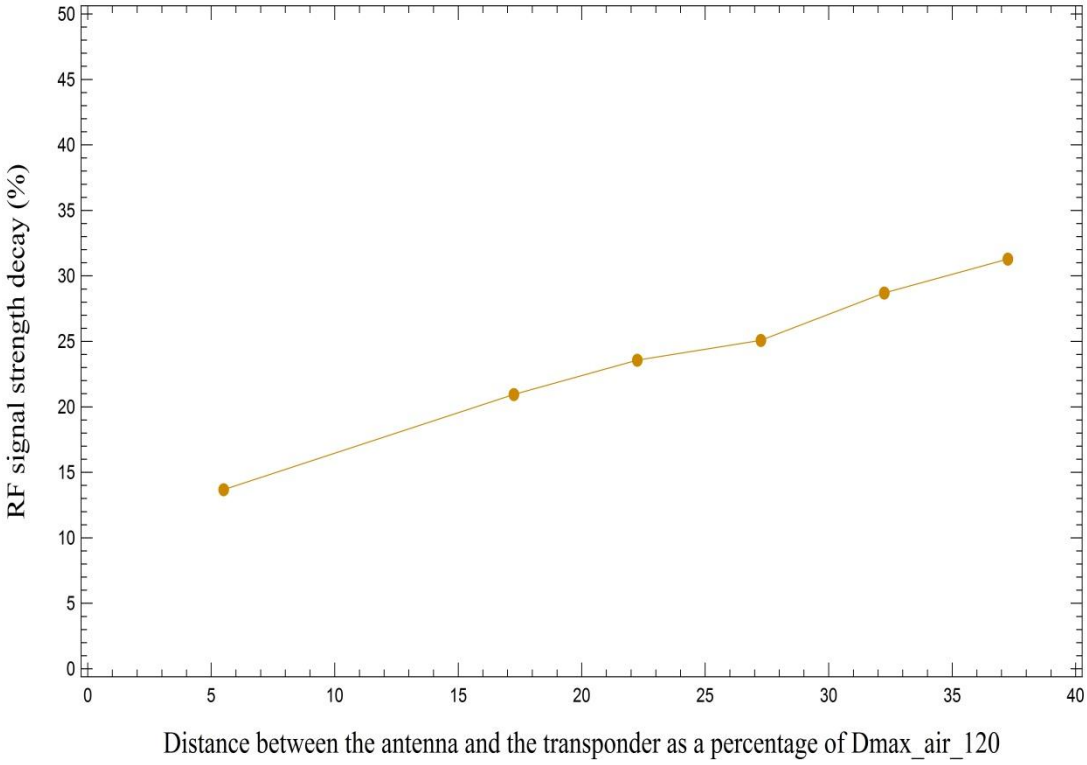

Figure 6-7 The RF signal strength decay curve for the erosion process experiments.

6.4.2. RF signal strength decay during the deposition (DEP) process

In these experimental series the TI LF passive RFID system with the 120 mm long transponders was used in measuring the height of deposition above the transponder

by relating the transponder's return RF signal strength with the thickness of the material deposited. The transponder was placed in a fixed distance from the RFID antenna (37% of $D_{max_air_120}$) and material was added above the transponder corresponding to distances between the RFID antenna and the surface of the sediment column of 5.5, 17, 22, 27, 32 and 37 of $D_{max_air_120}$ (see Figures 5-9 and 5-10 for details). At each experimental step, the distance between the RFID antenna and the water surface was constant at 0.045 m. As the height of the sediment column above the transponder increased, the transponder's return RF signal strength was recorded via a digital oscilloscope at the predetermined measurement points. Figure 6-8 shows the RF signal strength decay curve obtained during the deposition process experiments. The RF signal decay follows a horizontal line pattern, demonstrating that the decay of the RF signal strength is independent of the thickness of the material above the transponder.

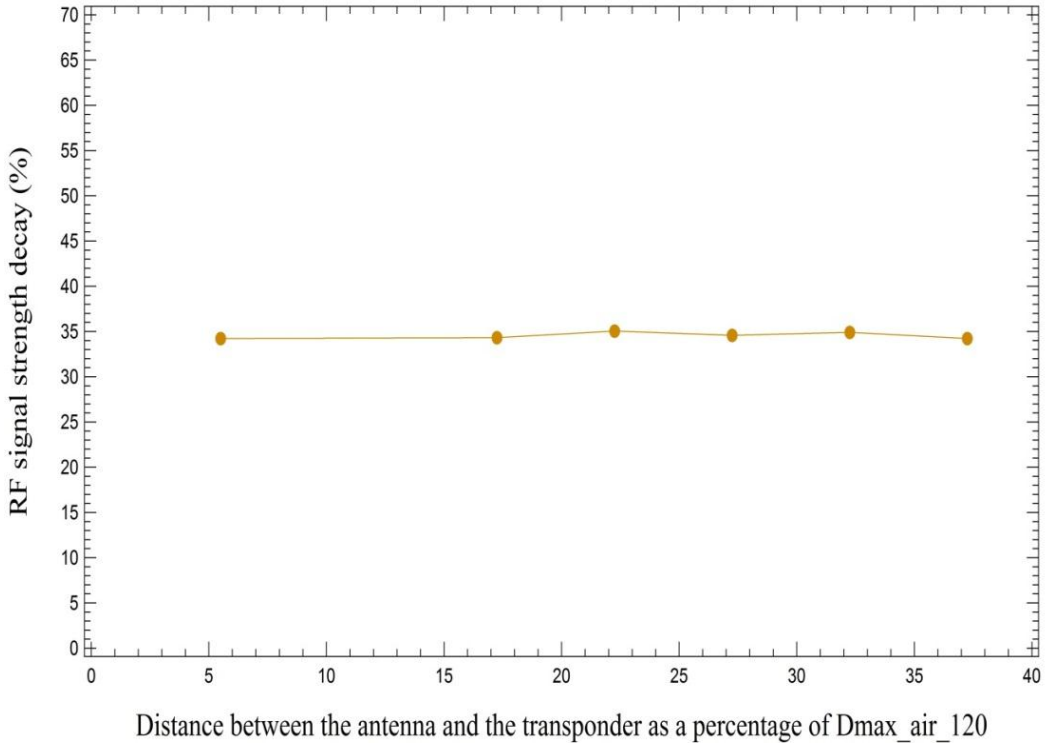

Figure 6-8 The RF signal strength decay curve for the deposition process experiments.

The key parameter that governs the RF signal decay is the antenna-transponder distance, since the longer the antenna-transponder distance, the greater the RF signal decay. The slight deviations of the RF signal decay values for the points considered herein from the exact horizontal line trend were attributed to the sensitivity of the TI LF passive RFID system and the digital oscilloscope used.

6.4.3. Quantify scour (SCR) using the Leopold chain method around a bridge pier model

The Leopold chain method results showed that the RFID system developed by HiTAG along with the 22 mm long transponders was able to successfully measure the scour depth evolution around a model bridge pier. These experiments were designed based on the results of the transponder orientation effect on the antenna-transponder maximum detection distance. The maximum antenna-transponder detection distance for the two transponder orientations (favorable - $D_{max_Leo_sc_22}$ vs. unfavorable - $D_{max_Leo_sc_unfav_22}$) towards the antenna plane were measured. For the case of favorable transponder orientation, the $D_{max_Leo_sc_22}$ was 0.43 m, while for the case of unfavorable orientation the maximum detection distance ($D_{max_Leo_sc_unfav_22}$) reduced to 0.101 m. The distance between the antenna and the upper and lower transponders on the chain were 0.235 and 0.407 m, respectively. In case of the upper transponder, the antenna-transponder detection distance was longer than the one corresponded to the unfavorable orientation so that when the transponder orientation changed to unfavorable due to scour evolution, the communication between the HiTAG RFID system and the transponder was disrupted. In case of the lower transponder, the antenna-transponder detection distance

was a bit shorter than the maximum detection distance ($D_{max_Leo_sc_22}$) to allow the system to detect the transponder 100% of the time. When the scour hole reached the depth of 10% of $D_{max_Leo_sc_22}$ (0.043 m), the communication between the antenna and the upper transponder was disrupted, since the transponder was unfavorably orientated to the RFID antenna plane. This change in the transponder orientation was an indication that the scour has reached the depth at which the transponder was initially buried. In the meantime, the other four transponders were successfully detected by the HiTAG RFID system, because they were favorably oriented with respect to the antenna plane. As the scour progressed, the second transponder orientation changed, when the scour hole reached 20% of $D_{max_Leo_sc_22}$ (0.086 m). At that point, the RFID antenna was not able to detect the first and the second transponders, while the rest three transponders were still detectable. Once the scour evolution reached the depth of 30% of $D_{max_Leo_sc_22}$ (0.129 m), 40% of $D_{max_Leo_sc_22}$ (0.172 m) and 50% of $D_{max_Leo_sc_22}$ (0.215 m), the third, fourth and fifth transponders respectively changed orientation and were not anymore detected by the system.

The Leopold chain method to quantify scour around a model bridge pier results showed that this is a reliable method to continuously monitor scour. The temporal resolution of this method can significantly increase by attaching more transponders on the chain (actually reducing the distance between two successive transponders). Moreover, this technique can be even more robust, if the transponders orientation is coupled with the transponder return RF signal strength decay, by developing the corresponding RF signal strength calibration curves for each transponder burial depth. This coupling will be the

basis for developing an advanced bridge scour monitoring system that will provide with continuous data about the scour evolution the bridge inspection personnel.

6.5. The RF signal strength vs. detection distance experiments

6.5.1. Development of a custom made RFID antenna for achieving the maximum antenna- transponder detection distance

A key parameter for attaining of the maximum possible antenna-transponder distance is the number of the wire loops that an RFID antenna is comprised of. The number of the wire loops of the RFID antenna affects the antenna inductance. The antenna inductance is a measure of the energy storage capacity of the antenna in its electromagnetic field. The antenna inductance was measured via an inductance meter that was connected to the two edges of the antenna wire. Table 5-3 demonstrates all the parameters taken into consideration for the development of the custom made RFID antenna, along with the antenna-transponder maximum detection distance achieved in each attempt. The RFID antennas constructed using 1 wire loop resulted in low inductance values and thus limited energy storage capacity leading to short antenna-transponder detection distances. Three-wire-loop antennas on the other hand, resulted in high antenna inductance values, close or exceeding the safety limit of the TI RFID system which was at 80 μH. Therefore, the 3-wire-loop antennas were disregarded as potentially harmful for the TI RFID system, despite the fact that these antennas demonstrated high energy storage capacity. The maximum antenna-transponder distance ($D_{max_air_cust_ant_120}$), 17.5 ft. (~5.3 m), was achieved with a 2-wire-loop antenna, although

that the 2-wire-loop antennas were characterized by moderate inductance values. The Q efficiency factor of the custom-made RFID antenna was employed in to ensure achieving the maximum antenna-transponder detection distance (17.5 ft.) by adjusting the loop spacing parameter. From the loop spacing values reported in Table 5-3, there is an optimum loop distance for each number of loops (e.g. $1^{3/8}$ in for a 2 loop antenna) where the maximum antenna-transponder detection distance obtains its maximum value. The reduction in the antenna-transponder detection distance was attributed to the fact that when the loop spacing was less than the optimum (for each number of loops), there was a strong interference between the electromagnetic fields of the neighboring wires, leading to shorter detection distances. On the other hand, when the loop spacing exceeded the optimum, there was a week interaction of the electromagnetic fields of the neighboring wires, resulting also in shorter antenna-transponder detection distances. The thickness of the wire used to build the antenna loops also affected the antenna performance. This can be attributed to the fact that the thicker the wire, the higher its electrical conductivity and therefore more energy can be stored in the electromagnetic field of the antenna. Finally, during the experiments, it occurred that the spikes/nails used to attach the wire on the antenna wooden frame can significantly affect the performance of the RFID antenna. For the antenna setup where the maximum antenna-transponder detection distance achieved (17.5 ft.), rusty spikes resulted in a reduction of 24% of $D_{max_air_cust_ant_120}$.

The development of a custom made RFID antenna considerably increased the maximum antenna-transponder detection distance given by the manufacturer for the TI rectangular loop shape RFID antenna and the TI 120 mm long transponders which is less than 2 m (TI Low Frequency 120mm Cylindrical Transponder Manual 2001). For the

same transponders (TI 120 mm long transponders) and the custom made RFID antenna, the maximum antenna-transponder detection distance increased by 265% of the $D_{max_air_120}$ (5.3 m). Also, in Dziadak et al. (2009) study a specially designed RFID antenna was used, with larger dimensions than the TI off the shelf RFID antennae, and they were able to achieve longer antenna-transponder detection distance. Although the increase in the maximum antenna-transponder detection distance is a key parameter for the successful implementation of the RFID technology in quantifying scour, the advantages of developing a custom made RFID antenna are not limited only to that, but also it allows the user to manipulate and optimize its size and shape based on the specific application and site requirements.

6.5.2. Development of the transponder return RF signal strength decay calibration curve in air using the custom made RFID antenna

Figure 6-9 presents the transponder return RF signal strength decay calibration curve for the TI LF passive RFID system with the 120 mm long transponders and the custom made RFID antenna in air. Although, the medium type in between the RFID antenna and the transponder affects the rate at which the RF signal strength decays (see Section 6.2.4), the distance between the RFID antenna and the transponder determines the RF signal decay (see Section 6.4.1). This experimental series was designed based on these interesting findings and therefore the transponder return RF signal strength decay calibration curve was built in air.

The transponder return RF signal strength follows an approximately linearly decaying pattern (Figure 6-9) as the distance between the antenna and the transponder

increased. The correlation, r^2, of the transponder return RF signal strength curve is close to unity (0.995), indicating a strongly linear relationship between the decay of the RF signal strength and the distance between the antenna and the transponder. This trend was expected since we already know from the electromagnetic theory that the RF signal strength linearly attenuates with the square of the distance traveled from the source. This linearly decay pattern of the RF signal strength is further supported by the findings of Ko 2010, where they plotted the signal strength in dBm (decibel) with the distance between the antenna and the transponder (m). In Barralet et al. (2009) study, they plotted the RSSI (Received Signal Strength Indicator) with the distance in logarithmic scale, in order to obtain a linear relationship, since dBm is a logarithmic unit.

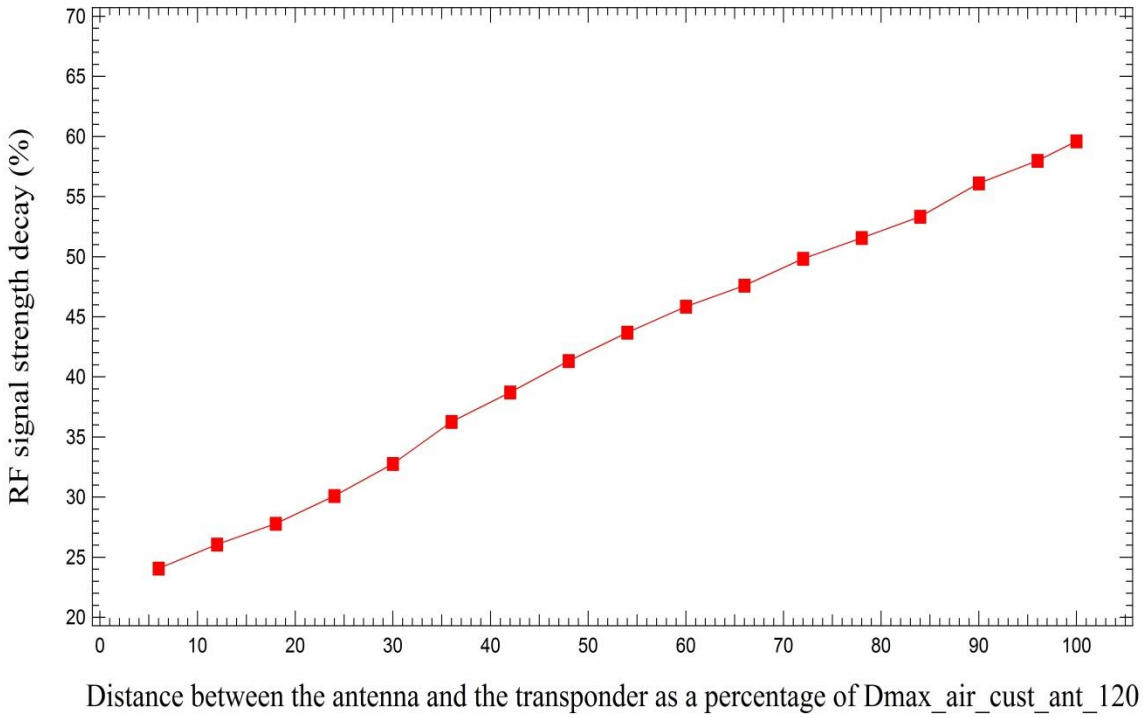

Figure 6-9 Transponder return RF signal strength decay calibration curve in air, using the custom made RFID antenna.

6.6. Uncertainty analysis

Uncertainty analysis is a powerful statistical tool that has been extensively used in engineering domain, where exact measurements are almost impossible to obtain, and provides information on the data quality, as well as reveals the weak points of the experimental procedure that need to be improved. In this study, an uncertainty analysis, based on the GUM (Guide to Expression of Uncertainty in Measurements) protocol (ISO/BIMP 1993), was conducted to provide an estimate of the combined uncertainties from all sources of error that contributed to the transponder return RF signal strength decay. The TI LF passive RFID system with the 120 mm long transponder, and the custom made excitation antenna were used, while the medium was air. The main sources of error were due to uncertainty in (a) the hardware accuracy (i.e., oscilloscope, measuring tape) and (b) environmental factors (see Chapter 2, section 2.5.2). These experiments were performed at Willow Creek Park and special care was taken to minimize the effects of the environmental factors on the RF signal. However, we cannot neglect the fact that there were some effects, even minimal, on the RF signal due to environmental factors, but we did not have the equipment to quantify them and therefore we are not going to include them into this uncertainty analysis. The level C of the confidence interval for the measured mean voltage values at each measurement point was 95%. A 95% confidence interval means that if the voltage measurement for a certain measurement point is repeated 100 times, then 95 times out of 100 the measured voltage value would be between the upper and lower limits estimated for this point. A number of 10 independent runs, under the same conditions, were performed to produce a large enough sample to get a sound estimation for the uncertainty lies in the final results.

The GUM uncertainty analysis followed herein was divided into five steps. The first step includes the development of the "reduction" equation (Equation 6-1), which is a mathematical expression that relates the variable of interest (measurand) with the input quantities. In this case the transponder return RF signal strength decay is the variable of interest, while the mean voltage values of the "charging" (V_{ch}) and "step" (V_{st}) parts of the RF signal are the input quantities.

$$RF = \left(1 - \frac{V_{st}}{V_{ch}}\right) \times 100 \qquad \text{Equation 6-1}$$

The second step is the evaluation of the standard uncertainty of each input quantity (i.e., V_{ch} and V_{st}). For each measurement point, the 10 independent repeated voltage values were used to compute the mean and standard deviation (std) for each input quantity. At this step, the digital oscilloscope accuracy (doa), 0.01%, and resolution (dor), 8-bit-type, were computed based on the information provided by the manufacturer (B+K Precision, 2530B User Manual 2011), along with the measuring tape accuracy (mta), 0.0007935 m. The assumptions made here were that since the digital oscilloscope and the measuring tape evaluation were carried out by means other than the statistical analysis of a series of observations, their distributions follow the rectangular distribution (ISO/BIMP 1993), where the standard uncertainty, u, of a value x_i is given by the Equation 6-2:

$$u(x_i) = \frac{\alpha_i}{\sqrt{3}} \qquad \text{Equation 6-2}$$

where α is the estimated semi-range of the uncertainty.

In the third step, the operational condition uncertainties for each input quantity were computed, based on the 10 independent repeated measurements. The operational condition uncertainties are the summation of the uncertainty components of each input quantity (Equations 6-3 & 6-4).

$$u(V_{ch})_i = \sqrt{(std(V_{ch})_i)^2 + (doa)^2 + (dor)^2 + (mta)^2} \qquad \text{Equation 6-3}$$

$$u(V_{st})_i = \sqrt{(std(V_{st})_i)^2 + (doa)^2 + (dor)^2 + (mta)^2} \qquad \text{Equation 6-4}$$

where $u(V_{ch})_i$ is the operational condition uncertainty for the *ith* measurement point of the input quantity V_{ch}; and

$u(V_{st})_i$ is the operational condition uncertainty for the *ith* measurement point of the input quantity V_{st};

The forth step includes the calculation of the combined standard uncertainty, u_c(RF), (Equation 6-5) for each measurement point. Here, the operational condition uncertainties are multiplied with the sensitivity coefficients. The sensitivity coefficients are the partial derivatives of the reduction equation with respect to each input quantity (Equations 6-6 & 6-7) and according to ISO/BIMP (1993), these partial derivatives are a measure of the variation in the values of the output estimates due to small changes in the value of the input estimates.

$$u_c(RF)_i = \sqrt{(u(V_{ch})_i)^2 \times \left(\frac{\partial RF}{\partial V_{chi}}\right)^2 + (u(V_{st})_i)^2 \times \left(\frac{\partial RF}{\partial V_{sti}}\right)^2} \quad \text{Equation 6-5}$$

$$\frac{\partial RF}{\partial V_{ch}} = \frac{100 \times Vst}{{V_{ch}}^2} \quad \text{Equation 6-6}$$

$$\frac{\partial RF}{\partial V_{st}} = -\frac{100}{V_{st}} \quad \text{Equation 6-7}$$

The final step in this uncertainty analysis, step 5, is the calculation of the expanded uncertainty, U, (Equation 6-8) for each measurement point, based on the 10 independent repeated measurements. Typically, the expanded uncertainty is expressed as a 95% confidence interval, at which the sample mean $(\bar{x})$ and the population mean (μ) are within two standard deviations of each other.

$$U = kU_c(RF)_i \quad \text{Equation 6-8}$$

where k is the coverage factor. Typically, for a 95% confidence interval, the value of k is 2 (ISO/BIMP 1993)

Figure 6-10 shows the 95% confidence intervals of the transponder return RF signal strength decay (%) for the TI LF passive RFID system with the 120 mm long transponders, along with the custom made excitation antenna, when air was in between

the antenna and the transponder. Each measurement point 95% confidence interval was computed following the ISO/BIMP (1993) uncertainty analysis protocol, and was based on the statistical analysis of a large sample of 10 independent repeated measurements. The maximum antenna-transponder detection distance for this setup was 17 ft. (5.2 m). As it was expected, the closer the transponder to the RFID antenna (until approximately 60% of $D_{max\ air_cust_ant_120}$), the lower the level of uncertainty in the RF signal strength decay. After that point (60% of $D_{max\ air_cust_ant_120}$), the uncertainty in the measurements dramatically increases, indicating that there is a significant deviation from the average measured RF signal strength. This abrupt change in the confidence interval limits can be attributed to the fact that the RF signal attenuates with the square of the distance traveled and that attenuation can be affected by environmental factors. The highest levels of uncertainty were observed for the measurement points located at 80 and 100% of $D_{max\ air_cust_ant_120}$, respectively. Although one would expect that the uncertainty would be higher for the measurement point located at $D_{max\ air_cust_ant_120}$, this irregularity is most probably related to the effects of the environmental factors on the RF signal propagation and attenuation.

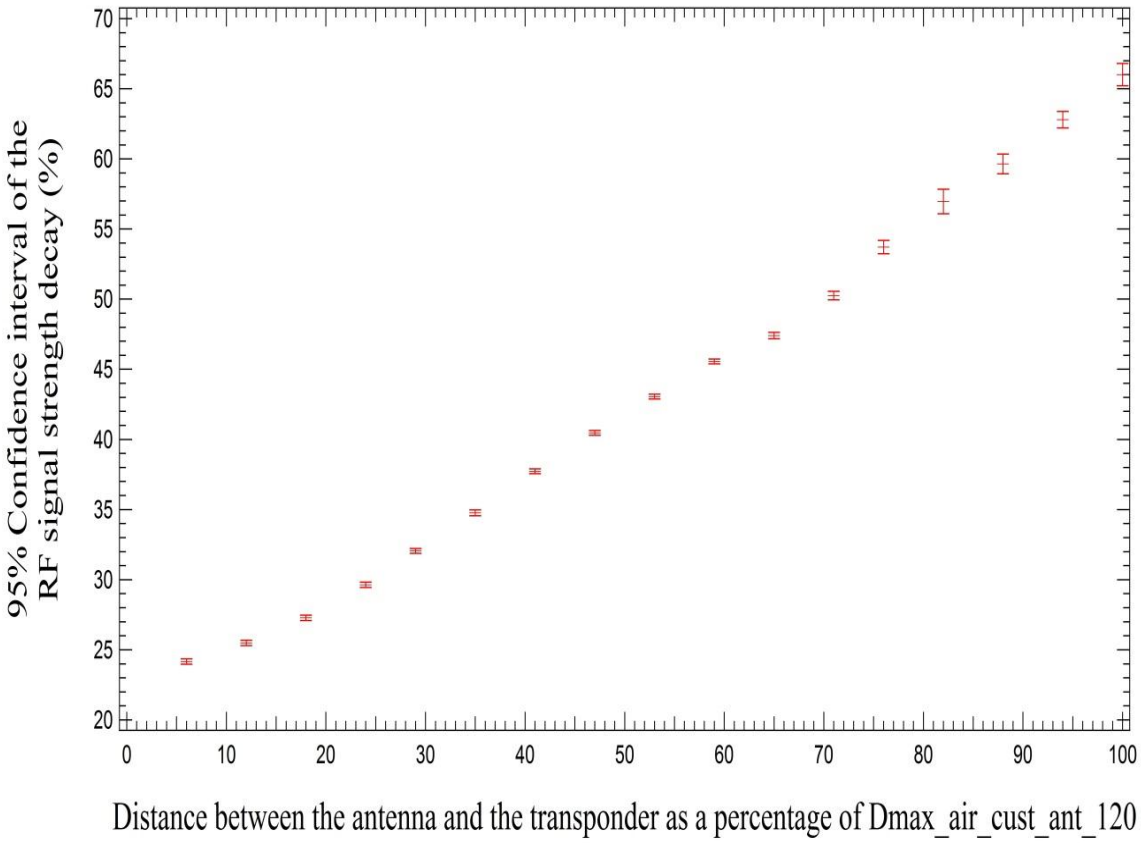

Figure 6-10 Uncertainty analysis plot for the transponder return RF signal strength decay using the ISO/BIMP (1993) protocol for the TI LF passive RFID system with the 120 mm transponders, along with the custom made RFID antenna, when AIR was in between the antenna and the transponder.

CHAPTER 7

CONCLUSIONS, CONTRIBUTIONS AND RECOMMENDATIONS

This research offers a new innovative approach for detecting sediment scour in natural environments and/or around hydraulic structures. The innovation lies on the utilization of the Low Frequency, passive RFID system to identify the onset of scour and provides a measure of the scour depth. The RFID technology has been around over the last twenty years for detecting object movement and quality of materials. The innovation of this research is not so much found on the development of a new RFID system, but on the introduction of the state-of-the-art methodology of utilizing the concept of the RF signal decay to investigate the problem at hand, scour.

Following that line of thinking, this research comprises of two major parts: (1) a parametric analysis to understand the governing variables affecting the performance of the RFID system in the context of the scour application; and (2) a RF signal strength decay vs. distance curve for different soil mediums, such as sand and gravel, as well as air and water.

A key finding of the parametric experiments is that the orientation of the transponder plays a significant role in terms of the detection efficiency of the RF signal. A transponder that is placed perpendicular to the excitation antenna plane provides the strongest signal and thus facilitates the largest detection distance. On the contrary, the transponder that is placed in parallel to the excitation antenna plane limits the detection distance. For these reasons, the perpendicular oriented transponder is defined in this

research as the favorable orientation transponder. We utilize this knowledge to identify the onset of scour during a scour evolution process.

Another significant finding of the parametric experiments is that medium matters. Transponders in sand, independent of the orientation of the excitation antenna, performed worse than transponders in air, water, and gravel. Sand affects the RF signal strength due to the influence of the quartz particles to the electromagnetic field generated by the excitation antenna and the transponder inner antenna by deteriorating the RF signal propagation. It was found that transponders in air performed the best and that is the reason in this research, but also for future studies related to this topic, that air should be used as the baseline or reference condition for any RF signal strength decay estimations.

Lastly, but not least, the material casing of the transponder used to encapsulate the transponder plays a role to the system performance. PVC was found to be the optimal solution due to the ease of use, cost, and endurance.

The second part of this research focuses on the RF signal strength decay vs. distance. This part of the research was significant for demonstrating the applicability of the RFID concept. No one could use the RFID concept, if the development of calibration curves that relate RF signal strength decay to distance, for different mediums, is not feasible. A precondition for performing this analysis is the use of a digital oscilloscope that can provide the voltage time series and typology characteristics at various distances, where the transponder is placed, each time. With the aid of the oscilloscope, the fraction of the reader-transponder communication RF signal corresponding to the transponder return signal part, which lasts for approximately 0.016 seconds, is analyzed. It is that

time fraction that is considered for the development of the RF signal strength vs. distance decay curves.

The findings from the analysis of the transponder return RF signal show the following: (1) that the RF signal strength vs. distance decay curves are overall well represented by a linear fit; (2) there is a shift between those line fits and a change in slope for different mediums. These findings led us to the following conclusions. First, if calibration lines are constructed reliably, then someone could extrapolate them to identify transponder locations for larger distances, and secondly, for each set of application the user must know the dominant soil structure, since the soil medium affects the gradient of the RF signal strength decay curve. In a nut shell, this research offers a new way of detecting scour in rivers with or without the presence of hydraulic structures with a lot of promise.

However, there are some caveats that must be addressed. First, an anti-collision must be available to prevent signal interference and camouflaging two neighboring transponders, when both transponders are located within the excitation antenna electromagnetic field. Second, new ways of installing the transponders must be identified, so the whole RFID technology is all well streamlined.

REFERENCES

Allan, J.C., Roger H, Tranquili, J.V. "The use of Passive Integrated Transponder (PIT) Tags to Trace Cobble Transport in a Mixed Sand-and-Gravel Beach on the High-Energy Oregon Coast, USA." *Marine Geology* 232, (2006): 63-86.

Al-Shamma'a, A.I., Shaw, A. and Saman, S. "Propagation of Electromagnetic Waves at MHz Frequencies through Seawater." *IEEE Transactions on Antennas and Propagation, November 2004* 52, no. 11 (2004).

Anderson, N.L., Ismael, A.M. and Thitimakorn, T. "Ground-Penetrating Radar: A Tool for Monitoring Bridge Scour." *Journal of Environmental and Engineering Geoscience* 13, (2007): 1-10.

Arkell, B., Leeks, G., Newson, M. and Oldfield, F. "Trapping and Tracing: Some Recent Observations of Supply and Transport of Coarse Sediment from Uplands Wales, in Modern and Ancient Fluvial Systems " *In J. D. Collinson and J. Lewin (Eds), Blackwell Publishing Ltd., Oxford, UK. Doi: 10.1002/9781444303773.ch8* (1982).

Ashworth, P.J. and Ferguson, R.I. "Size-Selective Entrainment of Bed Load in Gravel Bed Streams." *Water Resources Research* 25, no. 4 (1989): 627-634.

B+K Precision. "Model 2530B, 2532B 25 MHz and 40MHz Digital Storage Oscilloscope, User Manual." (2011).

Barralet, M., Huang, X., and Sharma, D.. "Effects of Antenna Polarization on RSSI Based Location Identification."IEEE, 2009.

Bradley, N.D., and Tucker, G.E. "Measuring Gravel Transport and Dispersion in Mountain River using Passive Radio Tracers." *Earth Surface Processes and Landforms* 37, no. 10 (2012): 1034-1045.

Breusers, H.N.C., Nicollet, G. and Shen, H.W. "Local Scour Around Cylindrical Piers." *Journal of Hydraulic Research, I.A.H.R.* 15, no. 3 (1977): 211-252.

Brunner, G.W. "HEC-RAS, River Analysis System Hydraulic Reference Manual, v. 4.1." *U.S. Army Corps of Engineers, Hydrologic Engineering Center (HEC)* (2010).

Camenen, B., Le Coz, J. Paquier, A. and Lagouy, M. "An Estimation of Gravel Mobility Over an Alpine River Gravel Bar (Arc En Maurienne, France) using PIT-Tag Tracers." *5th International Conference on Fluvial Hydraulics (River Flow 2010), Braunschweig, Germany, 8-10 September 2010* (.

Church, M. and Hassan, M.A. "Mobility of Bed Material in Harris Creek." *Water Resources Research 38, Doi: 10.1029/2001 WR000753:19-1-19-12* (2002).

Church, M. and Hassan, M.A. "Size and Distance of Travel of Unconstrained Clasts on a Streambed." *Water Resources Research* 28, (1992): 299-303.

Cormos, D.A., Letertre, T., Diet, A., and Azoulay, A. "Electromagnetic Environment of RFID Systems." Munich Germany, 2007.

Curtin, J., Kauffman, R.J., and Riggins, F.J. "Making the 'MOST'out of RFID Technology: A Research Agenda for the Study of the Adoption, Usage and Impact of RFID." *Information Technology and Management* 8, no. 2 (2007): 87-110.

Curtiss, G.M., Osborne, P.D. and Horner-Devine A.R. "Seasonal Patterns of Coarse Sediment Transport on a Mixed Sand and Gravel Beach due to Vessel Wakes, Wind Waves, and Tidal Currents." *Marine Geology* 259, (2009): 73-85.

Custer , S.G., Ergenzinger, P.J. and Anderson, B.C. "Electromagnetic Detection of Pebbles in Streams: A Method for Measurement of Sediment Transport Waves." *Flores (Eds) Recent Developments in Fluvial Dedimentology. Society of Paleontologists and Minerologists, Pp. 21-26* (1987).

Davoren, A. *Local Scour Around a Cylindrical Bridge Pier* Hydrology Centre, Ministry of Works and Development for the National Water and Soil Conservation Authority, 1985.

De Falco, F. and Mele, R. "The Monitoring of Bridges for Scour by Sonar and Sedimetri." *NDT&E International* 35, (2002): 117-123.

Deng, L. and Cai, C.S. "Bridge Scour: Prediction, Modeling, Monitoring, and Countermeasures-Review." *Pract. Period. Struct. Des. Constr.* 15, no. 2 (2010): 125-134.

Dongol, D.M.S. "Local Scour at Bridge Abutments." *Report no. 544, School of Engineering, the University of Auckland, Auckland, New Zealand* (1994).

Dziadak, K., Kumar, B. and Sommerville, J. "Model for the 3D Location of Buried Assets Based on RFID Technology." *Journal of Computing in Civil Engineering* 23, no. 3 (2009): 148-159.

Einstein A.H. "The Bed Load Transport as Probability Problem." *Mitteilung Der Versuchsanstalt Fuer Wasserbau an Der Eidgenossischen Technischen Hochschule. Zurich* (1937).

Einstein A.H. and Chien N. "Transport of Sediment Mixtures with Large Ranges of Grain Sizes." *U.S. Army Corps of Eng. MO River Div. Sediment Ser. Rep., 2.* (1953).

Emmett, W.W., Burrows, R.L. and Chacho, E.F.Jr. "Coarse Particle Transport in a Gravel Bed River." *3rd International Workshop on Gravel-Bed Rivers; Dynamics of*

Gravel-Bed Rivers, 25-29 September 1990, Florance, Italy, (Unpublished Manuscript) (1990).

Ergenzinger, P.J., Schmidt, K.H. and Busskamp, R. "The Pebble Transmitter System (PETS): First Results of a Technique for Studying Coarse Material Erosion, Transport and Deposition." *Zeit. Geomorph.,* 33, (1989): 503-508.

Ettema, R. "Scour at Bridge Piers." *Report no. 216, School of Engineering, the University of Auckland, Auckland, New Zealand* (1980).

Ettema, R., Nakato, T., and Muste, M. "An Illustrated Guide for Monitoring and Protecting Bridge Waterways Against Scour." *Iowa Highway Research Board Final Report, Project-515* (2006).

Forde, M.C., McCann, D.M., Clark, M.R., Broughton, K.J., Fenning, P.J. and Brown, A. "Radar Measurement of Bridge Scour." *NDT&E International* 32, (1999): 481-492.

Fukui, J. and Otuka, M. "Development of the New Ispection Method on Scour Condition Around Existing Bridge Foundations." *Proc., 1st Int. Conf. on Scour of Foundation, ICSF-1, Texas A&M Univ., College Station, Tex., 410–420.* (2002).

Gill, M.A. "Erosion of Sand Beds Around Spur Dikes." *Journal of the Hydraulics Division, A.S.C.E.* 107, no. HY3 (1972): 273-294.

Gorin, S.R. and Haeni, F.P. "Use of Surface-Geophysical Methods to Assess Riverbed Scour at Bridge Piers." *U.S. Geological Survey, Water-Resources Investigations Report 88-4212* (1989).

Gustafsson, M., and Nordebo, S. "Bandwidth, Q Factor, and Resonance Models of Antennas." *Progress in Electromagnetics Research* 62, (2006): 1-20.

Habersack, H.M. "Radio-Tracking Gravel Particles in a Large Braided River in New Zealand: A Field Test of Stochastic Theory of Bed Load Transport Proposed by Einstein." *Hydrological Processes* 15, (2001): 377-391.

Haeni, F., Buursink, M.L., Costa, J.L., Melcher, N.B., Cheng, R.T. and Plant, W.J. "Ground-Penetrating Radar Methods used in Surfacewater Discharge Measurements." *In Noon, D.A., Stickley, G.F. and Longstaff, D., Editors, GPR 2000, 8th International Conference on Ground Penetrating Radar, Gold Coast, Australia* (2000): 494-500.

Haschenburger, J.K. "Scour and Fill in a Gravel-Bed Channel: Observations and Stochastic Models." *PhD Thesis, University of British Columbia,* (1996).

Haschenburger, J.K. and Church, M. "Bed Material Transport Estimated from the Virtual Velocity of Sediment." *Earth Surface Processes and Landforms* 23, (1998): 791-808.

Hassan, M.A., Church, M. and Ashwrth, P. "Virtual Rate and Mean Distance of Travel of Individual Clasts in Gravel-Bed Channels." *Earth Surface Processes and Landforms,* 17, (1992): 617-627.

Hassan, M.A., Schick, P. and Laronne, J.B. "The Recovery of Flood-Dispersed Coarse Sediment Particle, a Three Dimensional Magnetic Tracing Method." *In Schick, A.P., Ed., Channel Processes; Water, Sediment and Catchment Controls: Catena Supplement, v. 5, p. 153-162* (1984).

Hassan, T. and Chatterjee, S. "A Taxonomy for RFID." *Proceedings of the 39th Annual Hawaii International Conference on System Sciences, 2006. HICSS '06.* (2006).

Hasted, J.B., ed. *Aqueous Dielectrics*. London: Chapman and Hall, 1973.

Hayes, D.C. and Drummond, F.E. "Use of Fathometers and Electrical Conductivity Probes to Monitor Riverbed Scour at Bridges and Piers." *Water Resources Investigations Rep. no. 94-4164, U.S. Geological Survey, Hartford, Connecticut* (1995).

Hendrick, R.R., Ely, L.L. and Papanicolaou, A.N. "The Role of Hydrologic Processes and Geomorphology on the Morphology and Evolution of Sediment Clusters in Gravel-Bed Rivers." *Geomorphology* 114, no. 3 (2010): 483-496.

Horne, W.A. "Scour Inspection using Ground Penetrating Radar." *Proceedings of National Conference on Hydraulic Engineering, San Francisco* (1993): 1888-1893.

Huang, H.P. and Chang, Y.T. "Robust Design for RFID System Testing and Applications."IEEE, 2007.

Hunt, B. E. "Scour Monitoring Programs for Bridge Health." *Transportation Research Record: Journal of the Transportation Research Board* (2005): 531-536.

ISO/BIMP. *Guide to the Expression of Uncertainty in Measurement*. 1st ed. Geneva, Switzerland: International Organisation for Standardisation, 1993.

Kattell, J., and Eriksson, M. "Bridge Scour Evaluation: Screening, Analysis, and Countermeasures." *Pub. Rep. no. 9877, USDA Forest Service, Washington, D.C.* (1998).

Keskilammi, M., Sydanheimo, L. and Kivikoski, M. "Radio Frequency Technology for Automated Manufacturing and Logistics Control. Part 1: Passive RFID Systems and

the Effects of Antenna Parameters on Operational Distance." *The International Journal of Advanced Manufactuting Technology* 112, no. 2 (2003): 510-520.

Kirkil, Gokhan. *Numerical Study of the Flow Field at Cylindrical Piers in an Alluvial Bed,* edited by Constantinescu, George, University of Iowa. Civil and Environmental Engineering 2008.

Kirkil, Gokhan. *Similitude of Coherent Eddies in Flume Experiments on Bridg Scour,* edited by Constantinescu, George, University of Iowa. Civil and Environmental Engineering 2004.

Ko, C.H. "RFID 3D Location Sensing Algorithms." *Automation in Construction* 19, (2010): 588-595.

Koken, M. and Constantinescu, G. "An Investigation of the Flow and Scour Mechanisms Around Isolated Spur Dikes in a Shallow Open Channel: 2. Conditions Corresponding to the Final Stages of the Erosion and Deposition Process." *Water Resources Research* 44, no. 16 (2008): 16.

Kuhnle, R.A., Alonso, C.V., Shields, F.D. "Local Scour Associated with Angled Spur Dikes." *Journal of Hydraulic Engineering* 128, no. 12 (2002): 1087-1093.

Kwan, T.F. "A Study of Abutment Scour." *Report no. 451, School of Engineering, the University of Auckland, Auckland, New Zealand* (1988).

Kwan, T.F. "Study of Abutment Scour." *Report no. 328, School of Engineering, the University of Auckland, Auckland, New Zealand* (1984).

Lagasse, P.F., Zevenbergen, L.A.W., School, J.D., and Clopper, P.E. "Bridge Scour and Stream Instability Countermeasures: Experience, Selection, and Design Guidelines." *Federal Highway Administration, Hydraulic Engineering Circular no. 23: FHWA NHI 01-003, U.S. Department of Transportation, Washington, D.C.* (2001).

Lagasse, P.F., Richardson, E.V. and Schall, J.D. "Fixed Instrumentation for Monitoring Scour at Bridges." *Transportation Research Record* 1647, no. 98-0057 (1998).

Lamarre, H., MacVicar, B. and Roy, A.G. "Using Passive Integrated Transponder (PIT) Tags to Investigate Sediment Transport in Gravel-Bed Rivers." *Journal of Sedimentary Research* 75, (2005): 736-741.

Laronne, J.B. and Duncan, M.J. "Bedload Transport Paths and Gravel Bar Formation." *In Billi, P., Hey, R. D., Thorne, C. R. and Tacconni, P. (Eds), Dynamics of Gravel-Bed Rivers, Wiley, Chichester, 177–200* (1992).

Lauth, T.J. and Papanicolaou, A.N. "Application of Radio Frequency Tracers to Individual and Group Particle Displacement within a Laboratory." *World Environmental and Water Resources Congress, 2009: Great Rivers* (2009).

Lauth, T.J. and Papanicolaou, A.N. "Experimental/feasibility Study of Radio Frequency Tracers for Monitoring Sediment Transport and Scour Around Bridges." *World Environmental and Water Resources Congress, 2008, Ahupua'a* (2008).

Lefter, J. "Instrumentation for Measuring Scour at Bridge Piers and Abutments." *National Cooperative Highway Research Program (NCHRP) Rep. no. 189, Transportation Research Board, Washington, D.C.* (1993).

Lemos, F.O. "General Report." *Proc., 16th. Congress, I.A.H.R., Sao Paulo, Brazil* (1975).

Leopold, L.B., Emmett, W.W. and Myrick, R.M. "Channel and Hillslope Processes in Semi-Arid Areas, New Mexico." *U.S. Geological Survey, Professional Paper 352-G* (1966): 193-253.

Liebault, F., Bellot, H., Chapuis, M., Klotz, S., and Deschatres, M. "Bedload Tracing in a High-Sediment-Load Mountain Stream." *Earth Surface Processes and Landforms* 37, (2012): 385-399.

Lin, Y.B., Chang, K.C., Lai, J.S. and Wu, I.W. "Applications of Optical Fiber Sensor on Local Scour Monitoring." *IEEE International Conference on Sensors, 2004, Vienna, Austria* (2004).

Lin, Y.B., Chen, J.C., Chang, K.C., Chern, J.C. and Lai, J.S. "Real-Time Monitoring of Local Scour by using Fiber Bragg Grating Sensors." *Smart Materials and Structures* 14, (2005): 664-670.

Lin, Y.B., Lai, J.S., Chang, K.C. and Li, L.S. "Flood Scour Monitoring System using Fiber Bragg Grating Sensors." *Smart Materials and Structures* (2006): 1950-1959.

MacVicar, B.J. and Roy A.G. "Sediment Mobility in a Forced Riffle-Pool." *Geomorphology* 125, (2011): 445-456.

Mason, R.R. and Shepard, D.M. "Field Performance of an Accoustic Scour-Depth Monitoring System." *Proceedings of Fundamentals and Advancements in Hydraulic Measurements and Experimentation, New York, 366-375* (1994).

McNamara, J.P. and Borden C. "Observations on the Movement of Coarse Gravel Implanted Motion-Sensing Radio Transmitters." *Hydrological Processes* 18, (2004): 1871-1884.

Melville, B.W. and Coleman, S. E. "Bridge Scour." *Water Resources, LLC, CO, USA* (2000).

Melville, B.W. "Local Scour at Bridge Sites." *Report no. 117, School of Engineering, the University of Auckland, Auckland, New Zealand* (1975).

Melville, B.W. and Chiew, Y.M. "Time Scale for Local Scour at Bridge Piers." *Journal of Hydraulic Engineering* 125, no. 1 (1999): 59-65.

Melville, B.W. and Sutherland, A.J. "Design Method for Local Scour at Bridge Piers." *Journal of Hydraulic Engineering* 114, no. 10 (1988): 1210-1226.

Merced Irrigation District (MID), Natural Resource Sciences, Inc. "Merced River Wing Dam Gravel Monitoring 2000-2002." *Final Report. March 2003. U.S. Fish Wildlife Service AFRP*. (2003).

Metje, N., Atkins, P.R., Brennan, M.J., Chapman, D.N., Lim, H.M., Machell, J., Muggleton, J.M., Pennock, S., Ratcliffe, J., Redfern, M., Rogers, C.D.F., Saul, A.J., Shan, Q., Swingler, S., and Thomas, A.N. "Mapping the Underworld - State-of-the-Art Review." *Tunnelling and Underground Space Technology* 22, no. 5-6 (2007): 568-586.

Millard, S.G., Bungey, J.H., Thomas, C., Soutsos, M.N., Shaw, M.R., and Patterson, A. "Assessing Bridge Pier Scour by Radar." *NDT&E Int.* 31, no. 4 (1998): 51-258.

Murillo, J.A. "The Scourge of Scour." *Civil Engineering* 57, no. 7 (1987): 66-69.

Nassif, H., Ertekin, A.O., and Davis, J. "Evaluation of Bridge Scour Monitoring Methods." *New Jersey Department of Transportation Final Report, FHWA-NJ-2003-009* (2002).

Nichols, M.H. "A Radio Frequency Identification System for Monitoring Coarse Sediment Particle Displacement." *Applied Engineering in Agriculture* 20, no. 6 (2004): 783-787.

O'Connor, K.M. and Dowding, C.H. "Real Time Monitoring of Infrastructure using TDR Technology: Case Histories." *Geophysics* (2006).

Papanicolaou, A.N., Bdour, A. and Wicklein, E. "One-Dimensional hydrodynamic/sediment Transport Model Applicable to Steep Mountain Streams." *Journal of Hydraulic Research* 42, no. 4 (2004): 357-375.

Papanicolaou, A.N., Elhakeem, M. and Tsakiris, A. "Autonomous Measurements of Bridge Pier and Abutment Scour using Motion-Sensing Radio Transmitters." *Iowa Highway Research Board Final Report, Project TR-595* (2010).

Park, I., Joengwoo, L. and Woncheol, C. "Assessment of Bridge Scour and Riverbed Variation by a Ground Penetrating Radar." *10th International Conference on Ground Penetrating Radar* (2004).

Richardson, E.V., Harrison, L.J., Richardson, J.R. and Davis, S.R. "Evaluating Scour at Bridges Second Edition (HEC-18)." *National Highway Institute Federal Highway Administration* (1993).

Saarenketo, T. "Electrical Properties of Water in Clay and Silty Soils." *Journal of Applied Geophysics* 40, (1998): 73-88.

Schall, J.D. and Price, G.R. *Portable Scour Monitoring Equipment*. Vol. 515 Transportation Research Board National Research, 2004.

Schmidt, K.H. and Ergenzinger, P. "Bedload Entrainment, Travel Lengths, Step Lengths, Rest Periods-Studied with Passive (Iron, Magnetic) and Active (Radio) Tracer Techniques." *Earth Surface Processes and Landforms,* 17, (1992): 147-165.

Schulz, W.L., Udd, E., Seim, J.M. and McGill, G.E. "Advanced Fiber Grating Sensor Systems for Bridges, Structures, and Highways." *Proc SPIE, 3325* (1998): 212-221.

SCOUR, W. I. S. B. "Uses." (2000).

Sear, D.A. "Event Bed Load Yield Measurement with Load Cell Bedload Traps and Prediction of Bed Load Yield from Hydrograph Shape." *Proceedings of the Oslo Workshop on Erosion and Sediment Transport Measurement in Rivers, Technological and Methodological Advances IAHS Publ. 283, Wallingford, Pp. 146–153.* (2003).

Sear, D.A., Lee, M.W.E., Oakey, D.J., Carling, P.A. and Collins, M.B. "Coarse Sediment Tracing Technology in Littoral and Fluvial Environments." *In Tracers in Geomorphology, Foster I.D.L. (Ed.). John Wiley and Sons: Chichester; 21-55* (2000).

Shaw, A., Al-Shamma'a, A.I., Wylie, S.R. and Toalm, D. "Experimental Investigations of Electromagnetic Wave Propagation in Seawater." *Proceedings of the 36th European Microwave Conference, September 2006, Manchester UK* (2006).

Shen, H.W., Schneider, V.R. and Karaki, S.S. "Mechanics of Locar Scour." *U.S. Department of Commerce, National Bureau of Standards, Institute for Applied Technology* (1966).

Shirhole, A.M. and Holt, R.C. "Planning for Comprehensive Bridge Safety Program." *Transportation Research Record 1290, Transportation Research Board, National Research Council, Washington, D.C., U.S.A.* 1, (1991): 39-50.

Strom, K. and Papanicolaou, A.N. "Case Study: Bed Stability Around the East Caisson of the Tacoma Narrows Bridge." *Journal of Hydraulic Engineering* 131, no. 2 (2005): 75-84.

Sumer, B.M., Kozakiewicz, A., Fredsoe, J., and Deigaard, R. "Velocity and Concentration Profiles in Sheet-Flow Layer of Movable Bed." *Journal of Hydraulic Engineering* 122, no. 10 (1996): 549.

Texas Instruments. "120mm Cylindrical Transponder." *Literature Number SCBS838* (2001).

Texas Instruments. "Antenna Reference Guide." *Literature Number SCBU025* (1996).

Texas Instruments. "Low Frequency 23mm Glass Transponder." *Literature Number SCBS841* (2001).

Texas Instruments. "Series 2000 Reader System Control Modules RI-CTL-MB2B RI-CTL-MB6B." *Literature Number SCBU044* (2008).

Texas Instruments. "Series 2000 Reader System High Performance Remote Antenna-Reader Frequency Module RI-RFM-008B Antenna Tuning Board RI-ACC-008B Reference Guide." *Literature Number SCBU023* (2002).

Ulaby, F.T., Moore, R.K. and Fung, A.K. "Microwave Remote Sensing: Active and Passive." *Vol. III, from Theory to Applications, Artech House, Norwood, Mass., 1986.* (1986).

Van Overmeeren, RA, Sariowan, S.V., and Gehrels, J.C. "Ground Penetrating Radar for Determining Volumetric Soil Water Content; Results of Comparative Measurements at Two Test Sites." *Journal of Hydrology* 197, no. 1-4 (1997): 316-338.

Van Wilson, K.Jr. "Scour at Sselected Bridge Sites in Mississippi." *U.S. Geological Survey, Water-Resources Investigations Report 94-4241* (1994).

Van Wilson, K.Jr. "Use of USGS Discharge Measurements to Determine Scour and Fill at Selected Stream Sites in Mississippi." *Proceedings of the Seventh Federal Interagency Sedimentation Conference, March 25 to 29, 2001, Reno, Nevada* (2001).

Weast, R.C. *Handbook of Chemistry and Physics*. 66th ed. Boca Raton, FL: CRC Press, 1986.

Webb, D.J., Anderson, N.L., Newton, T. and Cardimona, S. "Bridge Scour: Application of Ground Penetrating Radar." *Federal Highway Administration and Missouri Department of Transportation Special Publication* (2000).

Wilcock, P.R. "Entrainment, Displacement and Transport of Tracer Gravels." *Earth Surface Processes and Landforms* 22, (1997): 1125-1138.

Wraith, J.M. and Or, D. "Temperature Effects on Soil Bulk Dielectric Permittivity Measured by Time Domain Reflectometer: Experimental Evidence and Hypothesis Development." *Water Resources Research*, 35, no. 2 (1999): 361-369.

Yankielun, N.E. and Zabilansky, L. "Laboratory Investigation of Time-Domain Reflectometry System for Monitoring Bridge Scour." *Journal of Hydraulic Engineering* 125, no. 12 (1999): 1279-1284.

Yu, X. and Zabilansky, L.J. "Time Domain Reflectometry for Automatic Bridge Scour Monitoring." *Geotechnical Special Publication* 149, (2006): 152-159.

Ziegler, C.K., Israelsson, H.P., and Connolly, P.J. "Modeling Sediment Transport Dynamics in Thompson Island Pool, Upper Hudson River." *Water Quality and Ecosystem Modeling* 1, no. 1-4 (2000): 193-222.